2013-11-13

Synthesis and Characterization of High Nuclearity Bimetallic Group 8-Group 10 Transition Metal Cluster Complexes

Sumit Saha
University of Miami, sumitsahachem@gmail.com

UNIVERSITY OF MIAMI

SYNTHESIS AND CHARACTERIZATION OF HIGH NUCLEARITY BIMETALLIC GROUP 8-GROUP 10 TRANSITION METAL CLUSTER COMPLEXES

By

Sumit Saha

A DISSERTATION

Submitted to the Faculty
of the University of Miami
in partial fulfillment of the requirements for
the degree of Doctor of Philosophy

Coral Gables, Florida

December 2013

UNIVERSITY OF MIAMI

A dissertation submitted in partial fulfillment of
the requirements for the degree of
Doctor of Philosophy

SYNTHESIS AND CHARACTERIZATION OF HIGH NUCLEARITY BIMETALLIC GROUP 8-GROUP 10 TRANSITION METAL CLUSTER COMPLEXES

Sumit Saha

Approved:

_____ Burjor Captain, Ph.D. Professor of Chemistry	_____ Carl D. Hoff, Ph.D. Professor of Chemistry
_____ Jamie D. Walls, Ph.D. Professor of Chemistry	_____ M. Brian Blake, Ph.D. Dean of the Graduate School
_____ Ali Ghahremaninezhad, Ph.D. Professor of Civil, Architectural and Environmental Engineering	

SAHA, SUMIT (Ph.D., Chemistry)

Synthesis and Characterization of High Nuclearity Bimetallic Group 8-Group 10 Transition Metal Cluster Complexes. (December 2013)

Abstract of a dissertation at the University of Miami.

Dissertation supervised by Professor Burjor Captain.
No. of pages in text. (140)

In acetonitrile solvent, $Fe_5(CO)_{15}(\mu_5\text{-C})$, **2.1**, reacts with $Ni(COD)_2$ at room temperature to afford the iron-nickel complex $Fe_5Ni(NCMe)(CO)_{15}(\mu_6\text{-C})$, **2.3**. The acetonitrile ligand in **2.3** can be replaced by CO and NH_3 to yield $Fe_5Ni(CO)_{16}(\mu_6\text{-C})$, **2.4**, and $Fe_5Ni(NH_3)(CO)_{15}(\mu_6\text{-C})$, **2.6**, respectively. When refluxed in acetonitrile solvent, compound **2.3** loses a vertex to form the square pyramidal Fe_4Ni complex $Fe_4Ni(NCMe)_2(CO)_{12}(\mu_5\text{-C})$, **2.7**. Compound **2.7** readily converts to $Fe_4Ni(NCMe)(CO)_{13}(\mu_5\text{-C})$, **2.8**, by losing one of its acetonitrile ligands. Addition of acetonitrile to **2.8** gives compound **2.7**. When heated to 110 ºC under an atmosphere of CO, both compounds **2.7** and **2.8** furnish the octahedral Fe_4Ni_2 complex $Fe_4Ni_2(CO)_{15}(\mu_6\text{-C})$, **2.9**. (**Chapter 2**)

The reaction of $Ru_5(CO)_{15}(\mu_5\text{-C})$ with $Ni(COD)_2$ in acetonitrile at 80 °C affords the bimetallic octahedral ruthenium-nickel cluster complex $Ru_5Ni(NCMe)(CO)_{15}(\mu_6\text{-C})$, **3.1**. The acetonitrile ligand in **3.1** can be replaced by CO and NH_3 to yield $Ru_5Ni(CO)_{16}(\mu_6\text{-C})$, **3.2**, and $Ru_5Ni(NH_3)(CO)_{15}(\mu_6\text{-C})$, **3.3**, respectively. Photolysis of compound **3.1** in benzene and toluene solvent yielded the η^6-coordinated benzene and

toluene Ru_5Ni carbido cluster complexes $Ru_5Ni(CO)_{13}(\eta^6\text{-}C_6H_6)(\mu_6\text{-}C)$, **3.4** and $Ru_5Ni(CO)_{13}(\eta^6\text{-}C_7H_8)(\mu_6\text{-}C)$, **3.5** respectively. (**Chapter 3**)

In heptane solvent, $Ru_3(CO)_{12}$ reacts with tertiary butyl germane at reflux, to afford six new bimetallic ruthenium-germanium carbonyl cluster complexes $Ru_3(CO)_9(\mu_3\text{-}GeBu^t)_2$, **4.1**, $Ru_2(CO)_6(\mu\text{-}GeBu^tH)_3$, **4.2**, $Ru_4(CO)_{10}(\mu_4\text{-}Ge_2Bu^t_2)(\mu\text{-}GeBu^tH)_2$, **4.3**, $Ru_4(CO)_8(\mu_4\text{-}Ge_2Bu^t_2)(\mu\text{-}GeBu^tH)_2(\mu_3\text{-}GeBu^t)(H)$, **4.4,** $Ru_5(CO)_{12}(\mu_3\text{-}GeBu^t)_2(\mu_4\text{-}GeBu^t)(H)$, **4.5**, $Ru_6(CO)_{12}(\mu_3\text{-}GeBu^t)_4(H)_2$, **4.6**. Complex **4.2** was obtained as a result of cluster fragmentation while cluster condensation provided higher nuclearity ruthenium-germanium complexes **4.3** – **4.6** with varying Ru-Ge ratios. Addition of Bu^tGeH_3 to compound **4.3** yields compound $Ru_4(CO)_9(\mu_4\text{-}GeBu^t)_2(\mu\text{-}GeBu^tH)_3$, **4.7** releasing CO. (**Chapter 4**)

The reaction of $Ru_3(CO)_{12}$ with $Pt(IMes)_2$ in benzene solvent at room temperature afforded the monoplatinum–triruthenium cluster complex $Ru_3Pt(IMes)_2(CO)_{11}$, **5.1** in 21 % yield and the trigonal bipyramidal cluster complex $Ru_3Pt_2(IMes)_2(CO)_{12}$, **5.2** in 26 % yield. The reaction of $Ru(CO)_5$ with $Pt(IMes)_2$ in benzene solvent at 0 ^oC yielded two tri-nuclear cluster complexes, the monoplatinum–diruthenium $Ru_2Pt(IMes)(CO)_9$, **5.3** and the monoruthenium–diplatinum cluster complex $RuPt_2(IMes)_2(CO)_6$, **5.4**. The reaction of **5.2** with hydrogen at 80 ^oC afforded the tetrahydrido–tetraruthenium complex $Ru_4(IMes)(CO)_{11}(\mu\text{-}H)_4$, **5.5** and the dihydride–diruthenium–diplatinum complex $Ru_2Pt_2(IMes)_2(CO)_8(\mu\text{-}H)_2$, **5.6**. All six compounds were structurally characterized by single-crystal X-ray diffraction analyses. (**Chapter 5**)

"The whole of science is nothing more than a refinement of everyday thinking." – Albert Einstein

This thesis is dedicated to my parents
for their love, endless support
and encouragement

ACKNOWLEDGEMENTS

It is with great honor that I am able to dedicate this work to my parents and my younger brother. Without the guidance of my father Mr. Chandra Sekhar Saha, I would never have imagined myself as a chemist. Without the loving support of my mother Mrs. Mala Saha, there is simply no way I would be the person I am today. During this journey of my doctoral studies at the University of Miami, I am indebted to many people inside and outside the department for their help and immense support. First of all, I would like to convey my sincere gratitude to my research advisor Dr. Burjor Captain, who has been my mentor and friend over the past five years. His inspiration, consistent support, encouragement and enough freedom allowed me to think independently and implement my ideas to research. His friendly attitude, open mindedness and sense of humor created a healthy work environment. I am indeed fortunate enough to get the opportunity to work under his guidance.

I would like to thank Dr. Carl. D. Hoff for his intuitive, thought provoking ideas and motivation. I am deeply grateful to my other committee members Dr. Jamie D. Walls and Dr. Ali Ghahremaninezhad for their assistance and guidance during my work. I am very much thankful to Dr. Tegan Eve for his excellent guidance and help during my teaching assistantship in the Chemistry Department.

I convey my sincere thanks to our former postdoctoral fellow Dr. Lei Zhu and former graduate student Dr. Veeranna Yempally, who have shared their excellent research techniques with me and provided a helping hand in advancing my research in a fruitful direction. I am also thankful to the exceptional people I have shared the lab with during my time at the University of Miami: Dr. Derek Isrow and Anjaneyulu Koppaka.

I would like to thank the faculty members of the Department of Chemistry for their guidance, excellent teaching and research advice. I am indebted to our departmental staffs Sara, Lydia, Susana, Raul, Juanita, Jim Metcalf, Ed Torres and Dr. Hudson, they never let me feel that I am away from my family. I would like to thank the Department of Chemistry for providing me excellent research facilities.

Life is meaningless without family and friends. The enormous support provided by this special group of people has made my life complete. I am very lucky to have so many good friends around me during the past five years, few of them are Vikas, Arghya, Mehmet, Elam, Snigdhadeb, Debashis and Carl. Special thanks to my near and dear friends Himadri, Mayur, Rajib, Piu di and Sourav da for their love, care and support. These amazing people are like my family in Miami and we spent a lot of memorable fun times together.

Lastly, I would like to thank the University of Miami for five years of wonderful experiences as well as financial support. It is great to be a Miami Hurricane.

GO CANES!

TABLE OF CONTENTS

LIST OF FIGURES

CHAPTER 1

CHAPTER 2

CHAPTER 3

CHAPTER 4

CHAPTER 5

LIST OF SCHEMES

CHAPTER 1

CHAPTER 2

CHAPTER 3

CHAPTER 4

CHAPTER 5

LIST OF TABLES

APPENDIX A

APPENDIX B

APPENDIX C

APPENDIX D

Chapter 1: Introduction

1.1. Bimetallic carbonyl complexes

Metal carbonyl anions were the first reagents used to prepare complexes containing heteronuclear metal–metal bonds. One of the first bimetallic transition metal carbonyl complexes was prepared by Hieber when he was studying the chemistry of $[Co(CO)_4]^-$ in the 1930s. From the reaction of $AgNO_3$ with $NaCo(CO)_4$, the air and light sensitive compound $Ag_4[Co(CO)_4]_4$ was obtained.[1] The compound contains a planar Ag_4 core with a $Co(CO)_4$ group bridging each of the four Ag–Ag atom pairs, see Figure 1.1.

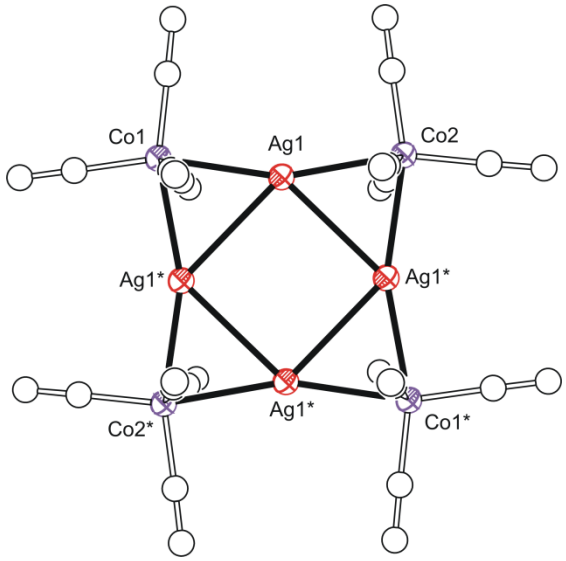

Figure 1.1. The molecular structure of $Ag_4[Co(CO)_4]_4$. (Adapted from Ref. 2)

The first compounds containing transition metal–gold and transition metal–copper bonds were obtained by Nyholm from reactions of metal carbonyl anions with gold and copper halides in 1964, e.g. $PPh_3AuCo(CO)_4$, $PPh_3AuMn(CO)_5$, $(PPh_3Au)_2Fe(CO)_4$, $PPh_3AuV(CO)_6$, (triars)$CuV(CO)_6$.[3] The first heteronuclear transition metal–transition metal carbonyl complexes appeared in the early 1960s. These included $Cp(CO)_3Mo–W(CO)_3Cp$,[4] $Cp(CO)_3$-Mo–$Fe(CO)_2Cp$,[5] $(CO)_5Mn–Fe(CO)_2Cp$[5] and $Cp(CO)Ni–Fe(CO)_2Cp$.[6] These were also made by the metal carbonyl anion/halide displacement

reactions. Vahrenkamp[7] showed some years later that these heterodinuclear compounds and many others can be made more conveniently by irradiation of mixtures of the appropriate homodinuclear compounds, e.g. UV irradiation of solutions containing $Mn_2(CO)_{10}$ and $Cp_2Fe_2(CO)_4$ gives $(CO)_5Mn–Fe(CO)_2Cp$ in a good yield. The metal–metal bonds in these compounds can be viewed as covalent heteronuclear bonds derived from two 17 electron metal-containing fragments.

Chini[8] was one of the pioneers of the redox ‘‘condensation’’ reaction of metal carbonyl anions with uncharged metal carbonyl complexes for preparing higher nuclearity heteronuclear metal clusters. Longoni’s nickel–platinum compounds: $[Ni_{38}Pt_6(CO)_{44}]^{6-}$ and $[Ni_{37}Pt_4(CO)_{46}]^{6-}$ are classic examples of metal segregated clusters that contain Pt_6 octahedral and Pt_4 tetrahedral cores inside octahedral and tetrahedral nickel shells, respectively, see Figure 1.2.[9,10]

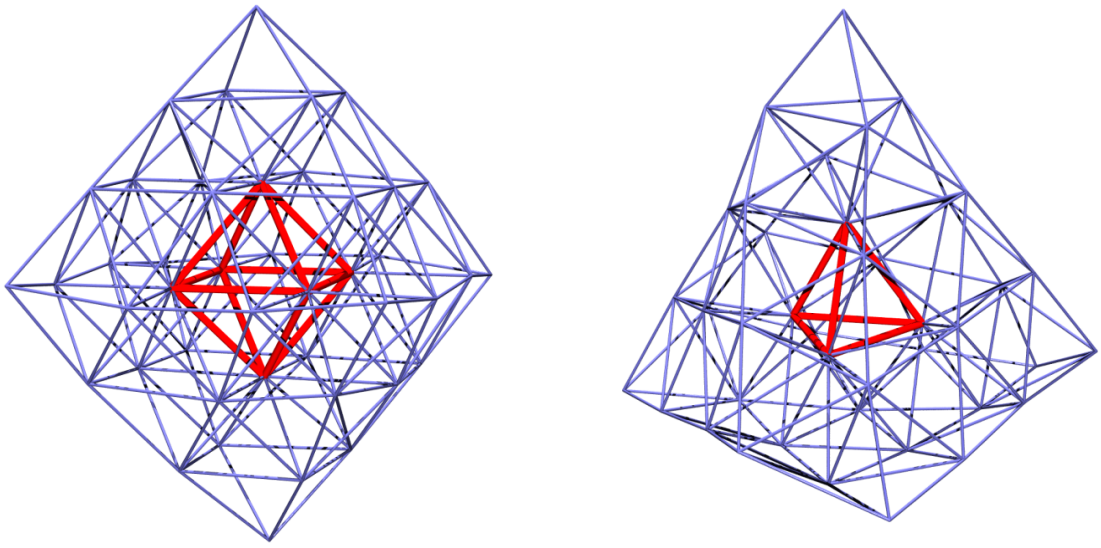

Figure 1.2. Representations of the metal framework in $[Ni_{38}Pt_6(CO)_{44}]^{6-}$ and $[Ni_{37}Pt_4(CO)_{46}]^{6-}$. The octahedral Pt_6 and tetrahedral Pt_4 groups are shown in red, and the frameworks of the Ni atoms are shown in blue. (Adapted from Ref. 2)

The Dahl group reported the novel nickel–silver cluster anion $[Ag_{16}Ni_{24}(CO)_{40}]^{4-}$ that contains a metallic core of 16 silver atoms,[11] see Figure 1.3.

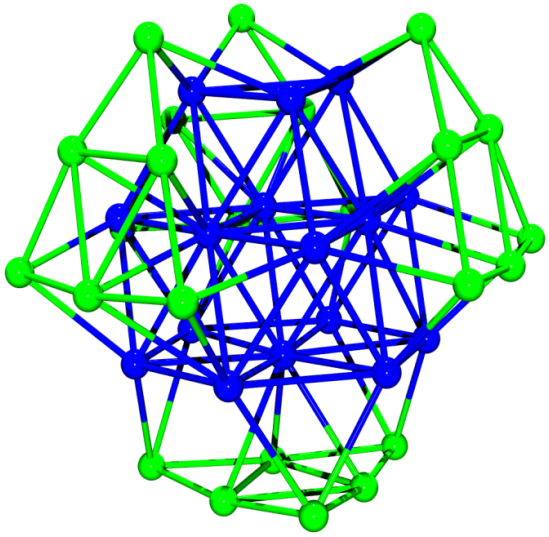

Figure 1.3. The structure of $[Ag_{16}Ni_{24}(CO)_{40}]^{4-}$. Ag atoms are shown in blue and Ni atoms are shown in green. The CO ligands have been omitted for clarity. (Adapted from Ref. 2)

1.2. Bimetallic cluster synthesis

Several synthetic methods exist for the formation and build-up of metal cluster complexes and these include ligand substitution, addition reactions, pyrolysis, metal-metal exchange and others. In ligand substitution reactions displacement of a ligand (anionic or neutral) from one metal is accompanied by simultaneous formation of a metal-metal bond with the other metal. The Cu-Fe cluster $[Cu_3Fe_3(CO)_{12}]^{3-}$ was obtained from the reaction of $[Fe(CO)_4]^{2-}$ with CuBr, see Scheme 1.1. The anionic halide ligand Br^- is a good leaving group and was displaced and simultaneous formation of the Fe-Cu bond occurred to yield the high nuclearity Cu-Fe cluster complex.[12]

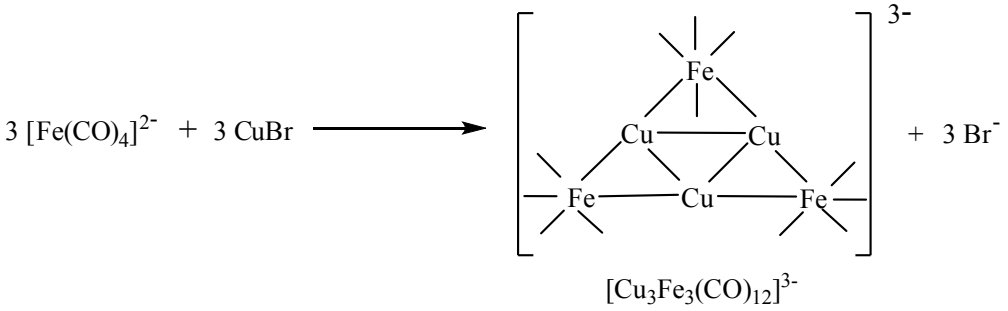

Scheme 1.1

In addition reactions one metal complex adds to another metal complex without displacing any of the ligands. However, these types of reactions are limited to compounds containing multiple bonds and to mononuclear species that are unsaturated. The $MeCpWCo(CO)_7$ without losing any of its ligands to form a CoW_3 tetrahedral cluster, see Scheme 1.2.[13]

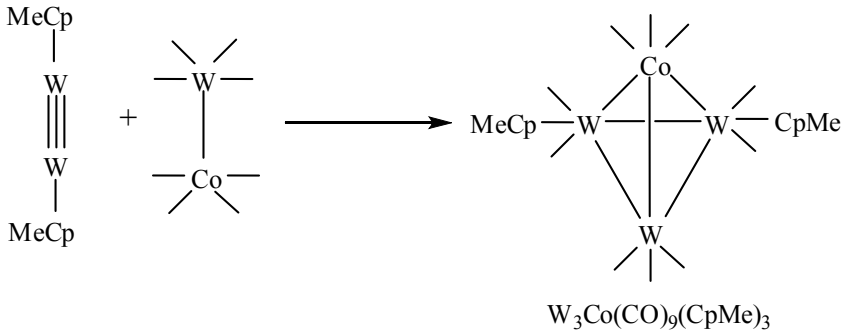

Scheme 1.2

Some of the most interesting clusters have been obtained by pyrolysis. The high nuclearity clusters are formed by condensation of small clusters, i.e. combination of the individual metal centers in the small clusters. The hexanuclear cluster $Ru_4Pt_2(CO)_{18}$ reacts with hydrogen at 97 ^oC to yield the high nuclearity tetrahydride cluster $Pt_3Ru_6(CO)_{21}H_4$.[14]

In substitution reactions, a metal atom replaces ligand bonded to the other metal and a metal-metal bond is formed. However, instead of displacing a ligand on the metal cluster, the metal atom itself can be substituted by another metal atom to result in a metal-metal exchange process and create mixed-metal clusters. An example of this kind of exchange process is seen in the reaction of the square pyramidal cluster $[Fe_5(C)(CO)_{15}]^{2-}$ with $Pt(PMePh)Cl_2$ where the platinum atom has replaced one of the iron atoms (an $Fe(CO)_2$ unit) on the base of the square pyramid, see Scheme 1.3.[15]

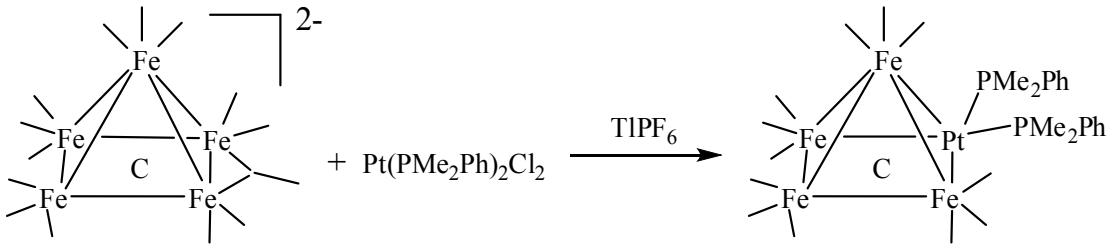

Scheme 1.3

1.3. Bimetallic cluster complexes: Applications to heterogeneous catalysis

Today the motivation for the study of bimetallic cluster complexes arises from the discoveries in the late 1960s when the platinum catalysts alloyed with iridium, rhenium or tin exhibited properties that were far superior to those of their components in the important industrial process known as petroleum reforming.[16] Later, platinum–rhodium catalysts were shown to be the most effective catalysts for the oxidation of hydrocarbons, carbon monoxide and simultaneous reduction of nitrogen oxides, NO_x. Today, supported platinum–rhodium catalysts are the active component of the three-way automotive catalytic converter.[17] It was shown that platinum–ruthenium mixtures are the most effective catalysts for the oxidation of methanol, and are the catalyst of choice at the anode of the Direct Methanol Fuel Cell.[18]

A vast number of precursor metal and mixed-metal carbonylates, of well-defined structure and stoichiometry, was available for the production of a wide range of novel nanocatalysts. The great merit of preparing bimetallic nanocatalysts from such precursors is that it guarantees as many subsequent elemental fingerprinting and electron microscopic imaging studies have repeatedly confirmed the integrity (and stoichiometry) of the nanoparticle catalyst. Bimetallic nanoparticle catalysts have been shown to exhibit superior catalytic properties, due to the presence of different metals such that one metal performs a certain role in a catalytic cycle and the other performs another function. For example, the nanoparticles of Pd and Ru alone were each far less active and less selective as hydrogenation catalysts than their Pd_6Ru_6 nanoparticle counterparts.[19] Thus, there was a pressing need for the discovery and development of single-step highly active and highly selective catalysts for the hydrogenation of a growing range of key organic compounds (Figure 1.4).[20]

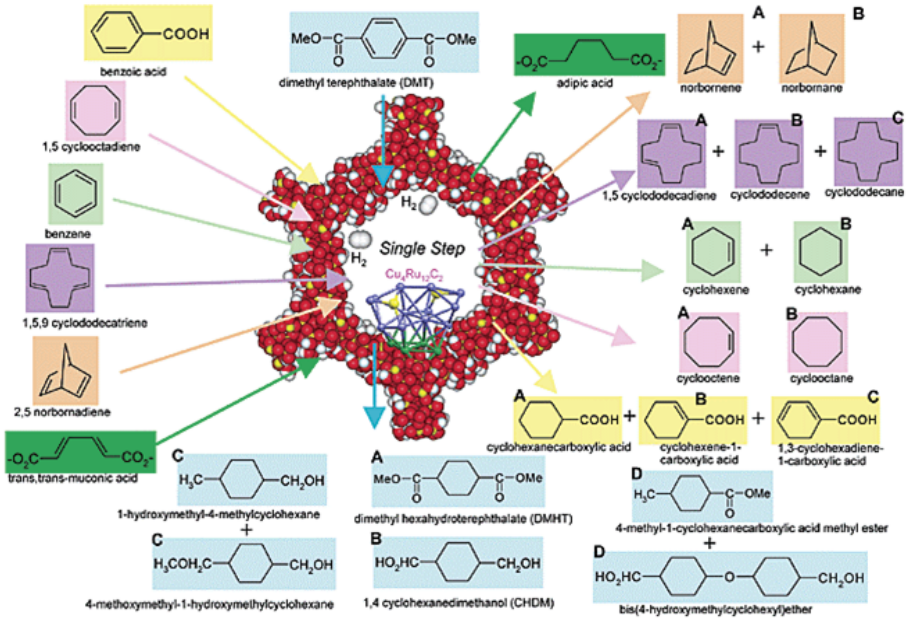

Figure 1.4. Single-step hydrogenation of some key organic compounds using highly active and selective anchored, bimetallic nanoparticle catalysts ($Cu_4Ru_{12}C_2$, in this case). (Adapted from Ref. 21)

1.4. Activation of small molecules at an unsaturated transition metal centers

Recent developments in probing techniques such as time resolved spectroscopy and neutron diffraction techniques have shed light on the binding of H_2 at a transition metal centers.[22,23] For example, the crucial step in activation of molecular hydrogen is its coordination at the metal center (see Scheme 1.4).

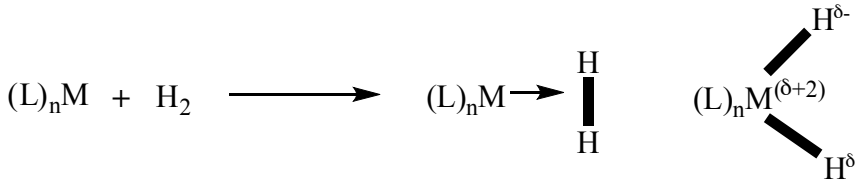

Scheme 1.4 M = Transition Metal, L = Ligand

Pioneering work by Kubas *et al.* on activation of di-hydrogen by the tungsten carbonyl complexes $W(CO)_3(PR_3)_2$ has revealed that back-donation of electrons is critical for the activation of hydrogen and stability of metal hydride complexes.[24,25] The back-donation of the electrons from the filled metal orbitals to the anti-bonding σ* orbital of hydrogen initiates cleavage of H-H bond. It was found that the ancillary ligands bonded to the metal center control the back-donation, and the nature of the formed metal-hydride complexes is dictated by the nature of the ligands.[24] Design of new ligands for application in the field of catalysis is another driving force for the advancement of organometallic chemistry.

For the activation of H_2 by transition metal complexes, the metal center should be either coordinately unsaturated or electronically unsaturated. The coordinative unsaturation can be attained by including a bulky chelating ligand, weakly bound solvent molecules, or labile CO ligands in the metal system.[26-28] The coordination of H_2 is facilitated by elimination of the solvent molecule or CO ligand. Crabtree *et al.* mimicked

the intramolecular heterolytic cleavage of H_2 by the Ir complex with weakly bound water molecule (see Scheme 1.5).[29]

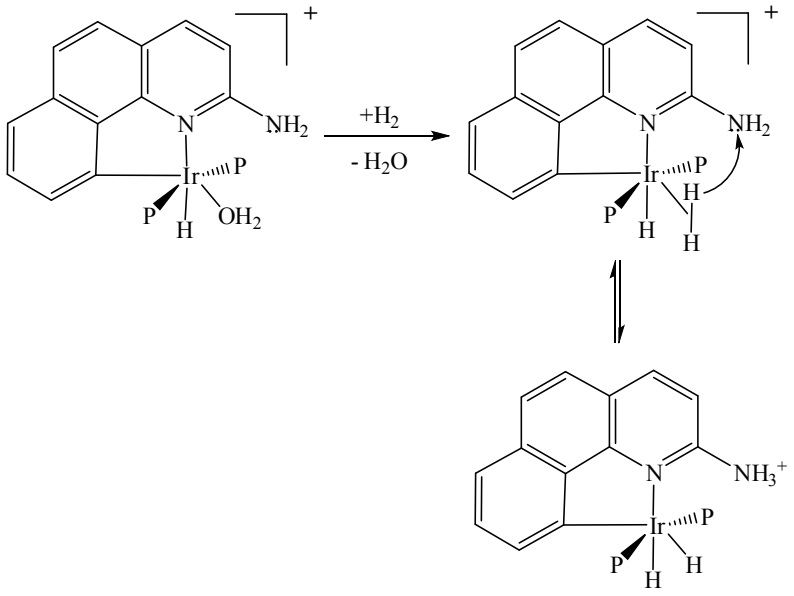

Scheme 1.5

Electronic unsaturation in transition metal complexes is induced by bulky ligands. As seen in Figure 1.5, the bulky ligands shield the metal center from the approach of large molecules, leaving enough room for the selective approach of small molecules.[30] Bulky ligands such as phosphines,[31] and N-heterocyclic carbenes[32-34] stabilize the reactive intermediates of transition metal complexes, where the metal is lacking the necessary number of electrons to attain an 18 electron configuration. Based on this approach, several unsaturated transition metal complexes have been synthesized and the reactivity of these complexes in small molecule activation is well known.[35-37]

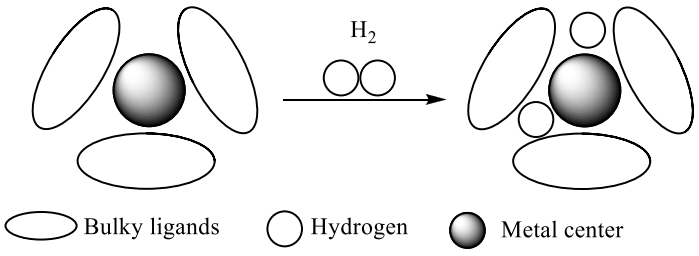

Figure 1.5. Activation of hydrogen at an unsaturated metal center.

1.5. Hydrogen activation by unsaturated mixed-metal cluster complexes

The safe and efficient utilization of hydrogen for energy-related purposes is going to require catalysts.[38] The activation of hydrogen by metals is a fundamental step in nearly all catalytic hydrogenation reactions.[39] Over the years, hydrogen-rich polynuclear metal complexes have captured the attention of cluster chemists. There are a number of reported examples in which mononuclear metal complexes are condensed under the influence of hydrogen to form high nuclearity complexes containing large number of hydride ligands.

In early work, Stone and co-workers showed that the unsaturated 58-electron complex $[PtOs_3(CO)_{10}(PCy_3)(\mu\text{-}H)_2]$, **1.1** adds hydrogen reversibly to yield the tetrahydrido complex $[PtOs_3(CO)_{10}(PCy_3)(\mu\text{-}H)_4]$, **1.2** but the addition reaction requires a pressure of 200 atm H_2 (see Scheme 1.6).[40] When the H_2 pressure is released, compound **1.2** is converted back into **1.1**.

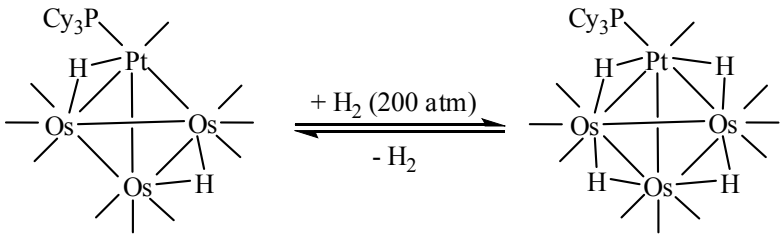

1.1 **1.2**

Scheme 1.6

Adams *et al.* have shown that stable, highly unsaturated mixed-metal cluster complexes can be prepared by the reactions of $[Pt(P^tBu_3)_2]$ with selected polynuclear metal carbonyl cluster complexes. For example, the reaction of $[Pt(P^tBu_3)_2]$ with $[Re_2(CO)_{10}]$ yielded the highly unsaturated heterometallic complex $[Pt_3Re_2(CO)_6(P^tBu_3)_3]$, **1.3**.[41]

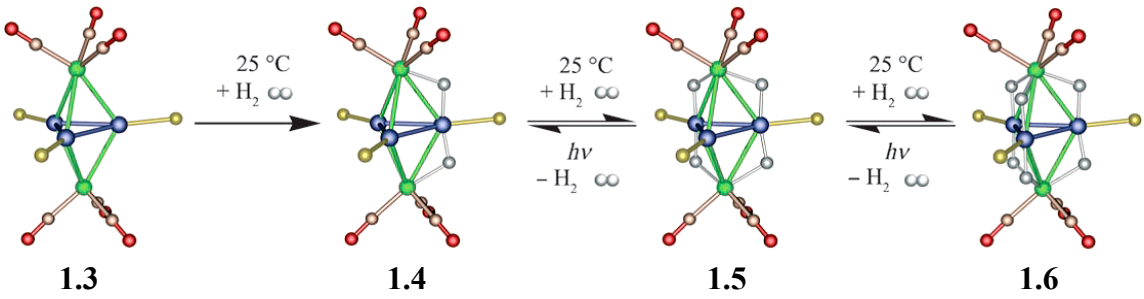

1.3 **1.4** **1.5** **1.6**

Figure 1.6. Reversible addition of H_2 to the $\{Pt_3Re_2\}$ cluster complex **1.3**. Blue Pt, green Rh, yellow P, red O, light brown C, gray H.

Most interestingly, they also found that this complex sequentially adds three equivalents of hydrogen to yield a series of three hydride-containing compounds – the dihydrido, tetrahydrido and hexahydrido complexes $[Pt_3Re_2(CO)_6(P^tBu_3)_3(\mu\text{-}H)_2]$, **1.4**, $[Pt_3Re_2(CO)_6(P^tBu_3)_3(\mu\text{-}H)_4]$, **1.5**, and $[Pt_3Re_2(CO)_6(P^tBu_3)_3(\mu\text{-}H)_6]$, **1.6**, respectively (see Figure 1.6) at room temperature.

Another very interesting highly unsaturated mixed-metal cluster complex is the 54-electron platinum–rhenium complex $[Pt_2Re_2(CO)_7(P^tBu_3)_2(\mu\text{-}H)_2]$, **1.7**, which was obtained from the reaction of $[Pt(P^tBu_3)_2]$ with $[PtRe_2(CO)_9(P^tBu_3)(\mu\text{-}H)_2]$.[42] Complex **1.7** also adds hydrogen at room temperature and 1 atm H_2, but, unlike the reaction of **1.3**, only one equivalent of H_2 is added to **1.7** to yield the 56-electron tetrahydrido cluster complex $[Pt_2Re_2(CO)_7(P^tBu_3)_2(\mu\text{-}H)_4]$, **1.8**, (see Figure 1.7), once again without any evidence of ligand loss. Most importantly, the addition of H_2 to **1.7** is fully reversible.

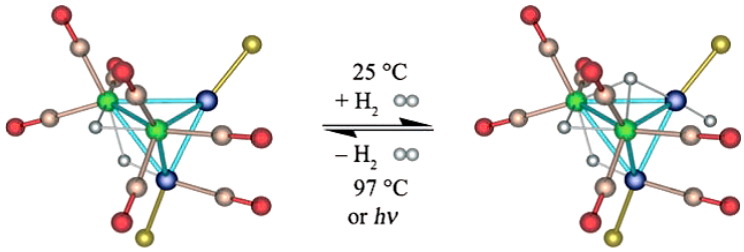

1.7 **1.8**

Figure 1.7. Reversible addition of hydrogen to the $\{Pt_2Re_2\}$ cluster complex **1.7**.

1.6. Statement of purpose

The scope to create new heteronuclear clusters is endless as there are so many ways to achieve them. To understand the concepts, models and applications of metal clusters above, there needs to be available clusters. Furthermore, bimetallic nanoparticles, prepared from bimetallic molecular cluster complexes have been shown to be viable precursors to heterogeneous catalysts in several industrial processes. Thus the quest to synthesize potential heterogeneous catalysts and to synthesize bulky unsaturated bimetallic complexes for the application in small molecules activation motivated us to investigate high nuclearity bimetallic transition metal cluster complexes.

Chapter 2: Synthesis and structural characterization of bimetallic iron-nickel carbido cluster complexes

2.1. Background

In past years Adams *et. al.* synthesized and characterized a plenty of ruthenium-platinum bimetallic cluster complexes and most of them can serve as precursors for the heterogeneous catalysis. These bimetallic nanoparticle catalysts have been shown to exhibit superior catalytic properties. But ruthenium and platinum are very expensive metals and they are also very rare. Thus the nanocatalysts made by these metals are less attractive to industry. Our goal was to synthesize bimetallic cluster complexes containing cheap metals. So we replaced ruthenium with iron and platinum with nickel. Both the iron and nickel are very cheap metals and abundant on the earth. Bimetallic nanoparticle catalysts containing iron and nickel would be a cheaper and attractive option for the application in heterogeneous catalysis in several industrial processes.

A recent and now widely used approach for preparing bimetallic nanoparticle catalysts is from bimetallic molecular cluster complexes.[43] Bimetallic nanoparticle catalysts have been shown to exhibit superior catalytic properties,[44] due to the presence of different metals such that one metal performs a certain role in a catalytic cycle and the other performs another function.[45] Supported bimetallic Fe-Ni particles have also been of interest in heterogeneous catalysis.[46] For example, it has been shown that it is possible to increase the activity of Ni based catalysts by alloying it with Fe for the hydrogenation of CO to methane, an important reaction that is used in several industrial processes.[46a]

Recently, mixed-metal nitride clusters of Fe-Ni were obtained using the nitrido anion $[Fe_4(CO)_{12}(N)]^-$.[47] Iron carbide carbonyl cluster complexes, especially $Fe_5(CO)_{15}(\mu_5\text{-}C)$, **2.1**, have always been of considerable interest to metal cluster

researchers,[48] and in a previous study we reported that **2.1** reacts with $NiCp_2$ via metal-metal exchange and metal cluster rearrangement processes, to yield the bimetallic Ni-Fe carbide containing cluster complex, $NiFe_4(Cp)_2(CO)_{10}(\mu_5\text{-}C)$, **2.2**, see Scheme 2.1.[49]

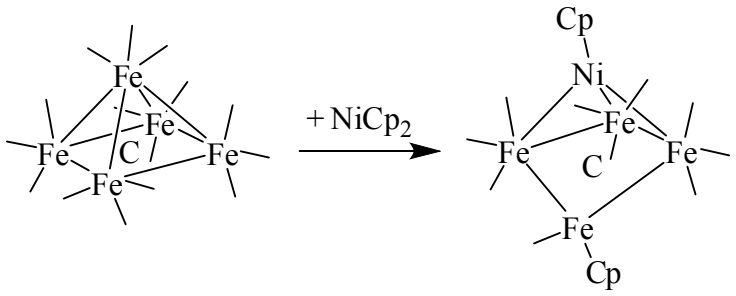

2.1 **2.2**

Scheme 2.1

In this chapter, we have reported the reaction of **2.1** with bis(1,5-cyclooctadiene)nickel(0), $Ni(COD)_2$, in acetonitrile solvent to afford the nickel-iron complex $Fe_5Ni(NCMe)(CO)_{15}(\mu_6\text{-}C)$, **2.3**. In addition, some chemistry with **2.3** was also studied which gave new Fe-Ni carbide clusters with varying Fe-Ni ratios.

2.2. Results and discussion

The reaction of $Fe_5(CO)_{15}(\mu_5\text{-}C)$, **2.1**, with $Ni(COD)_2$ in acetonitrile solvent at room temperature afforded the new bimetallic Fe-Ni cluster complex $Fe_5Ni(NCMe)(CO)_{15}(\mu_6\text{-}C)$, **2.3**, in 54 % yield. Compound **2.3** was characterized by a combination of IR, ^1H NMR, mass spectrometry, and single crystal X-ray diffraction analyses. An ORTEP showing the molecular structure of **2.3** is shown in Figure 2.1. Selected bond distances and angles are listed in Table A.3.

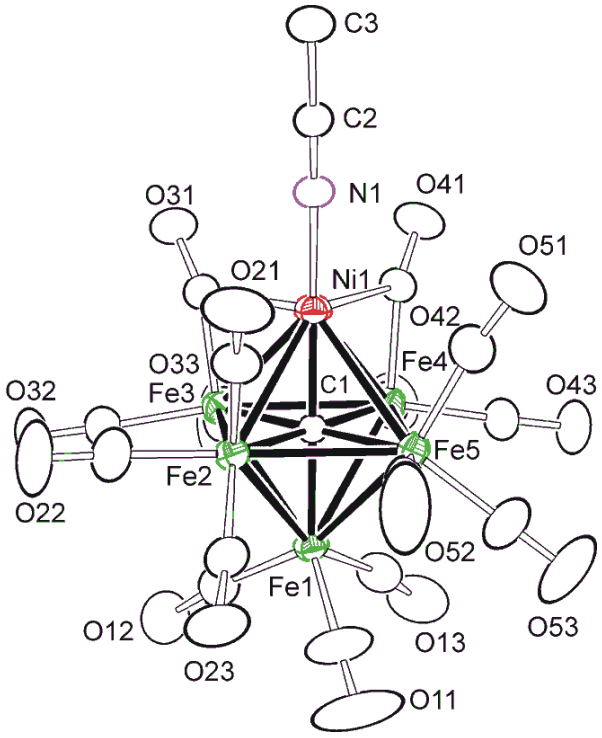

Figure 2.1. An ORTEP diagram of the molecular structure of $Fe_5Ni(NCMe)(CO)_{15}(\mu_6\text{-}C)$, **2.3**, showing 40% thermal ellipsoid probability.

Compound **2.3** consist of an octahedral cluster of five iron atoms and one nickel atom with the carbide ligand encapsulated in the center of the Fe_5Ni octahedron. The Ni-Carbide distance of 1.831(3) Å, is not significantly different from the Fe-Carbide distances, range 1.888(3)-1.916(3) Å. Also the Fe-Carbide distances are similar to the Fe-Carbide distances in **2.1**, range 1.87(3) – 1.96(3) Å, and in the hexanuclear iron carbide anionic cluster complex $[PPN]_2[Fe_6(CO)_{15}(SO_2)(\mu_6\text{-}C)]$,[52] range 1.870(10) – 1.915(7) Å. There is a terminal acetonitrile ligand from the reaction solvent that is coordinated to the Ni atom. There are two bridging CO ligands and these bridge the Ni(1) – Fe(3) bond (2.5653(7) Å), and the Ni(1) – Fe(4) bond (2.5424(7) Å) and these two metal-metal bonds are shorter than all the other metal-metal bonds in the octahedral framework, range 2.6671(7) - 2.7214(7) Å. Compound **2.3** contains 86 cluster valance electrons which is in

accord to conventional electron counting theories if all six transition metal atoms formally have an 18-electron configuration.[53]

When solutions of **2.3** were exposed to carbon monoxide gas, compound **2.3** reacts with CO at 110 °C to furnish the binary carbonyl cluster complex $Fe_5Ni(CO)_{16}(\mu_6\text{-}C)$, **2.4**, in 61 % yield. Compound **2.4** was prepared a number of years ago by Muetterties,[48b] and its structure was formulated accurately based on IR, mass spectrometry and elemental analyses. We have now obtained a crystal structure for compound **2.4** which is shown in Figure 2.2. Selected bond distances and angles are listed in Table A.4. As can be seen in Figure 2.2 the structure is very similar to compound **2.3** where the acetonitrile ligand on the Ni atom has been replaced by a carbonyl group.

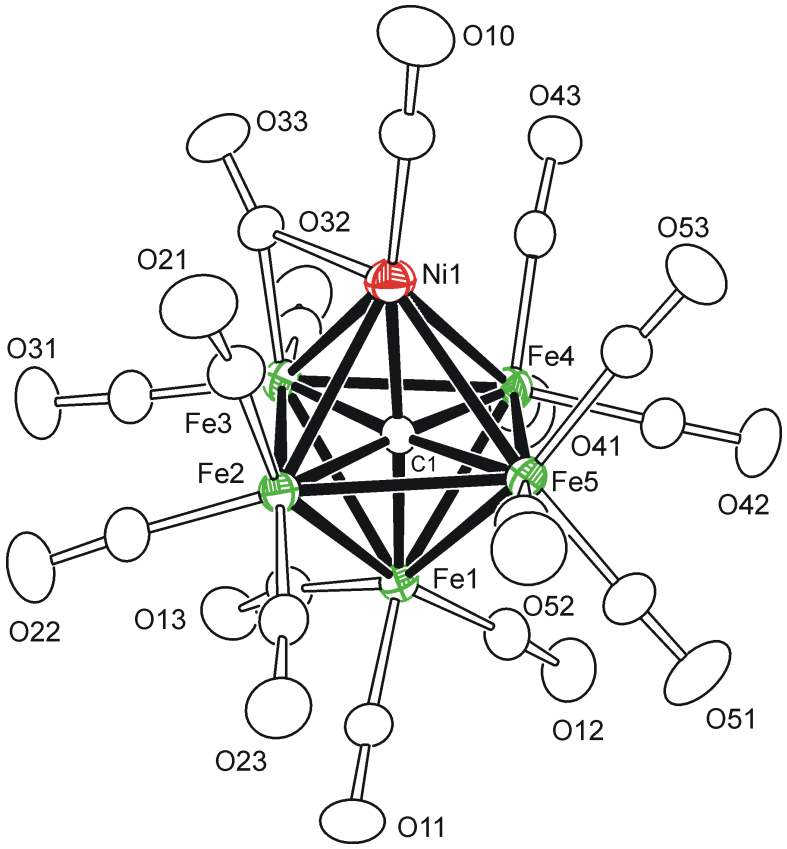

Figure 2.2. An ORTEP diagram of the molecular structure of $Fe_5Ni(CO)_{16}(\mu_6\text{-}C)$, **2.4**, showing 40% thermal ellipsoid probability.

Compound **2.4** is isostructural to the known platinum-ruthenium mixed-metal cluster complex $PtRu_5(CO)_{16}(\mu_6\text{-C})$, **2.5**,[54] that was prepared previously by Adams. Just like in compound **2.5**, one of the metal-metal bonds has a bridging carbonyl group, Ni(1) – Fe(3) = 2.5095(7) Å, which is considerably shorter than all the other metal-metal bonds in **2.4**. Compound **2.4** can be prepared by the reaction of the dianion $[NEt_4]_2[Fe_5(CO)_{14}(\mu_5\text{-C})]$ with $Ni(COD)_2$ to yield $[Fe_5Ni(CO)_{14}(COD)(\mu_5\text{-C})]^{2-}$. Substitution of the COD group with CO followed by oxidation with Fe^{3+} then gives the desired compound **2.4**.[48b] The yield of this reaction is not reported and in our hands we were able to obtain a maximum yield of 15 % following this previously reported procedure. Our preparation is a more convenient and perhaps "better" yielding procedure for the synthesis of compound **2.4**.

Both compounds **2.3** and **2.4** react with ammonia gas at 0 °C, to give the compound $Fe_5Ni(NH_3)(CO)_{15}(\mu_6\text{-C})$, **2.6**, in 82 % and 77 % yields respectively. The solid state structure of **2.6** is shown in Figure 2.3 and selected bond distances and angles are listed in Table A.3. The structure of compound 2.6 is similar to both compounds 2.3 and 2.4 however there now is an ammonia ligand on the Ni atom.

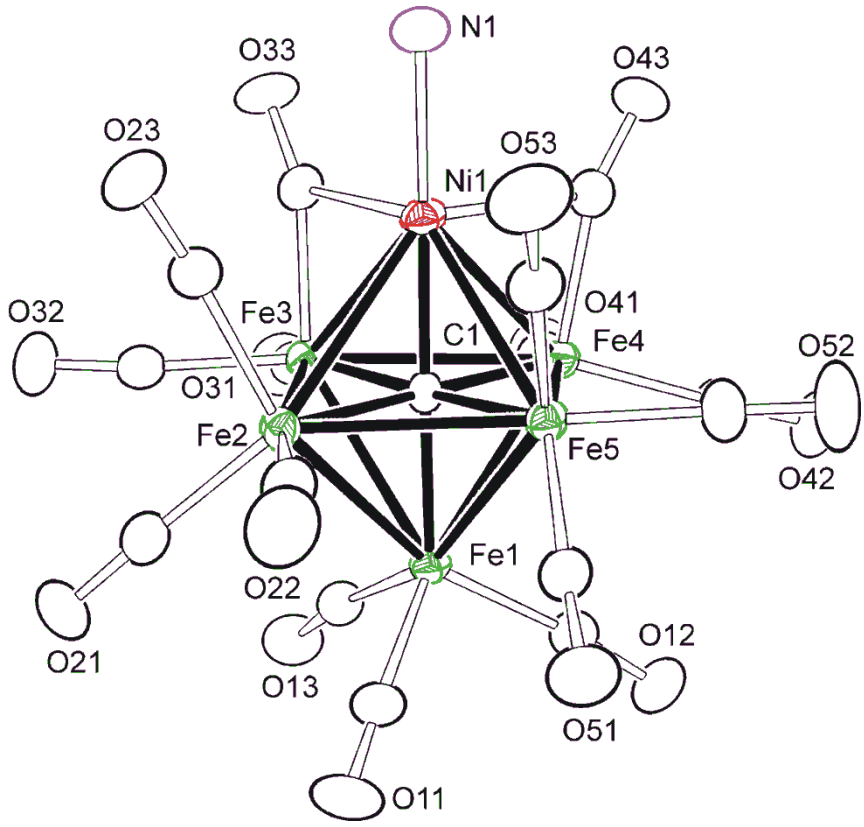

Figure 2.3. An ORTEP diagram of the molecular structure of $Fe_5Ni(NH_3)(CO)_{15}(\mu_6\text{-}C)$, **2.6**, showing 40% thermal ellipsoid probability.

It is interesting to note here that the replacement of the acetonitrile ligand in **2.3** by an ammonia group and replacement of a carbonyl ligand by an ammonia group is very facile. This is surprising since both CO and NCMe are betting coordinating ligands than ammonia as both CO and NCMe are good sigma donors as well as good pi- acceptor ligands, whereas an NH_3 ligand is only capable of sigma donation.[55,56]

Thermolysis of compound **2.3** up to temperatures of 110 °C in solvents other than acetonitrile (benzene and toluene solvent at reflux) decomposed compound **2.3** to give insoluble, probably metallic particles. However, when compound **2.3** was refluxed in acetonitrile solvent the new Fe_4Ni carbido cluster complex $Fe_4Ni(NCMe)_2(CO)_{12}(\mu_5\text{-}C)$,

2.7, was obtained in 68 % yield. An ORTEP showing the molecular structure of **2.7** is shown in Figure 2.4 and selected bond distances and angles are listed in Table A.5.

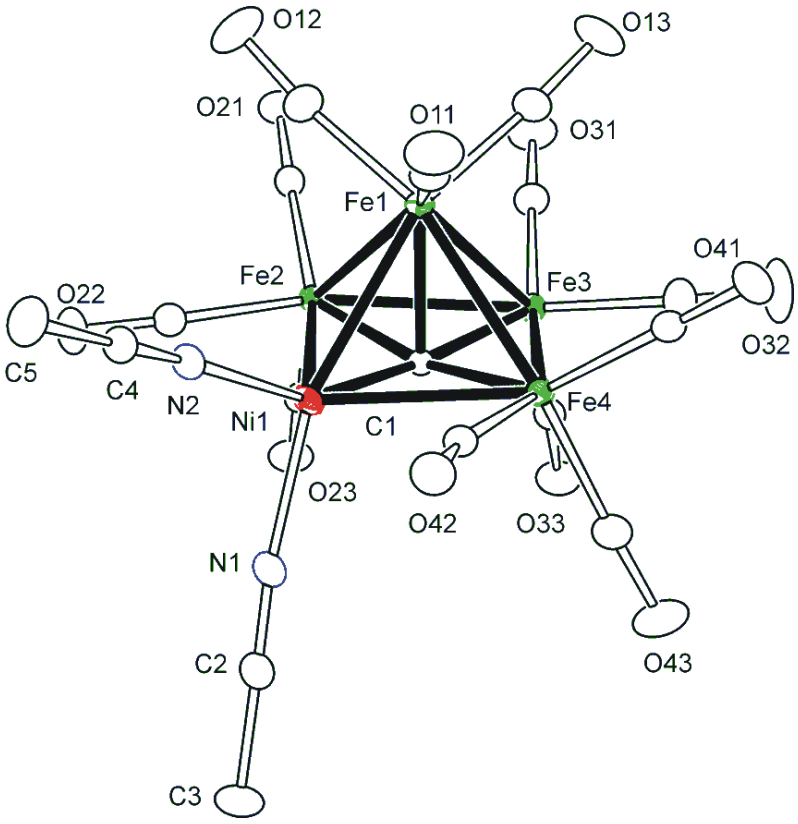

Figure 2.4. An ORTEP diagram of the molecular structure of $Fe_4Ni(NCMe)_2(CO)_{12}(\mu_5$-C), **2.7**, showing 50% thermal ellipsoid probability.

This complex consists of a square pyramidal cluster of four iron atoms and one nickel atom with a peripheral or exposed carbide ligand in the center of the base of the square pyramid. The nickel atom in **2.7** is not in the apical position but occupies one of the basal positions of the square pyramid. The two acetonitrile ligands are terminally coordinated to the nickel atom. The ^{1}H NMR spectrum for **2.7** should show two resonances for the methyl groups on each of the NCMe ligands, as the two NCMe ligands are inequivalent. Atom N(1) on one the NCMe groups has approximate trans coordination to the Ni(1)-

Fe(1) bond, N(1)-Ni(1)-Fe(1) = 159.67(3)°, whereas atom N(2) on the other NCMe group is coordinated approximately cis to the same bond, N(2)-Ni(1)-Fe(1) = 103.73(3)°. However, ^{1}H NMR at room temperature showed a single resonance indicating that the two NCMe groups are rapidly exchanging on the NMR timescale, via most probably a mechanism involving a polytopal rearrangement process on the nickel atom. It is well known that CO, CNR, NCR and phosphine ligands undergo rapid exchange process.[57]

Photolysis of compound **2.3** at room temperature in benzene solvent, however, afforded another Fe_4Ni carbido cluster complex $Fe_4Ni(NCMe)(CO)_{13}(\mu_5\text{-}C)$, **2.8**, in 63 % yield. The molecular structure of **2.8** is shown in Figure 2.5 and selected bond distances and angles are listed in Table A.5. The structure of **2.8** is very similar to that of **2.7**, where in place of one of the NCMe ligands on the nickel atom in **2.7**, there is a terminal carbonyl ligand. All the bond lengths in **2.8** are very similar to those found in **2.7**, see Table A.5. When compound **2.8** is dissolved in acetonitrile solvent at room temperature, substitution of a CO ligand with acetonitrile occurs to give compound **2.7** in 97 % yield.

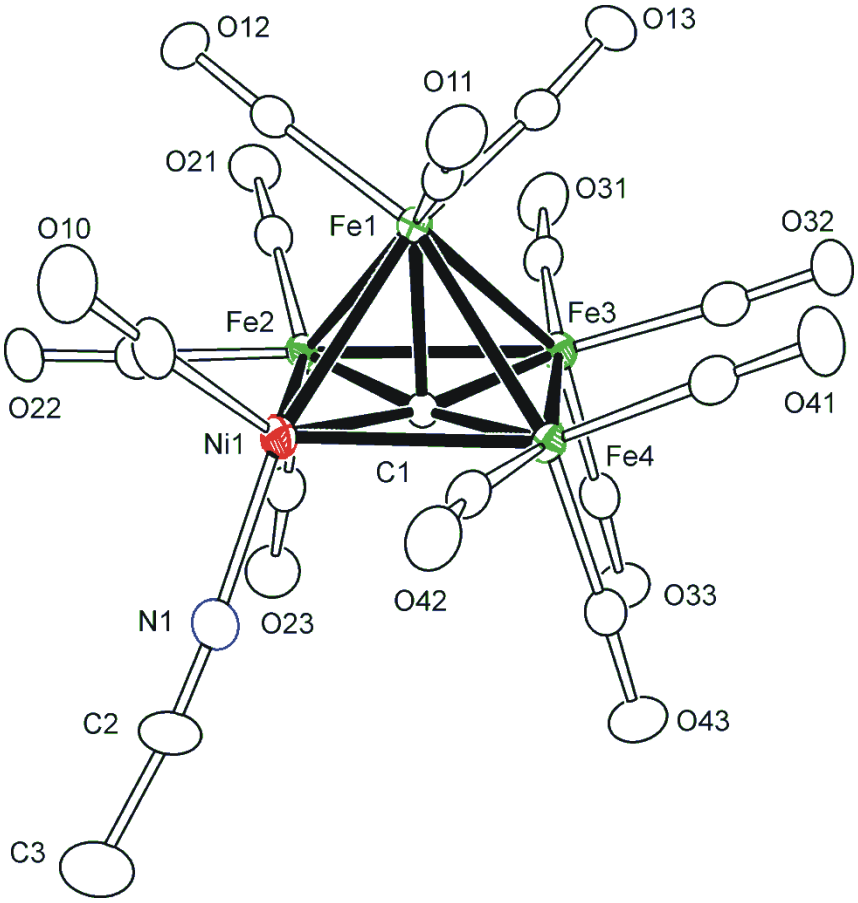

Figure 2.5. An ORTEP diagram of the molecular structure of $Fe_4Ni(NCMe)(CO)_{13}(\mu_5\text{-}C)$, **2.8**, showing 50% thermal ellipsoid probability.

Interestingly when CO was added at room temperature to **2.7** to obtain **2.8**, the new compound $Fe_4Ni_2(CO)_{15}(\mu_6\text{-}C)$**, 2.9** was obtained. Compound **2.7** when dissolved in solvents other than acteonitrile, such as methylene chloride, slowly "decomposes" to **2.8** in 68 % yield. Compound **2.9** as shown in Figure 2.6 (selected bond distances and angles are listed in Table A.6) contains an octahedral cluster comprised of four iron atoms and two nickel atoms. The two nickel atoms are bonded to each other, with one nickel atom occupying an apical position and the other, one of the positions on the square plane of the octahedron.

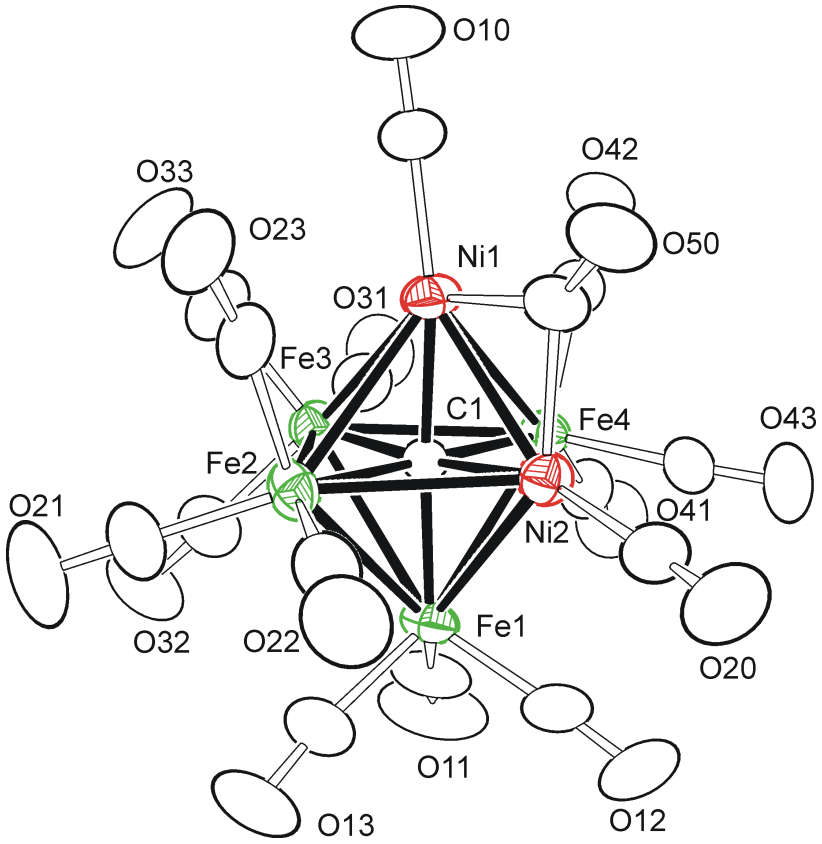

Figure 2.6. An ORTEP diagram of the molecular structure of $Fe_4Ni_2(CO)_{15}(\mu_6\text{-}C)$, **2.9**, showing 40% thermal ellipsoid probability.

Just as in compounds **2.3**, **2.4** and **2.6**, there is a carbon ligand that is encapsulated in the center of the Fe_4Ni_2 octahedron, Metal-Carbide distances range 1.861(5) - 1.908(5) Å. The Ni(1)-Ni(2) bond distance of 2.4642(11) Å is significantly shorter than that found in the nitrido dianionic cluster complex, $[HNi_2Fe_4(CO)_{13}(\mu_6\text{-}C)]^{2-}$, **2.10**, (2.724(1) Å),[47] and can be attributed to the carbonyl ligand that bridges the Ni(1)-Ni(2) edge of the octahedron. The other metal-metal bond distances are similar to those found in **2.10**. With 15 CO ligands the cluster valence count is 86 which is consistent for a *closo* octahedron structure as seen in the solid state for **2.10**.[53]

Bimetallic Fe-Ni cluster complexes from the reaction of **2.1** with $Ni(COD)_2$ were only obtained when the solvent acetonitrile was used. In the other common solvents and/or at elevated temperatures, the reaction of **2.1** with $Ni(COD)_2$ does proceed, however, mainly with decomposition of the starting materials and we were unable to isolate and characterize any Ni-Fe bimetallic complexes. As possible control experiments, there was no reaction of $Ni(COD)_2$ with acetonitrile. In fact $Ni(COD)_2$ is not soluble in acetonitrile solvent at room temperature. When **2.1** was dissolved in acetonitrile solvent at room temperature, compound **2.1** slowly degraded to the trinuclear cluster $Fe_3(CO)_{12}$. However, when both **2.1** and $Ni(COD)_2$ were dissolved in acetonitrile solvent at room temperature as mentioned above, complex **2.3** formed in 54% yield. It is known and has been shown that the Ru analog of **2.1**, $Ru_5(CO)_{15}(\mu_5\text{-C})$ **2.11**, in acetonitrile solvent forms the open metal framework structure, $Ru_5(CO)_{15}(\mu_5\text{-C})(NCMe)$ **2.12**,[58] as shown in Scheme 2.2 via bond homolysis of the square pyramidal geometry of **2.11** that can provide vacant coordination sites without cluster fragmentation. However, we were not able to detect the presence of such a species when **2.1** was dissolved in acetonitrile but believe that such a process followed by migration of the acetonitrile ligand to nickel perhaps facilitates the facile formation of **2.3**.

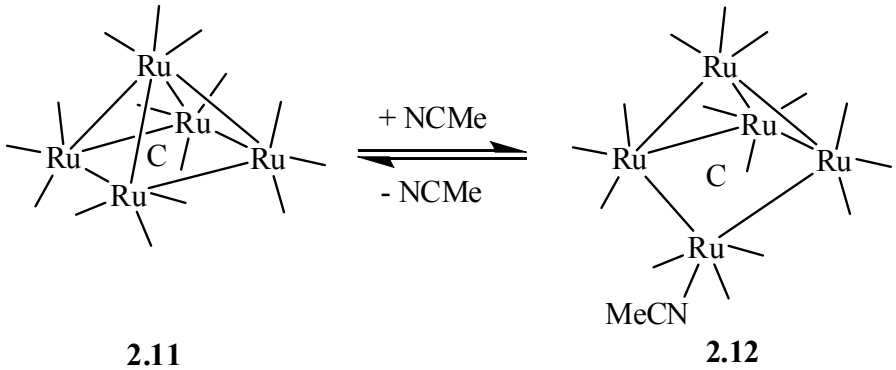

2.11 **2.12**

Scheme 2.2

2.3. Conclusions

A summary of the products that were obtained in this study is shown in Scheme 2.3. The pentairon carbide carbonyl cluster **2.1** reacts with $Ni(COD)_2$ in acetonitrile solvent at room temperature to yield the $NiFe_5$ octahedral cluster, **2.3**, which has an acetonitrile ligand from the reaction solvent on the nickel atom. The acetonitrile ligand in **2.3** can be displaced by CO to yield the binary carbonyl cluster complex **2.4**. Ammonia gas can also replace the acetonitrile ligand in **2.3** to yield complex **2.6**. Appropriately compound **2.4** can be converted to **2.6** by reacting with ammonia gas. Compound **2.3** when dissolved in acetonitrile solvent and heated to reflux results in removal of a vertex occupied by an iron atom in **2.3** along with substitution of a CO ligand with acetonitrile to give a *nido* octahedral (square pyramidal) cluster **2.7**. Compound **2.7** is stable in the solid state and in acetonitrile solvent, but loses one of its acetonitrile ligands in methylene chloride solvent to yield complex **2.8**. Compound **2.8** can be converted to **2.7** by dissolving **2.8** in acetonitrile solvent. Compound **2.7** reacts with CO to form the Fe_4Ni_2 octahedral cluster **2.9** via first forming compound **2.8**. Studies of some of these compounds to serve as molecular precursors to new nickel-iron nanoparticle catalysts for applications in heterogeneous catalysis[43] are in progress.

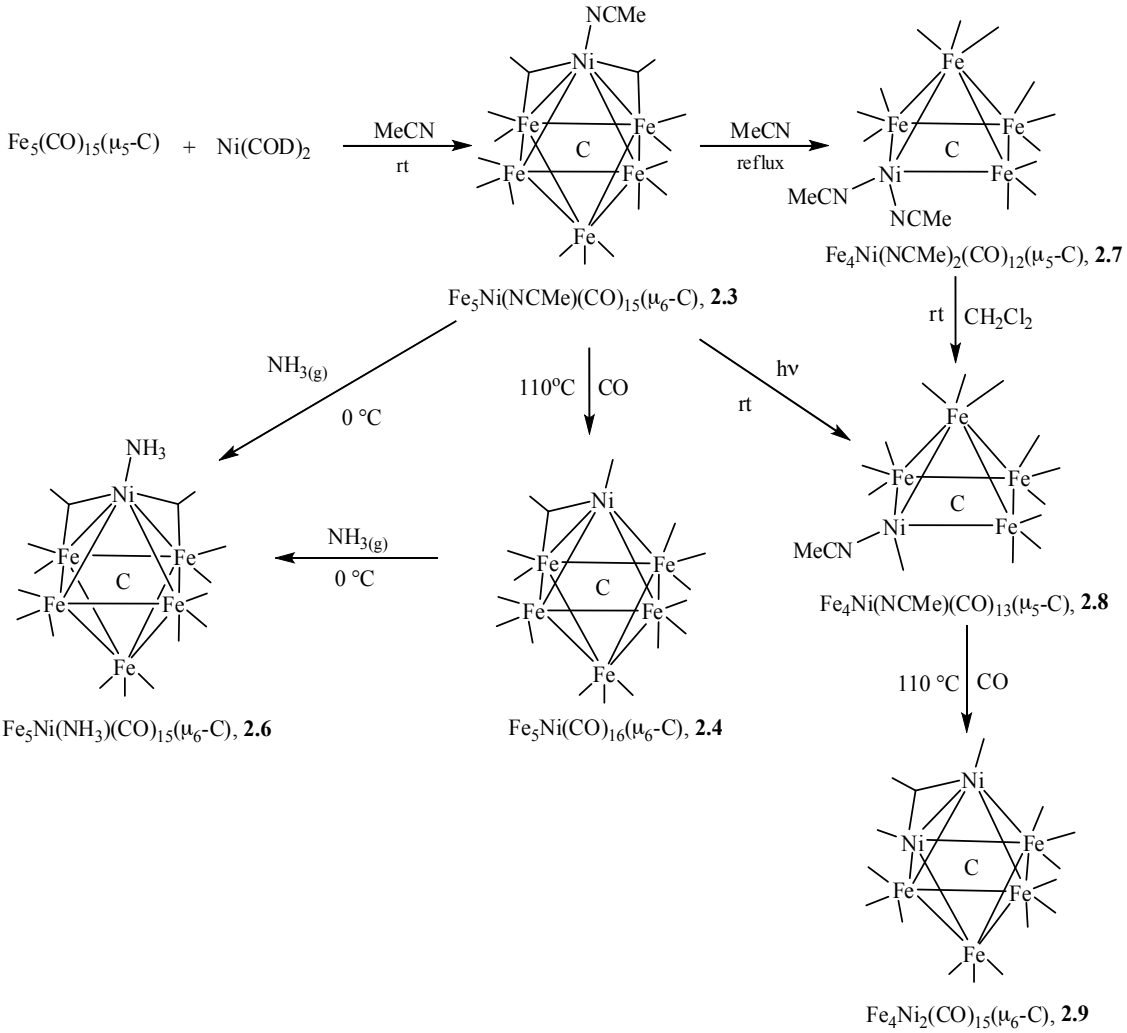

Scheme 2.3

2.4. Experimental section

General data

Unless indicated otherwise, all reactions were performed under an atmosphere of Argon. Reagent grade solvents were dried by the standard procedures and were freshly distilled prior to use. Infrared spectra were recorded on a Nicolet 380 FT-IR spectrophotometer. ^{1}H NMR were recorded on a Bruker 400 spectrometer operating at 399.993 MHz. Elemental analyses were performed by Columbia Analytical Services (Tucson, AZ). Mass spectrometric measurements performed by direct–exposure probe

using electron impact ionization (EI) were made on a VG 70S instrument and electrospray mass spectrometric measurements were obtained on a MicroMass Q-Tof spectrometer at the University of South Carolina, Columbia, SC. Bis(1,5-cyclooctadiene)nickel(0), $Ni(COD)_2$, was purchased from Strem Chemicals, used without further purification, and stored and handled in a drybox. NH_3 was purchase form Matheson Tri-Gas as pure ammonia gas. $Fe_5(CO)_{15}(\mu_5\text{-C})$, **2.1**, was prepared according to the previously published procedure.[48b] Product separations were performed by TLC in air on Analtech silica gel GF 250 or 500 μm glass plates. Silica gel (60-200μm, 70-230 mesh) used for chromatographic separations was purchased from Silicycle. Florisil (F100-500, 60-100 mesh) used for product purifications was purchased from Fisher Scientific.

Preparation of $Fe_5Ni(NCMe)(CO)_{15}(\mu_6\text{-C})$, 2.3

A 100 mg (0.14 mmol) amount of **2.1** and 58 mg (0.21 mmol) amount of $Ni(COD)_2$ were dissolved in 20 mL of acetonitrile in a 50 mL 3-neck round-bottom flask. The solution was stirred at room temperature for 10 min. at which time IR showed complete consumption of the starting material, **2.1**. The solvent was removed *in vacuo* and the residue was washed with hexane several times to remove any green side product of $Fe_3(CO)_{12}$. The purple colored residue was dissolved in methylene chloride and filtered through florisil to give 61.8 mg of **2.3** (54% yield). Spectral data for **2.3**: IR ν_{CO} (cm^{-1} in hexane): 2078(w), 2064 (w), 2032 (s), 2007 (v); ^1H NMR ($CDCl_3$ in ppm): δ = 2.59 (s, 3 H, CH_3). EI/MS: *m/z* 769 (M^+), 657(M^+- 4CO), 601 (M^+- 2CO), 545 (M^+- 2CO), 461 (M^+- 3CO). The isotope distribution pattern is consistent with the presence of one nickel atom and five iron atoms.

Preparation of $Fe_5Ni(CO)_{16}(\mu_6\text{-}C)$, 2.4

A 100 mg (0.12 mmol) amount of **2.3** was dissolved in 20 mL of toluene in a 50 mL 3-neck round-bottom flask equipped with a reflux condenser. Carbon monoxide gas (1 atm) was bubbled through the solution and the solution was refluxed at 110 °C with stirring for 1 h. The solvent was removed *in vacuo* and the product was separated on a silica gel column to yield a purple band of **2.4** (60 mg, 61% yield) eluted by pure hexane. The compound was identified by IR in the ν_{CO} region.[6b] Spectral data for **2.4**: IR ν_{CO} (cm^{-1} in hexane): 2100(w), 2064 (m), 2042 (s), 2039 (s), 2015 (m), 1883(vw, br).

Preparation of $Fe_5Ni(NH_3)(CO)_{15}(\mu_6\text{-}C)$, 2.6 from $Fe_5Ni(NCMe)(CO)_{15}(\mu_6\text{-}C)$, 2.3

A 10.3 mg (0.013 mmol) amount of **2.3** was dissolved in 8 mL of methylene chloride in a 50 mL 3-neck round-bottom flask. Ammonia gas (1 atm) was bubbled through the solution and the solution was stirred at 0 °C (maintained in an ice bath) for about15 min. at which time TLC showed complete consumption of the starting material. The solvent was removed *in vacuo* and the product was re-dissolved in methylene chloride and filtered through florisil to give 8.1 mg of **2.6** (82% yield). Spectral data for **2.6**: IR ν_{CO} (cm^{-1} in hexane): 2074(w), 2050 (w), 2033 (s), 2023 (m, sh), 2006 (w); ^1H NMR ($CDCl_3$ in ppm): δ = 3.30 (s, 3 H, NH_3). EI/MS: *m/z* 786 (M^+), 730(M^+- 2CO), 674 (M^+- 2CO), 646 (M^+- CO), 618 (M^+- CO), 590(M^+- CO), 562 (M^+- CO). The isotope distribution pattern is consistent with the presence of one nickel atom and five iron atoms. Elemental Anal. Calc.: C, 24.41; H, 0.38; N, 1.77 % Found: C, 24.36; H, 0.64; N, 1.72 %.

Preparation of $Fe_5Ni(NH_3)(CO)_{15}(\mu_6\text{-}C)$, 2.6 from $Fe_5Ni(CO)_{16}(\mu_6\text{-}C)$, 2.4

A 15 mg (0.018 mmol) amount of **2.4** was dissolved in 20 mL of methylene chloride in a 50 mL 3-neck round-bottom flask. Then ammonia gas (1 atm) was bubbled through the solution and the solution was stirred at 0 °C (maintained in an ice bath) for 10 min. at which time IR showed complete consumption of the starting material. The solvent was removed *in vacuo* and the product was re-dissolved in methylene chloride and filtered through florisil to give 11.4 mg of 6 (77% yield).

Note: In both cases the reactions do proceed at room temperature, however owing to some decomposition the yields at 0 °C are better.

Preparation of $Fe_4Ni(NCMe)_2(CO)_{12}(\mu_5\text{-}C)$, 2.7

A 21 mg (0.026 mmol) amount of **2.3** was dissolved in 15 mL of acetonitrile in a 50 mL 3-neck round-bottom flask equipped with a reflux condenser. The solution was then heated to reflux with stirring for 10 min. at which time IR showed complete consumption of the starting material. The solvent was removed *in vacuo* and the product was dissolved in acetonitrile and filtered through silica gel to give 12.6 mg of **2.7** (68% yield). Spectral data for **2.7**: IR ν_{CO} (cm^{-1} in methylene chloride): 2087(w), 2066 (w), 2054 (m), 2030 (s), 2016 (vs), 1941 (w,br); ^1H NMR ($CDCl_3$ in ppm): δ = 2.45 (s, 6H, CH_3). Elemental Anal. Calc.: C, 28.66; H, 0.85; N, 3.93 % Found: C, 28.51; H, 0.88; N, 3.93 %.

Note: Compound **2.7** slowly decomposes when dissolved in solvents other than acetonitrile.

Photolysis of $Fe_5Ni(NCMe)(CO)_{15}(\mu_6\text{-}C)$, 2.3 to $Fe_4Ni(NCMe)(CO)_{13}(\mu_5\text{-}C)$, 2.8

A 15 mg (0.018 mmol) amount of **2.3** was dissolved in 10 mL of benzene in a 50 mL 3-neck round-bottom flask equipped with a reflux condenser. The solution was irradiated using a high-pressure mercury UV lamp (American Ultraviolet Co.) at the 125 wpi (watts per inch) setting for 25 min. at which time IR showed complete consumption of the starting material. The solvent was removed *in vacuo* and the product was dissolved in methylene chloride and filtered through silica gel to give 8.2 mg of **2.8** (63% yield). Spectral data for **2.8**: IR ν_{CO} (cm^{-1} in hexane): 2111(w), 2075 (w), 2065 (w), 2054 (m), 2043 (w), 2033 (s), 2017 (m), 2010 (m), 1942 (w); ^1H NMR ($CDCl_3$ in ppm): δ = 2.31 (s, 3H, CH_3). EI/MS: *m/z* 699 (M^+). The isotope distribution pattern is consistent with the presence of one nickel atom and four iron atoms.

Conversion of $Fe_4Ni(NCMe)_2(CO)_{12}(\mu_5\text{-}C)$, 2.7 to $Fe_4Ni(NCMe)(CO)_{13}(\mu_5\text{-}C)$, 2.8

An 31.9 mg (0.045 mmol) amount of **2.7** was dissolved in 10 mL of methylene chloride in a 50 mL 3-neck round-bottom flask. Then the solution was stirred at room temperature for 15 min. at which time IR showed complete consumption of the starting material. The solvent was removed *in vacuo* and the product was re-dissolved in methylene chloride and filtered through silica gel to give 21.5 mg of **2.8** (68% yield).

Conversion of $Fe_4Ni(NCMe)(CO)_{13}(\mu_5\text{-}C)$, 2.8 to $Fe_4Ni(NCMe)_2(CO)_{12}(\mu_5\text{-}C)$, 2.7

A 21.5 mg (0.031 mmol) amount of **2.8** was dissolved in 10 mL of acetonitrile in a 50 mL 3-neck round-bottom flask. Then the solution was stirred at room temperature for 15 min. at which time IR showed complete consumption of the starting material. The reaction solution was filtered through silica gel to give 21.2 mg of **2.7** (97% yield).

Preparation of $Fe_4Ni_2(CO)_{15}(\mu_6\text{-C})$, 2.9 from $Fe_4Ni(NCMe)_2(CO)_{12}(\mu_5\text{-C})$, 2.7

A 21.2 mg (0.029 mmol) amount of **2.7** was dissolved in 15 mL of toluene in a 50 mL 3-neck round-bottom flask equipped with a reflux condenser. Then carbon monoxide gas (1 atm) was bubbled through the solution and the solution was then heated to reflux with stirring for 30 min. at which time IR showed complete consumption of the starting material. The solvent was removed *in vacuo* and the product was dissolved in methylene chloride and filtered through silica gel to give 10.4 mg of **2.9** (45% yield). Spectral data for **2.9**: IR ν_{CO} (cm^{-1} in hexane): 2111(w), 2076 (m), 2065 (m), 2054 (w), 2043 (s), 2033 (m), 2028 (m), 2022 (m), 1963 (w). EI/MS: *m/z* 772 (M^+), 744(M^+- CO), 716 (M^+- CO). The isotope distribution pattern is consistent with the presence of two nickel atoms and four iron atoms.

Preparation of $Fe_4Ni_2(CO)_{15}(\mu_6\text{-C})$, 2.9 from $Fe_4Ni(NCMe)(CO)_{13}(\mu_5\text{-C})$, 2.8

A 21.5 mg (0.031 mmol) amount of **2.8** was dissolved in 15 mL of toluene in a 50 mL 3-neck round-bottom flask equipped with a reflux condenser. Then carbon monoxide gas (1 atm) was bubbled through the solution and the solution was then heated to reflux with stirring for 30 min. at which time IR showed complete consumption of the starting material. The solvent was removed *in vacuo* and the product was dissolved in methylene chloride and filtered through silica gel to give 10.4 mg of **2.9** (44% yield).

2.5. Crystallographic analyses

Single crystals of **2.3**, **2.4**, **2.6**, **2.8** and **2.9** suitable for diffraction analysis were all grown by slow evaporation of solvent from solutions in hexane/methylene chloride solvent mixture at -20 °C. Single crystals of **2.7** suitable for diffraction analysis were grown by slow evaporation of solvent from a solution of hexane/methylene

chloride/acetonitrile solvent mixture at – 20 °C. The data crystals for **2.3**, **2.4**, **2.6** and **2.9** were glued onto the end of a thin glass fiber. Data crystals for **2.7** and **2.8** were mounted onto the end of a thin glass fiber using Paratone-N. X-ray intensity data were measured by using a Bruker SMART APEX2 CCD-based diffractometer using Mo Kα radiation (λ = 0.71073 Å).[50] The raw data frames were integrated with the SAINT+ program by using a narrow-frame integration algorithm.[50] Corrections for Lorentz and polarization effects were also applied with SAINT+. An empirical absorption correction based on the multiple measurement of equivalent reflections was applied using the program SADABS. All structures were solved by a combination of direct methods and difference Fourier syntheses, and refined by full-matrix least-squares on F^2, by using the SHELXTL software package.[51] All non-hydrogen atoms were refined with anisotropic displacement parameters. Hydrogen atoms were placed in geometrically idealized positions and included as standard riding atoms during the least-squares refinements. Crystal data, data collection parameters, and results of the analyses are listed in Tables A.1 and A.2.

Compounds **2.3** and **2.6** crystallized in the orthorhombic crystal system. The systematic absences in the intensity data were consistent with either of the space groups *Pnma* or $Pna2_1$. The structure could only be solved in the latter space group. Compound **2.4** crystallized in the triclinic crystal system. The space group $P\ \bar{1}$ was assumed and confirmed by the successful solution and refinement of the structure. Compounds **2.7**, **2.8** and **2.9** crystallized in the monoclinic crystal system. For compounds **2.7** and **2.9** the systematic absences in the intensity data were consistent with the unique space group $P2_1/c$ and for compound **2.8** the systematic absences in the intensity data were consistent with the unique space group $P2_1/n$.

Chapter 3: Bimetallic octahedral ruthenium-nickel carbido cluster complexes. synthesis and structural characterization

3.1. Background

After synthesizing six new iron-nickel carbide cluster complexes with varying iron-nickel ratios, we wanted to synthesize similar carbide cluster complexes with ruthenium (replacing iron) and nickel. As ruthenium and iron are in the same group in the periodic table (Group 8), we thought we would be able to synthesize new ruthenium-nickel carbide cluster complexes with varying ruthenium -nickel ratios for the application in heterogeneous catalysis. Thus we investigate the reaction of $Ru_5(CO)_{15}(\mu_5\text{-}C)$ with $Ni(COD)_2$.

Bimetallic nanoparticle catalysts have been shown to exhibit superior catalytic properties,[44] due to the presence of different metals such that one metal performs a certain role in a catalytic cycle and the other performs another function.[45] Ruthenium based catalysts modified with Group 10 metals have been shown previously to be more active and selective in a number of industrially important hydrogenation processes.[59,60] Supported bimetallic Ru-Ni particles have been of interest in heterogeneous catalysis. For example, It has been shown that the bimetallic cluster $(C_5H_5)NiRu_3H_3(CO)_9$ acts as an effective heterogeneous catalyst for the hydrogenation, dehydrogenation and isomerization of linear and cyclic monoenes and dienes and aromatic hydrocarbons.[61] The hydrogenation of carbon monoxide was also studied over various titania-supported Ru-Ni bimetallic catalysts.[62] Recently bimetallic Ru-Ni catalysts are used for steam reforming of ethylene, a key component of biomass derived tars.[63] There is extensive literature on ruthenium complexes containing group 10 elements, however there are only few examples of ruthenium-nickel complexes.[64-66]

In a previous study we reported the reaction of $Fe_5(CO)_{15}(\mu_5\text{-C})$ with bis(1,5-cyclooctadiene)nickel(0), $Ni(COD)_2$, in acetonitrile solvent to afford the nickel-iron complex $Fe_5Ni(NCMe)(CO)_{15}(\mu_6\text{-C})$, **2.3**. Replacement of the acetonitrile ligand with CO gave the binary carbonyl cluster complex $Fe_5Ni(CO)_{16}(\mu_6\text{-C})$, **2.4** (Scheme 3.1). Additional chemistry with **2.3** was also studied which gave new Fe-Ni carbide clusters with varying Fe-Ni ratios.[67]

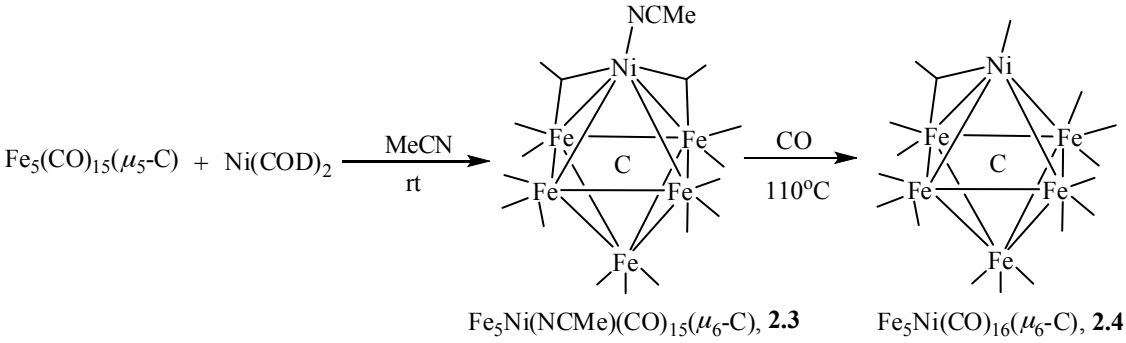

Scheme 3.1

In this chapter, we have reported the reaction of $Ru_5(CO)_{15}(\mu_5\text{-C})$ with $Ni(COD)_2$ in acetonitrile solvent to afford the nickel-ruthenium complex $Ru_5Ni(NCMe)(CO)_{15}(\mu_6\text{-C})$, **3.1**, and its subsequent reactions with CO and ammonia gas to yield the complexes $Ru_5Ni(CO)_{16}(\mu_6\text{-C})$, **3.2**, and $Ru_5Ni(NH_3)(CO)_{15}(\mu_6\text{-C})$, **3.3**, respectively. Furthermore, photolysis of **3.1** in benzene and toluene solvents furnished the arene coordinated bimetallic cluster complexes $Ru_5Ni(CO)_{13}(\eta^6\text{-}C_6H_6)(\mu_6\text{-C})$, **3.4**, and $Ru_5Ni(CO)_{13}(\eta^6\text{-}C_7H_8)(\mu_6\text{-C})$, **3.5**.

3.2. Results and discussion

The bimetallic cluster complex $Ru_5Ni(NCMe)(CO)_{15}(\mu_6\text{-C})$, **3.1**, was obtained in 37 % yield from the reaction of $Ru_5(CO)_{15}(\mu_5\text{-C})$, with $Ni(COD)_2$ in acetonitrile solvent under refluxing conditions. Compound **3.1** was characterized by a combination of IR, ^1H

NMR, mass spectrometry, and single crystal X-ray diffraction analyses. An ORTEP showing the molecular structure of **3.1** is shown in Figure 3.1. Selected bond distances and angles are listed in Table B.3.

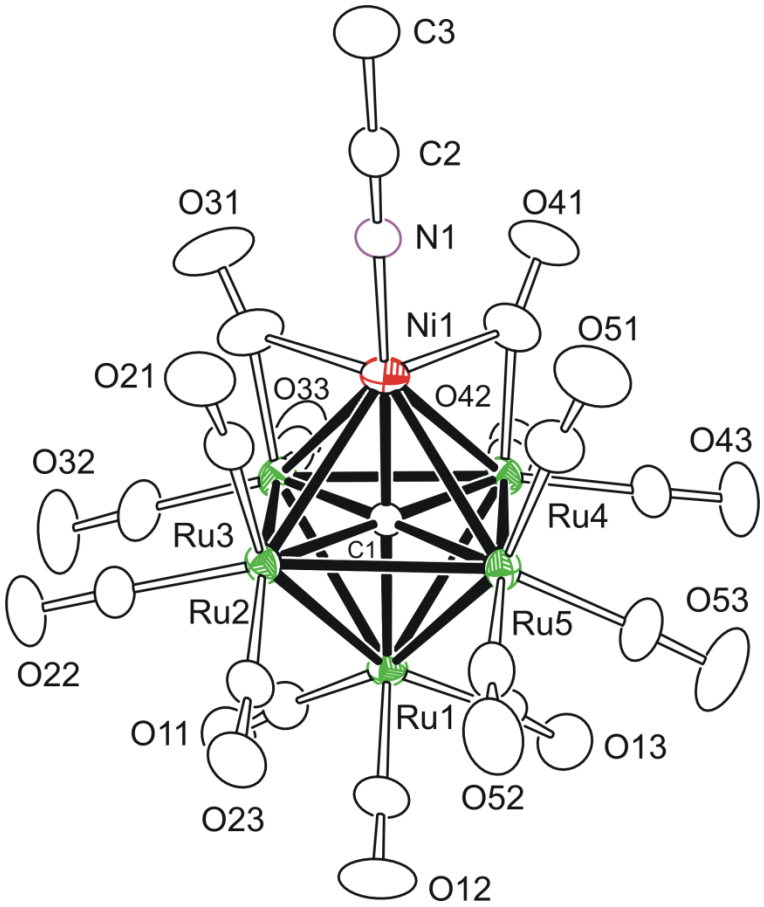

Figure 3.1. An ORTEP diagram of the molecular structure of $Ru_5Ni(NCMe)(CO)_{15}(\mu_6\text{-}C)$, **3.1**, showing 30% thermal ellipsoid probability.

Compound **3.1** is isostructural to the iron analog cluster **2.3**, consisting of an octahedron of one nickel atom and five ruthenium atoms. The carbide ligand is encapsulated in the center of the Ru_5Ni octahedron and the acetonitrile ligand from the reaction solvent is terminally coordinated to the nickel atom. The Ni-Carbide distance of 1.862(4) Å is not significantly different from the Ru-Carbide distances, range 2.033(4)-

2.059(4) Å. Also the Ru-Carbide distances are similar to the Ru-Carbide distances in $Ru_5(CO)_{15}(\mu_5\text{-C})$, range 2.01(2) – 2.10(2) Å. There are two bridging CO ligands and these bridge the Ni(1) – Ru(3) bond (2.6914(7) Å), and the Ni(1) – Ru(4) bond (2.6756(7) Å) and these two metal-metal bonds are shorter than all the other metal-metal bonds, range 2.8394(7) - 2.9210(5) Å. As expected compound **3.1** contains 86 cluster valence electrons which is in accord with the Polyhedral Skeletal Electron Pair theory.[53]

When carbon monoxide gas was purged through solutions of **3.1** at 110 °C, replacement of the acetonitrile ligand with CO gave the complex $Ru_5Ni(CO)_{16}(\mu_6\text{-C})$, **3.2**, in 97 % yield. Compound **3.2** was characterized crystallographically and its molecular structure is shown in Figure 3.2. Selected bond distances and angles are listed in Table B.4.

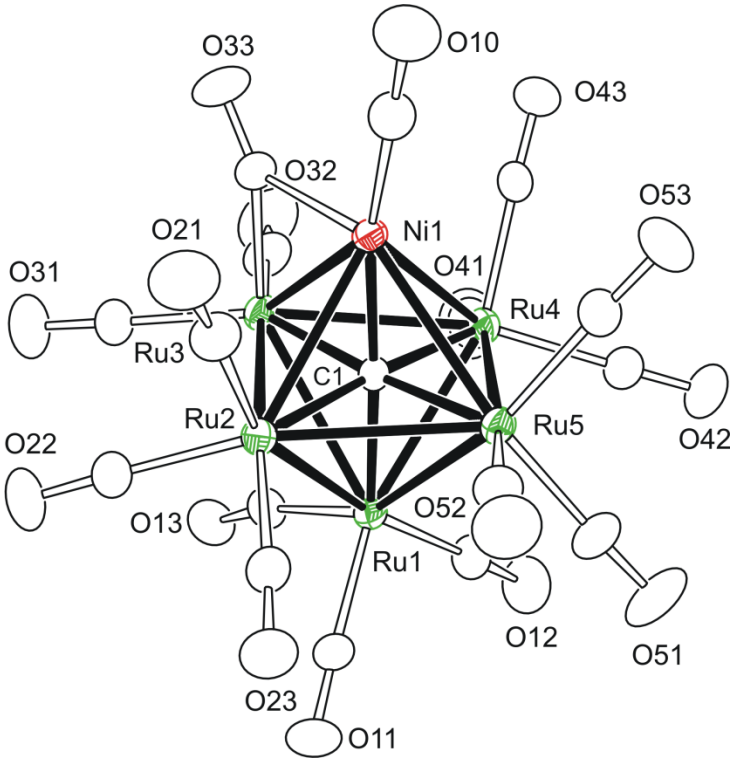

Figure 3.2. An ORTEP diagram of the molecular structure of $Ru_5Ni(CO)_{16}(\mu_6\text{-C})$, **3.2**, showing 30% thermal ellipsoid probability.

Compound **3.2** is isostructural to the known platinum-ruthenium mixed-metal cluster complex $PtRu_5(CO)_{16}(\mu_6\text{-}C)$, **3.6**,[54] that was reported previously, and is isostructural and isomorphous to the Fe_5Ni carbido cluster **2.4**. Also as in **3.6**, one of the metal-metal bonds has a bridging carbonyl group, Ni(1) – Ru(3) = 2.6624(6) Å, which is considerably shorter than all the other metal-metal bonds in **3.2**.

When solutions of **3.1** and **3.2** were exposed to ammonia gas at 0 °C, the complex $Ru_5Ni(NH_3)(CO)_{15}(\mu_6\text{-}C)$, **3.3**, was formed and isolated in 97 % and 50 % yields, respectively. As in the case with **2.3** and **2.4**, both reactions do proceed at room temperature, however owing to some decomposition the yields at 0 °C are better. The solid state structure of **3.3** is shown in Figure 3.3 and selected bond distances and angles are listed in Table B.3.

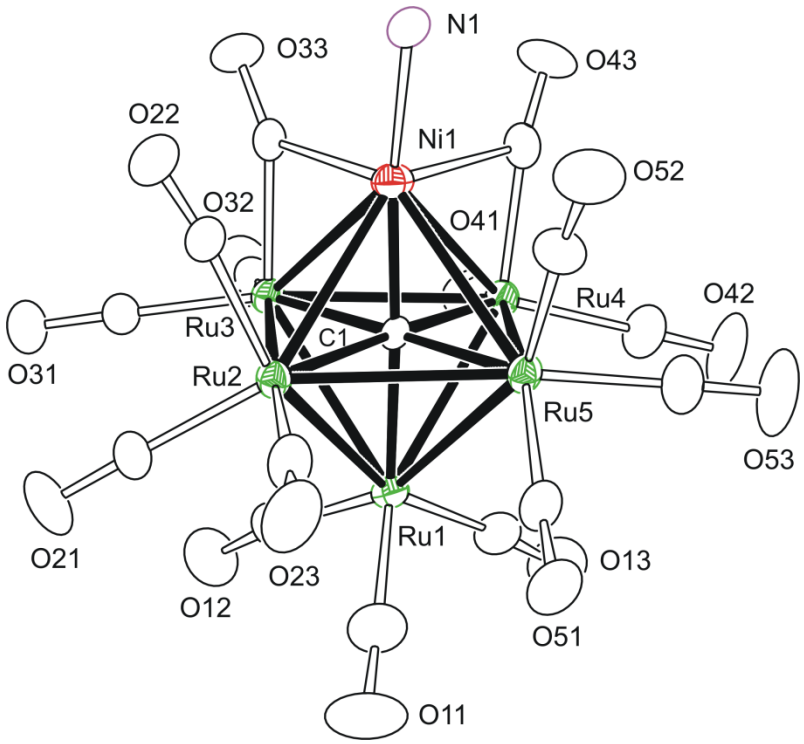

Figure 3.3. An ORTEP diagram of the molecular structure of $Ru_5Ni(NH_3)(CO)_{15}(\mu_6\text{-}C)$, **3.3**, showing 30% thermal ellipsoid probability.

The structure of compound **3.3** is similar to the iron-nickel cluster complex $Fe_5Ni(NH_3)(CO)_{15}(\mu_6\text{-C})$ previously reported by us. There are two bridging CO ligands and these bridge the Ni(1) – Ru(3) bond (2.6506(13) Å), and the Ni(1) – Ru(4) bond (2.7060(14) Å) and these two metal-metal bonds are shorter than all the other metal-metal bonds in the octahedral framework, range 2.852(1) - 2.919(1) Å.

The isolation and characterization of compounds **3.1-3.3** has proven to be relatively straightforward considering our investigations of the related iron-nickel cluster system. The choice of acetonitrile solvent in the reaction medium is essential to form the Ru_5Ni octahedral framework. It has been shown that $Ru_5(CO)_{15}(\mu_5\text{-C})$ will readily add small molecules such as acetonitrile to yield an open $Ru_5(\mu_5\text{-C})$ cluster, $Ru_5(CO)_{15}(NCMe)(\mu_5\text{-C})$, where one ruthenium atom bridges a butterfly arrangement of four other ruthenium atoms.[58] The opening of the $Ru_5(\mu_5\text{-C})$ cluster facilitates the reaction with $Ni(COD)_2$ by providing vacant coordination sites that are not accompanied by cluster degradation. Migration of the acetonitrile ligand to the nickel atom with subsequent loss of the labile COD groups in $Ni(COD)_2$ gives the parent complex **3.1**. The iron analog compound **2.3** undergoes cluster fragmentation when exposed to UV radiation and heat to form Fe_4Ni and Fe_4Ni_2 carbido clusters. In our efforts to see if indeed similar reactivity was observed with the ruthenium-nickel complex **3.1** we performed the respective experiments.

When an acetonitrile solution of **3.1** was heated to reflux, instead of the anticipated five metal as in $Fe_4Ni(\mu_5\text{-C})$ cluster, no reaction was observed. Only when irradiated did we see formation of products. Photolysis of **3.1** in benzene solvent resulted in the formation of the new complex $Ru5Ni(CO)_{13}(\eta^6\text{-}C_6H_6)(\mu_6\text{-C})$, **3.4**, in 33 % yield as

the major product. Compound **3.4** was characterized crystallographically and its molecular structure is shown in Figure 3.4.

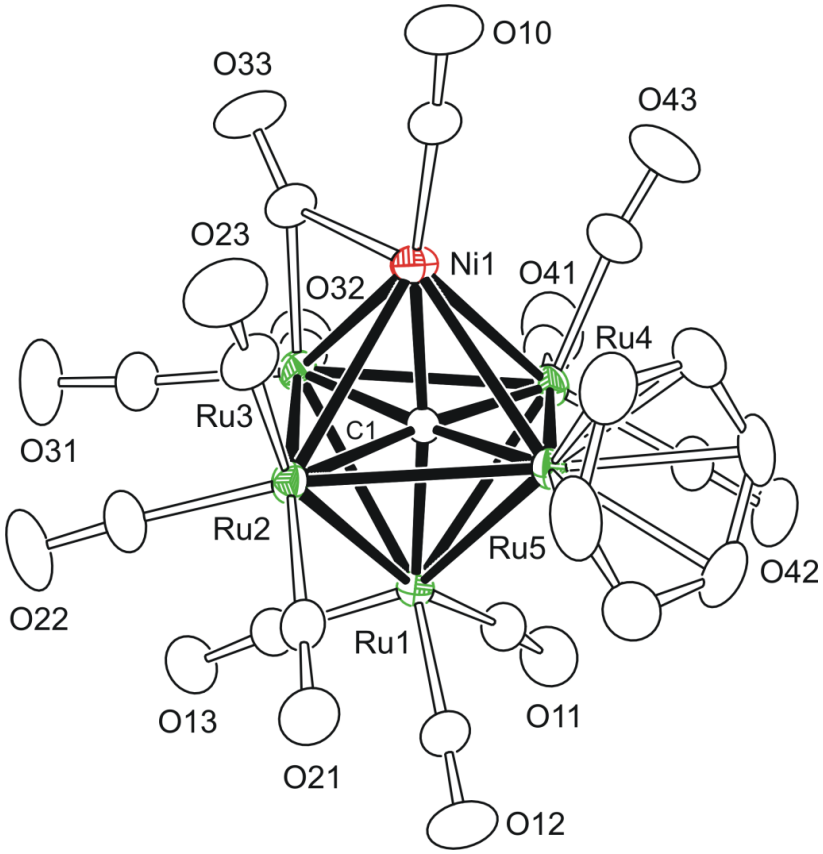

Figure 3.4. An ORTEP diagram of the molecular structure of $Ru_5Ni(CO)_{13}(\eta^6\text{-}C_6H_6)(\mu_6\text{-}C)$, **3.4**, showing 30% thermal ellipsoid probability.

As seen in Figure 3.4, compound **3.4** consists of a $Ru_5Ni(\mu_6\text{-}C)$ cluster where one of the ruthenium vertices is coordinated to a benzene molecule in an η^6- fashion. There are many examples of arene ligands coordinated to metal carbonyl cluster complexes,[69] the first being $Ru_6(CO)_{14}(\eta^6\text{-}C_6H_6)(\mu_6\text{-}C)$ that was reported some years ago. There have also been examples of metal carbonyl clusters to contain bis(arene) ligands and in some/one case where a metal cluster is "sandwiched" between two $\eta^6\text{-}C_6H_6$ ligands [69e,70]. However, there have not been many examples of mixed-metal clusters containing the η^6-

C_6H_6 ligand. The bimetallic complexes that do contain the arene ligand were prepared using an already coordinated benzene ligand in the starting reactant as seen in the complexes, $Ru_5(CO)_{12}(\eta^6\text{-}C_6H_6)(\mu_6\text{-}C)[PtPBu^t_3]$[69h,71]. In the photolysis reaction of **3.1**, the complexes $Ru_5Ni(CO)_{16}(\mu_6\text{-}C)$, $Ru_6(CO)_{17}(\mu_6\text{-}C)$, $Ru_5(CO)_{15}(\mu_5\text{-}C)$, $Ru_5(CO)_{12}(\eta^6\text{-}C_6H_6)(\mu_5\text{-}C)$ and $Ru_5Ni(NCMe)(CO)_{15}(\mu_6\text{-}C)$ were also obtained in minor/trace amounts.

Photolysis of a toluene solution of **3.1** furnished the complex $Ru_5Ni(CO)_{13}(\eta^6\text{-}C_7H_8)(\mu_6\text{-}C)$, **3.5** in 37 % yield, see Figure 3.5. Compound **3.5** is very similar in structure to **3.4** where in place of the benzene ligand there is now an $\eta^6\text{-}C_7H_8$ group coordinated to one of the ruthenium vertices (Table B.5). The $\eta^6\text{-}C_7H_8$ coordination mode has been observed previously in the homometallic carbide cluster $Ru_6(CO)_{14}(\eta^6\text{-}C_7H_8)(\mu_6\text{-}C)$.[69d,72]

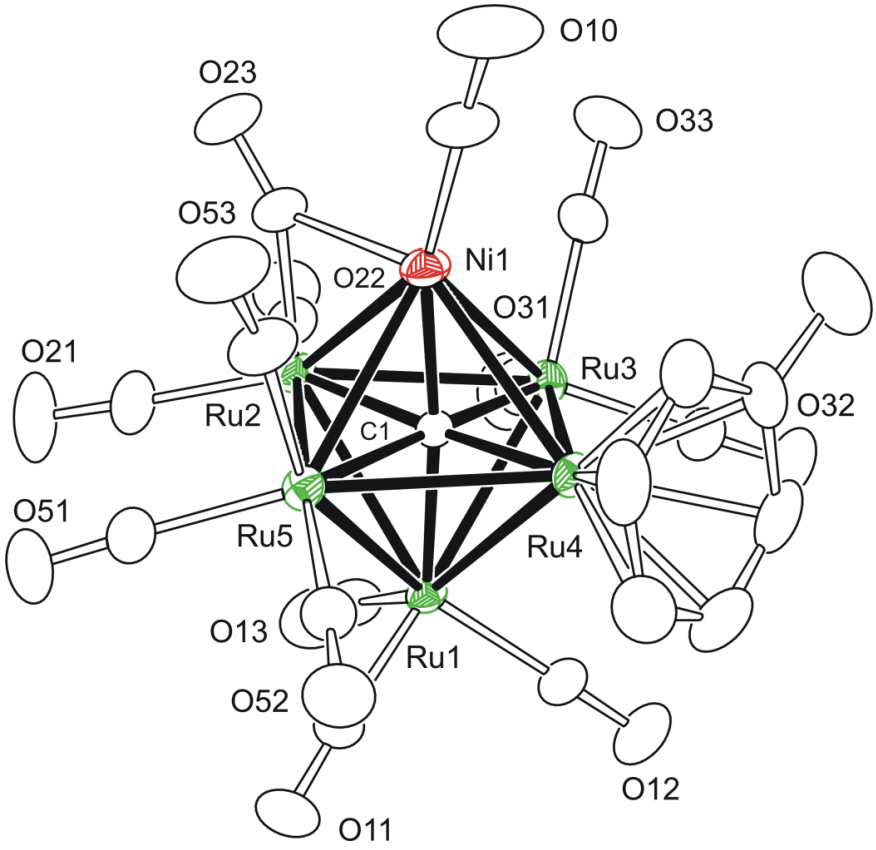

Figure 3.5. An ORTEP diagram of the molecular structure of $Ru_5Ni(CO)_{13}(\eta^6\text{-}C_7H_8)(\mu_6\text{-}C)$, **3.5**, showing 30% thermal ellipsoid probability.

The improved synthesis of the various arene coordinated ruthenium carbide clusters is accomplished using cyclohexadiene under thermal conditions or in the presence of trimethylamine *N*-oxide as a decarbonylating reagent to furnish the cyclohexadiene coordinated carbide cluster first, followed by loss of H_2 to yield the benzene coordinated cluster.[69e-f,70a] In our bimetallic system the arene coordinated complexes **3.4** and **3.5** are formed directly from benzene or toluene solvent in reasonable yields under photolytic conditions. Compounds **3.4** and **3.5** can also be obtained from the binary cluster **3.2** under similar conditions.

3.3. Conclusions

A series of Ru-Ni carbide cluster complexes have been prepared in reasonable yields and a summary of the products that were obtained is shown in Scheme 3.2. The pentaruthenium carbide carbonyl cluster $Ru_5(CO)_{15}(\mu_5\text{-C})$ reacts with $Ni(COD)_2$ in acetonitrile solvent at room temperature to yield the $NiRu_5$ octahedral cluster, **3.1**, which has an acetonitrile ligand from the reaction solvent on the nickel atom. The acetonitrile ligand in **3.1** can be displaced by CO to yield the binary carbonyl cluster complex **3.2**. Ammonia gas can also replace the acetonitrile ligand in **3.1** to yield complex **3.3**. Appropriately, compound **3.2** can be converted to **3.3** by reacting with ammonia gas. Photolysis of compound **3.1** in benzene and toluene solvent afforded η^6-coordinated benzene and toluene Ru_5Ni carbido cluster complexes **3.4** and **3.5**, respectively. Studies of some of these compounds to serve as molecular precursors to new nickel-ruthenium nanoparticle catalysts for applications in heterogeneous catalysis are underway.

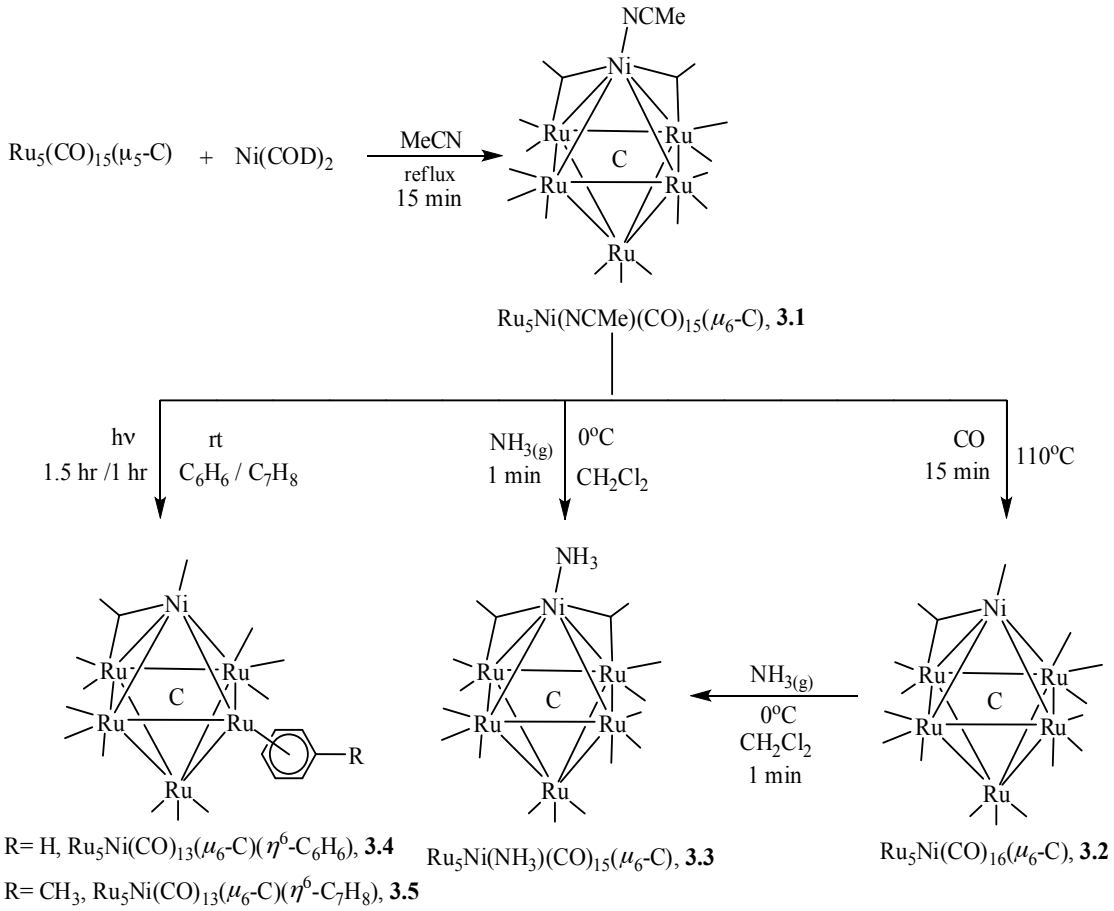

Scheme 3.2

3.4. Experimental section

General data

Unless indicated otherwise, all reactions were performed under an atmosphere of Argon. Reagent grade solvents were dried by the standard procedures and were freshly distilled prior to use. Infrared spectra were recorded on a Nicolet 380 FT-IR spectrophotometer. ^{1}H NMR were recorded on a Bruker 400 spectrometer operating at 399.993 MHz. Mass spectrometric measurements performed by direct–exposure probe using electron impact ionization (EI) were made on a VG 70S instrument at the University of South Carolina, Columbia, SC. Bis(1,5-cyclooctadiene)nickel(0), $Ni(COD)_2$, was purchased from Strem Chemicals, used without further purification, and

stored and handled in a drybox. NH_3 was purchased from Matheson Tri-Gas as pure ammonia gas. $Ru_5(CO)_{15}(\mu_5\text{-C})$ was prepared according to the previously published procedure.[68] Product separations were performed by TLC in air on Analtech silica gel GF 250 or 500 μm glass plates. Silica gel (60-200μm, 70-230 mesh) used for chromatographic separations was purchased from Silicycle. Florisil (F100-500, 60-100 mesh) used for product purifications was purchased from Fisher Scientific.

Preparation of $Ru_5Ni(NCMe)(CO)_{15}(\mu_6\text{-C})$, 3.1

A 100 mg (0.11 mmol) amount of $Ru_5(CO)_{15}(\mu_5\text{-C})$ and 40 mg (0.15 mmol) amount of $Ni(COD)_2$ were dissolved in 20 mL of acetonitrile in a 50 mL 3-neck round-bottom flask equipped with a reflux condenser. The solution was then heated to reflux with stirring for 15 min. at which time IR showed complete consumption of the starting material, $Ru_5(CO)_{15}(\mu_5\text{-C})$. The solvent was removed *in vacuo* and the product was separated by column chromatography using 1:1 hexane/methylene chloride solvent mixture to yield 41 mg (37% yield) of brown $Ru_5Ni(NCMe)(CO)_{15}(\mu_6\text{-C})$, **3.1** and a trace amount of $Ru_5(CO)_{15}(\mu_5\text{-C})$. Spectral data for **3.1**: IR ν_{CO} (cm^{-1} in methylene chloride): 2086 (w), 2045 (s), 2019 (m), 1987 (w, br), 1868 (vw, br). ^1H NMR ($CDCl_3$ in ppm): δ = 2.49 (s, 3 H, CH_3). EI/MS: *m/z* 1038 (M^+). The isotope distribution pattern is consistent with the presence of one nickel atom and five ruthenium atoms.

Preparation of $Ru_5Ni(CO)_{16}(\mu_6\text{-C})$, 3.2

A 50 mg (0.05 mmol) amount of **3.1** was dissolved in 20 mL of toluene in a 50 mL 3-neck round-bottom flask equipped with a reflux condenser. Carbon monoxide gas (1 atm) was bubbled through the solution and the solution was refluxed at 110 °C with stirring for 15 min. at which time IR showed complete consumption of the starting

material **3.1**. The solvent was removed *in vacuo* and the product was re-dissolved in methylene chloride and filtered through florisil to give 48 mg of **3.2** (97% yield). Spectral data for **3.2**: IR ν_{CO} (cm^{-1} in hexane): 2104 (vw), 2062 (s), 2050 (m), 2038 (w), 2030 (w), 2001 (w), 1885 (vw, br). EI/MS: *m/z* 1025 (M^+), 940(M^+- 3CO), 912 (M^+- 4CO), 856 (M^+- 6CO). The isotope distribution pattern is consistent with the presence of one nickel atom and five ruthenium atoms.

Preparation of $Ru_5Ni(NH_3)(CO)_{15}(\mu_6\text{-}C)$, 3.3 from $Ru_5Ni(NCMe)(CO)_{15}(\mu_6\text{-}C)$, 3.1

A 20 mg (0.019 mmol) amount of **3.1** was dissolved in 10 mL of methylene chloride in a 50 mL 3-neck round-bottom flask. Ammonia gas (1 atm) was bubbled through the solution and the solution was stirred at 0 °C (maintained in an ice bath) for approx. 1 min. at which time TLC showed complete consumption of the starting material. The reaction solution was filtered through florisil to give 19 mg of **3.3** (97% yield). Spectral data for **3.3**: IR ν_{CO} (cm^{-1} in methylene chloride): 2085 (w), 2044 (s), 2019 (m), 1980 (vw, br), 1870 (vw, br). ^1H NMR (CD_2Cl_2 in ppm): δ = 2.95 (s, 3 H, NH_3). EI/MS: *m/z* 1013 (M^+), showing successive loss of 8 CO ligands. The isotope distribution pattern is consistent with the presence of one nickel atom and five ruthenium atoms.

Preparation of $Ru_5Ni(NH_3)(CO)_{15}(\mu_6\text{-}C)$, 3.3 from $Ru_5Ni(CO)_{16}(\mu_6\text{-}C)$, 3.2

A 24 mg (0.023 mmol) amount of **3.2** was dissolved in 10 mL of methylene chloride in a 50 mL 3-neck round-bottom flask. Then ammonia gas (1 atm) was bubbled through the solution and the solution was stirred at 0 °C (maintained in an ice bath) for approx. 1 min. at which time IR showed complete consumption of the starting material, **3.2**. The solvent was removed *in vacuo* and the product was separated on a silica gel

column to yield a brown band of **3.3** (12 mg, 50% yield) eluted by 1:1 hexane/methylene chloride solvent mixture.

Note: In both cases the reactions do proceed at room temperature, however owing to decomposition the yields at 0 °C are better.

Preparation of $Ru_5Ni(CO)_{13}(\eta^6\text{-}C_6H_6)(\mu_6\text{-}C)$, 3.4 from $Ru_5Ni(NCMe)(CO)_{15}(\mu_6\text{-}C)$, 3.1

A 20 mg (0.019 mmol) amount of **3.1** was dissolved in 20 mL of benzene in a 50 mL 3-neck round-bottom flask equipped with a reflux condenser. The solution was irradiated using a high-pressure mercury 1000 W UV lamp (American Ultraviolet Co.) at the 250 wpi (watts per inch) setting for 90 min. at which time IR showed complete consumption of the starting material, **3.1**. The solvent was removed *in vacuo* and the product was separated by TLC on silica gel by using 1:1 hexane/methylene chloride solvent mixture to yield 6.4 mg (33% yield) of green $Ru_5Ni(CO)_{13}(\eta^6\text{-}C_6H_6)(\mu_6\text{-}C)$, **3.4** and trace amounts of $Ru_5Ni(CO)_{16}(\mu_6\text{-}C)$, $Ru_6(CO)_{17}(\mu_6\text{-}C)$, $Ru_5(CO)_{15}(\mu_5\text{-}C)$, $Ru_5(CO)_{12}(\eta^6\text{-}C_6H_6)(\mu_5\text{-}C)$ and $Ru_5Ni(NCMe)(CO)_{15}(\mu_6\text{-}C)$. Spectral data for **3.4**: IR ν_{CO} (cm^{-1} in methylene chloride): 2075 (m), 2043 (vs), 2034 (vs), 2018 (s), 1971 (w), 1853 (vw, br); ^1H NMR (CD_2Cl_2 in ppm): $\delta = 5.85$ (s, 6 H, C_6H_6). EI/MS: *m/z* 1018-1019 (M^+), showing successive loss of 13 CO ligands. The isotope distribution pattern is consistent with the presence of one nickel atom and five ruthenium atoms.

Preparation of $Ru_5Ni(CO)_{13}(\eta^6\text{-}C_6H_6)(\mu_6\text{-}C)$, 3.4 from $Ru_5Ni(CO)_{16}(\mu_6\text{-}C)$, 3.2

A 20 mg (0.019 mmol) amount of **3.2** was dissolved in 20 mL of benzene in a 50 mL 3-neck round-bottom flask equipped with a reflux condenser. The solution was irradiated using a high-pressure mercury 1000 W UV lamp (American Ultraviolet Co.) at the 250 wpi setting for 90 min. The solvent was removed *in vacuo* and the product was

separated by TLC on silica gel by using 1:1 hexane/methylene chloride solvent mixture to yield 5.2 mg (26 % yield) of green $Ru_5Ni(CO)_{13}(\eta^6\text{-}C_6H_6)(\mu_6\text{-}C)$, **3.4**.

Preparation of $Ru_5Ni(CO)_{13}(\eta^6\text{-}C_7H_8)(\mu_6\text{-}C)$, 3.5 from $Ru_5Ni(NCMe)(CO)_{15}(\mu_6\text{-}C)$, 3.1

A 20 mg (0.019 mmol) amount of **3.1** was dissolved in 20 mL of toluene in a 50 mL 3-neck round-bottom flask equipped with a reflux condenser. The solution was irradiated using a high-pressure mercury 1000 W UV lamp (American Ultraviolet Co.) at the 250 wpi setting for 60 min. at which time IR showed complete consumption of the starting material, **3.1**. The solvent was removed *in vacuo* and the product was separated by TLC on silica gel by using 1:1 hexane/methylene chloride solvent mixture to yield 7.3 mg (37% yield) of green $Ru_5Ni(CO)_{13}(\eta^6\text{-}C_7H_8)(\mu_6\text{-}C)$, **3.5** and trace amounts of $Ru_5Ni(CO)_{16}(\mu_6\text{-}C)$, $Ru_6(CO)_{17}(\mu_6\text{-}C)$, $Ru_5(CO)_{15}(\mu_5\text{-}C)$, and $Ru_5Ni(MeCN)(CO)_{15}(\mu_6\text{-}C)$. Spectral data for **3.5**: IR ν_{CO} (cm^{-1} in methylene chloride): 2074 (m), 2042 (vs), 2032 (vs), 2017 (s), 1967 (w), 1844 (vw, br); ^1H NMR (CD_2Cl_2 in ppm): δ = 5.80 (d, 2 H, CH), 5.75 (t, 2 H, CH), 5.67 (t, 1 H, CH), 2.38 (s, 3H, CH_3). EI/MS: *m/z* 1033-1034 (M^+), showing successive loss of 9 CO ligands. The isotope distribution pattern is consistent with the presence of one nickel atom and five ruthenium atoms.

Preparation of $Ru_5Ni(CO)_{13}(\eta^6\text{-}C_7H_8)(\mu_6\text{-}C)$, 3.5 from $Ru_5Ni(CO)_{16}(\mu_6\text{-}C)$, 3.2

A 20 mg (0.019 mmol) amount of **3.2** was dissolved in 20 mL of toluene in a 50 mL 3-neck round-bottom flask equipped with a reflux condenser. The solution was irradiated using a high-pressure mercury 1000 W UV lamp (American Ultraviolet Co.) at the 250 wpi setting for 60 min. The solvent was removed *in vacuo* and the product was separated by TLC on silica gel by using 1:1 hexane/methylene chloride solvent mixture to yield 2.5 mg (12% yield) of green $Ru_5Ni(CO)_{13}(\eta^6\text{-}C_7H_8)(\mu_6\text{-}C)$, **3.5**.

3.5. Crystallographic analyses

Single crystals of **3.1**, **3.2, 3.3, 3.4** and **3.5** suitable for diffraction analysis were all grown by slow evaporation of solvent from solutions in a hexane/methylene chloride solvent mixture at – 20 °C. The data crystals for **3.1**, **3.2, 3.3, 3.4** and **3.5** were glued onto the end of a thin glass fiber. X-ray intensity data were measured by using a Bruker SMART APEX2 CCD-based diffractometer using Mo Kα radiation (λ = 0.71073 Å).[50] The raw data frames were integrated with the SAINT+ program by using a narrow-frame integration algorithm.[50] Corrections for Lorentz and polarization effects were also applied with SAINT+. An empirical absorption correction based on the multiple measurement of equivalent reflections was applied using the program SADABS. All structures were solved by a combination of direct methods and difference Fourier syntheses, and refined by full-matrix least-squares on F^2, by using the SHELXTL software package.[51] All non-hydrogen atoms were refined with anisotropic displacement parameters. Hydrogen atoms were placed in geometrically idealized positions and included as standard riding atoms during the least-squares refinements. Crystal data, data collection parameters, and results of the analyses are listed in Tables B.1 and B.2.

Compound **3.1** crystallized in the orthorhombic crystal system. The systematic absences in the intensity data were consistent with the space groups *Pnma* and $Pna2_1$. The structure could only be solved in the latter space group. Compounds **3.2** and **3.3** crystallized in the triclinic crystal system. The space group $P\ \bar{1}$ was assumed and confirmed by the successful refinement of the structures. With Z = 4, there are 2 formula equivalents of complex **3.3** present in the asymmetric crystal unit. Compound **3.4** crystallized in the orthorhombic crystal system. The systematic absences in the intensity

data were consistent with the unique space group *Pbca*. Compound **3.5** crystallized in the monoclinic crystal system. The systematic absences in the intensity data were consistent with the unique space group $P2_1/n$. With Z = 8, there are 2 formula equivalents of the complex present in the asymmetric crystal unit.

Chapter 4: Build-up of a Ru_6 octahedral cluster core stabilized by *tert*-butyl germyl ligands

4.1. Background

Electronic unsaturation in transition metal complexes is induced by bulky ligands. The bulky ligands shield the metal center from the approach of large molecules, leaving enough room for the selective approach of small molecules. Based on this approach, we wanted to synthesize the transition metal cluster complexes with bulky tin ligands for the application in small molecule activation. But due to the lack of reactivity of the tertiary butyl tin hydride with iron-nickel and ruthenium-nickel carbide complexes, we started to investigate the reaction of bulky tertiary butyl germane with ruthenium carbonyl complexes.

In recent years bimetallic nanoparticles, prepared from bimetallic molecular cluster complexes have been shown to be viable precursors to nanoscale catalysts.[43] Under heterogeneous condition bimetallic nanoparticle catalysts exhibit superior catalytic properties.[44] Germanium has been shown to modify the reactivity of important heterogeneous catalysts.[73] For example when germanium is used as a promoter in a carbon-supported palladium catalyst, an increase in catalytic activity and selectivity was observed in the hydrogenation of C=C double bonds conjugated with hydroxyl, carbonyl or phenyl groups.[74] Ruthenium carbonyl cluster complexes when combined with Group 14 elements such as germanium and tin, exhibit interesting catalytic properties.[75] It is known that germanes react with transition metal complexes via oxidative addition of the Ge-H bond and form the metal germyl complexes. Adams and coworkers have done extensive work on ruthenium cluster complexes with triphenylgermane.[76-81] There are

only a few examples of transition metal (Fe, Ni, Co, Mo, W) cluster complexes containing tertiary butyl germane ligand reported in the literature.[82-84]

Ruthenium clusters containing the tertiary butyl germane group have not yet been investigated. Thus, we have now studied the reactions of $GeBu^tH_3$ with $Ru_3(CO)_{12}$ and have obtained seven new ruthenium carbonyl cluster complexes containing $GeBu^t$ groups. Cleavage of hydride from tertiary butyl germane ligand facilitates the high incorporation of germanium ligands into these clusters. The synthesis and structural characterization of these new compounds is presented in this chapter.

4.2. Results and discussion

Six new bimetallic ruthenium-germanium carbonyl cluster complexes $Ru_3(CO)_9(\mu_3\text{-}GeBu^t)_2$, **4.1**, $Ru_2(CO)_6(\mu\text{-}GeBu^tH)_3$, **4.2**, $Ru_4(CO)_{10}(\mu_4\text{-}Ge_2Bu^t_2)(\mu\text{-}GeBu^tH)_2$, **4.3**, $Ru_4(CO)_8(\mu_4\text{-}Ge_2Bu^t_2)(\mu\text{-}GeBu^tH)_2(\mu_3\text{-}GeBu^t)(H)$, **4.4**, $Ru_5(CO)_{12}(\mu_3\text{-}GeBu^t)_2(\mu_4\text{-}GeBu^t)(H)$, **4.5**, $Ru_6(CO)_{12}(\mu_3\text{-}GeBu^t)_4(H)_2$, **4.6**, $Ru_4(CO)_9(\mu_4\text{-}GeBu^t)_2(\mu_2\text{-}GeBu^tH)_3$, **4.7** were obtained from the reaction of $Ru_3(CO)_{12}$ with tertiary butyl germane, Bu^tGeH_3, in heptane solvent at reflux condition for 45 min. When tertiary butyl germane was added to the compound **4.3** and was refluxed at 98 ^oC, another new compound **4.7** was yielded. All these seven compounds were structurally characterized by a combination of IR, ^1H NMR, mass spectrometry and single-crystal X-ray diffraction analyses. One of the products, compound **4.1**, shows the addition of $GeBu^t$ groups to the intact starting Ru_3 cluster. An ORTEP diagram of the molecular structure of **4.1** is shown in Figure 4.1. Selected bond distances and angles are listed in Table C.4. The compound contains a Ru_3 triangle that is capped on either side by $\mu_3\text{-}GeBu^t$ ligands to afford a trigonal bipyramidal Ru_3Ge_2 cluster. With three carbonyl ligands on each ruthenium atom, the complex is

electron precise having 48 cluster valence electrons. This molecule possess approximate C_{3h} symmetry and is similar in structure to the previously reported compound (μ_3-GeEt)$_2$Fe$_3$(CO)$_9$, which has a Fe_3Ge_2 trigonal bipyramidal configuration.[85]

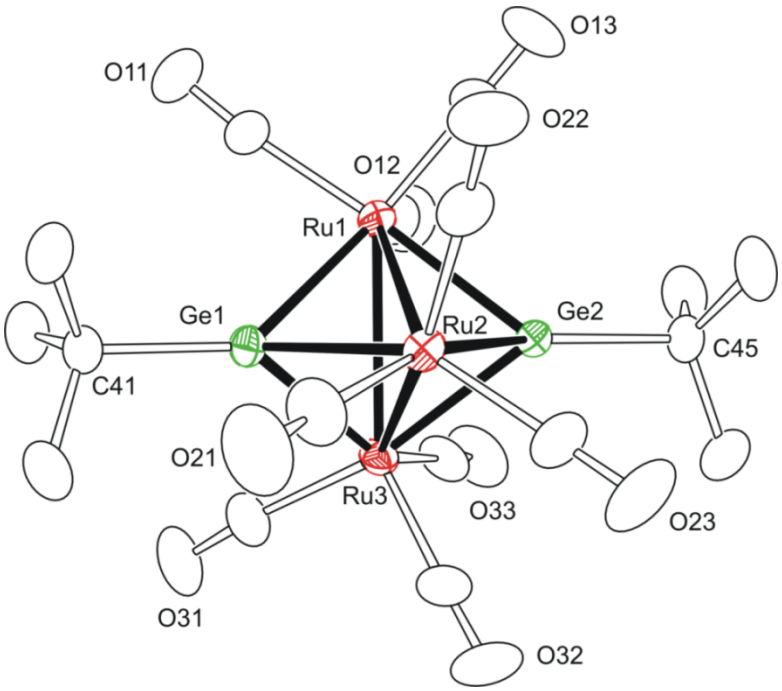

Figure 4.1. An ORTEP diagram of the molecular structure of $Ru_3(CO)_9(\mu_3\text{-}GeBu^t)_2$, **4.1**, showing 30% thermal ellipsoid probability.

Elucidation of the structure of compound **4.2** in the solid state as seen in Figure 4.2 provides evidence for cluster fragmentation in the reaction system. Compound **4.2** is a dinuclear ruthenium complex where the Ru-Ru vector is bridged by three μ-GeBu^{t}H groups. The molecule crystallized in the hexagonal crystal system and has crystallographic C_{3h} symmetry. Overall, the molecule can be viewed to possess approximate D_{3h} symmetry and appropriately shows two peaks in its IR spectrum which are assigned to the A_2'' mode (2034 cm^{-1}) and an E′ mode (2001 cm^{-1}). As expected the ^{1}H NMR spectrum shows a singlet resonance for the hydride ligands on Ge at 7.92 ppm and for the Bu^t protons at 1.25 ppm. The downfield Ge-H resonance is consistent with

those observed in the germylene-bridged diiron complexes $Cp_2Fe_2(CO)_3(\mu\text{-}GeH^tBu)$ and $Cp_2Fe_2(CO)_2(\mu\text{-}GeH^tBu)_2$;[82] and $[RhIr(H)_2(CO)_2(\mu\text{-}GeH^tBu)(dppm)_2]$ and $[RhIr(CO)_2((\mu\text{-}Ge\ HPh)(\mu\text{-}GePh_2(dppm)_2]$.[86] The resonance of the germanium-bonded hydrogen atom of the $GeBu^tH_3$ ligand lies at δ = 3.74 ppm, while the Ge-H rseonances in **4.2** and in a few previously reported compounds appears significantly deshielded from 3.74 ppm. In 1969 Elder *et al.* reported the complex $Fe_2(GeMe_2)_3(CO)_6$, which has a Fe_2Ge_3 core.[87] A similar molecular structure for the osmium analog, $Os_2(GeMe_2)_3(CO)_6$, was reported by Leong *et al.*[88] A few years ago, V. A. Du *et al.* obtained the compound, $Fe_2(CO)_6(SiCl_2)_3$, via thermolysis of $Fe(CO)_4(SiCl_3)_2$.[89]

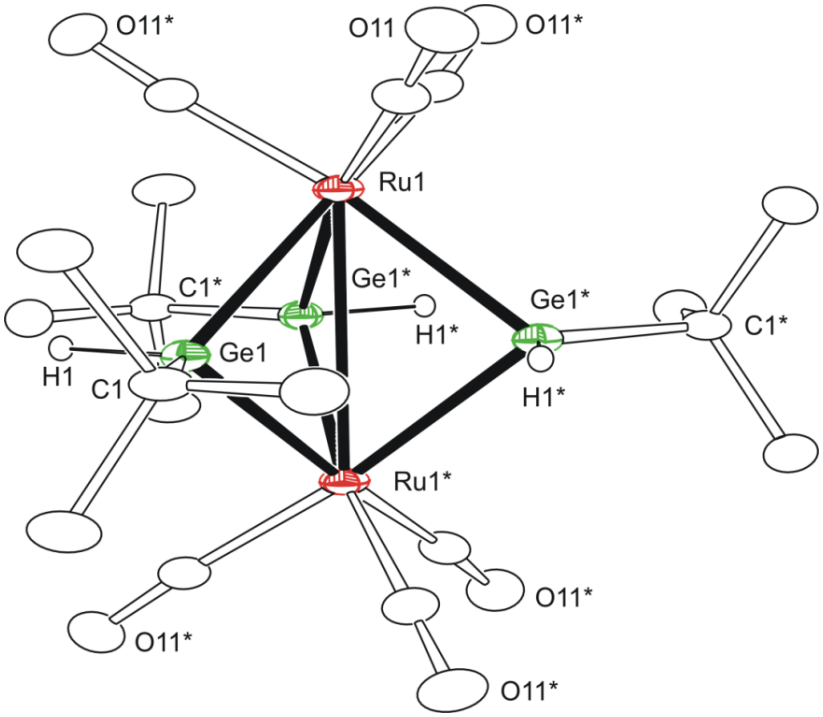

Figure 4.2. An ORTEP diagram of the molecular structure of $Ru_2(CO)_6(\mu\text{-}GeBu^tH)_3$, **4.2**, showing 30% thermal ellipsoid probability.

In addition to this fragmentation product **4.2**, four new complexes as a result of cluster condensation were also obtained. The molecular structure of **4.3** is shown in

Figure 4.3. Compound **4.3** contains an octahedral cluster comprised of four ruthenium atoms and two germanium atoms. There are two μ-GeBu^{t}H groups that bridge two of the Ru-Ru bonds in **4.3**. Each of the Ge atoms in the octahedral core contains a terminal Bu^t group. With 10 CO ligands, the cluster valence electron count is 66 which is consistent for a *closo* octahedron based on the Polyhedral Skeletal Electron Pair Theory [10M + 2 + 4n = 10(4) + 2 + 4(6) = 66 e$^-$].[90] Adams *et al.* reported an octahedral cluster, $Ru_4(\mu_4\text{-}GePh)_2(\mu\text{-}GePh_2)_2(CO)_{10}$, comprised of four ruthenium atoms and two germanium atoms containing two μ-$GePh_2$ groups that bridge two of the Ru-Ru bonds which is very similar to our compound **4.3**.[80] They also reported another octahedral cluster, $Ru_4(\mu_4\text{-}SnPh)_2(\mu\text{-}SnPh_2)_2(CO)_{10}$, comprised of four ruthenium atoms and two tin atoms containing two μ-$SnPh_2$ groups that bridge two of the Ru-Ru bonds.[91]

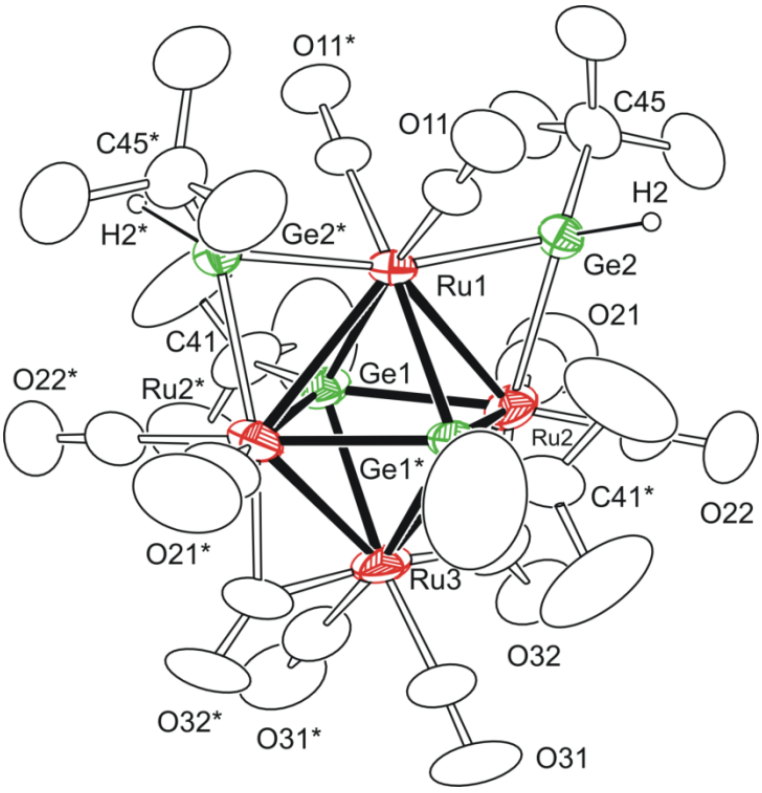

Figure 4.3 An ORTEP diagram of the molecular structure of $Ru_4(CO)_{10}(\mu_4\text{-}Ge_2Bu^t_2)(\mu\text{-}GeBu^tH)_2$, **4.3**, showing 30% thermal ellipsoid probability.

Compound **4.4**, which also contains four ruthenium atoms, was isolated from the reaction mixture. As can be seen in Figure 4.4, this complex also consists of a Ru_4Ge_2 octahedral cluster as in **4.3**. However, unlike in **4.3** the two Ge atoms are now bonded to each other. The Ge-Ge bond distance of 2.4490(8) Å is similar to those found in Ge_2Ph_6, 2.446(1) Å[92]; $C_{56}H_{56}Ge_4O_2$, 2.4418(5) Å[93]; $[Pt(PPh_3)_2(H)(GeHMesGeH_2Mes)]$, 2.4571(12) Å[94]; and $Cp_2HfGe_2(Me_3Si)_4.PMe_3$, 2.4538(9) Å[95]. Compound **4.4** in addition to also having two μ-GeBu^{t}H groups bridging two of the Ru-Ru bonds, there is also a triply bridging μ_3-GeBu^t group that caps the Ru1-Ru2-Ru2* triangular face. Appropriately, the complex contains one hydride ligand which is a triple bridge on the Ru3-Ru2-Ru2* face and was located and refined crystallographically.

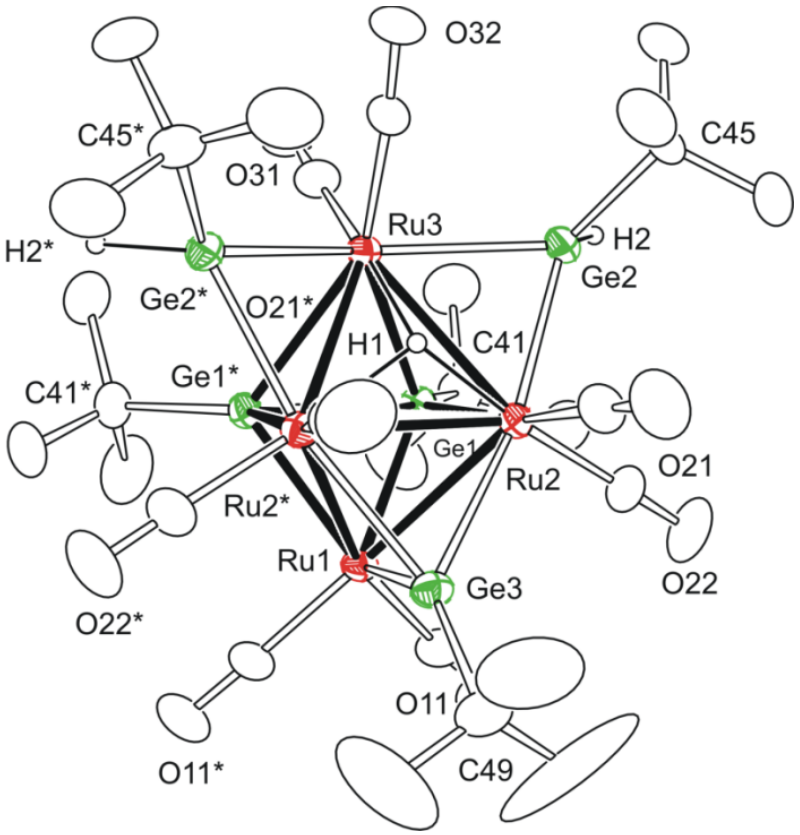

Figure 4.4. An ORTEP diagram of the molecular structure of $Ru_4(CO)_8(\mu_4\text{-}Ge_2Bu^t_2)(\mu\text{-}GeBu^tH)_2(\mu_3\text{-}GeBu^t)(H)$, **4.4**, showing 30% thermal ellipsoid probability.

^{1}H NMR confirmed the presence of the hydride ligand which showed a high-field singlet at -20.84 ppm. With 8 CO ligands, just like in **4.3** the cluster valence electron count remains at 66 in accordance with a *closo* octahedral structure. All the Ru-Ru bonds are similar in length and the presence of a hydride ligand does not increase any of Ru-Ru bond lengths.

Two higher nuclearity ruthenium cluster complexes $Ru_5(CO)_{12}(\mu_3\text{-}GeBu^t)_2(\mu_4\text{-}GeBu^t)(H)$, **4.5**, and $Ru_6(CO)_{12}(\mu_3\text{-}GeBu^t)_4(H)_2$, **4.6**, were also obtained. An ORTEP diagram of the molecular structure of **4.5** is shown in Figure 4.5. Selected bond distances and angles are listed in Table C.8. The compound contains an octahedral cluster comprised of five ruthenium atoms and one germanium atom. Two μ_3-GeBu^t groups are present as triply bridging ligands capping two of the Ru_3 faces. One of the other Ru_3 faces (Ru1-Ru1*-Ru3) contains a triply bridging hydride ligand which was located and refined crystallographically. The hydride peak was observed as a high-field resonance in its ^{1}H NMR spectrum, $\delta = -22.77$. The cluster valence electron count is 76 which is consistent for a *closo* octahedron structure, where five of the vertices are occupied by a transition metal atom [10M + 2 + 4n = 10(5) + 2 + 4(6) = 76 e$^-$]. A similar cluster, $Ru_5(CO)_{11}(\eta^5\text{-}C_6H_6)(\mu_4\text{-}SnPh)(\mu_3\text{-}CPh)$, was isolated by Adams where the octahedron consists of five ruthenium atoms and one tin atom.[96]

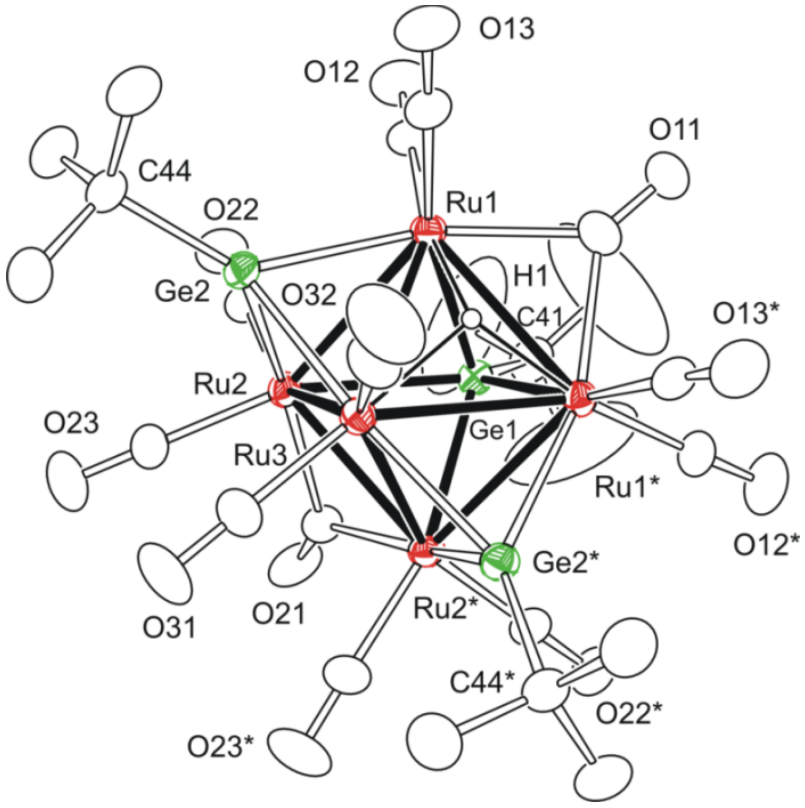

Figure 4.5. An ORTEP diagram of the molecular structure of $Ru_5(CO)_{12}(\mu_3\text{-}GeBu^t)_2(\mu_4\text{-}GeBu^t)(H)$, **4.5**, showing 30% thermal ellipsoid probability.

Compound **4.6**, see Figure 4.6, is a Ru_6 octahedron with four triply bridging μ_3-$GeBu^t$ groups. With 12 CO ligands and two face bridging hydride ligands the cluster valence count is 86 e^- which is exactly the number expected for an octahedral cluster of six metal atoms. These two hydride ligands (located and refined crystallographically) are equivalent and appear as one high-field resonance, at -26.77 ppm, in the ^1H NMR spectrum of the compound. The Ru2-Ru4 bond distance (2.9414(5) Å) is larger than Ru2-Ru3 bond distance (2.8730(5) Å) and can be explained due to the presence of a bridging hydride ligand.[97] There have been previous reports of bridging SnL_2 in Ru_6 octahedral clusters, $Ru_6(CO)_{16}(\mu\text{-}SnCl_2)(\mu_6\text{-}C)$[98] and $Ru_6(CO)_{13}(\mu\text{-}SnPh_2)(\eta^6\text{-}C_6H_6)(\mu_6\text{-}C)$[76], however these contain the encapsulated carbide ligand.

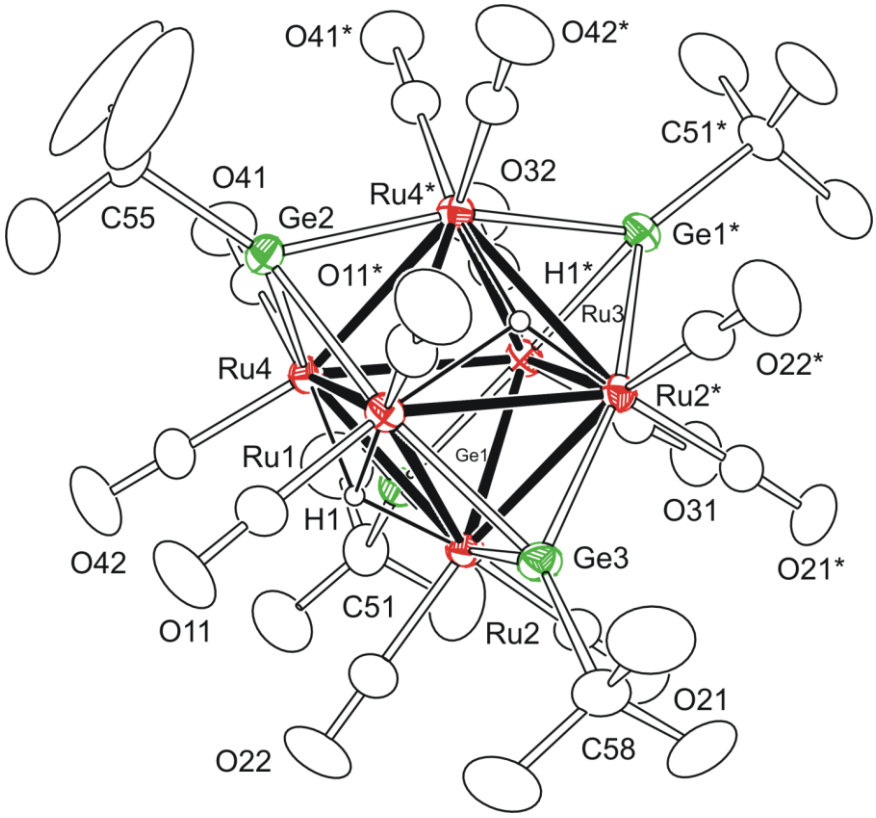

Figure 4.6. An ORTEP diagram of the molecular structure of $Ru_6(CO)_{12}(\mu_3\text{-}GeBu^t)_4(H)_2$, **4.6**, showing 30% thermal ellipsoid probability.

When one equivalent of tertiary butyl germane, $ButGeH_3$ was added to the compound **4.3** and refluxed in heptane solvent, we expected to obtain compound **4.4**. But instead another new compound, **4.7** was yielded. Compound **4.7** contains an octahedral cluster comprised of four ruthenium atoms and two germanium atoms, as shown in Figure 4.7. Selected bond distances and angles are listed in Table C.10. Each of the Ge atoms in the octahedral core contains a terminal Bu^t group. There are three μ-$GeBu^tH$ groups that bridge two of the Ru-Ru bonds of this compound. In this compound, one μ-$GeBu^tH$ group replaced one of the two bridging carbonyl groups from compound **4.3**; as a result compound **4.7** contains only one bridging CO ligand.

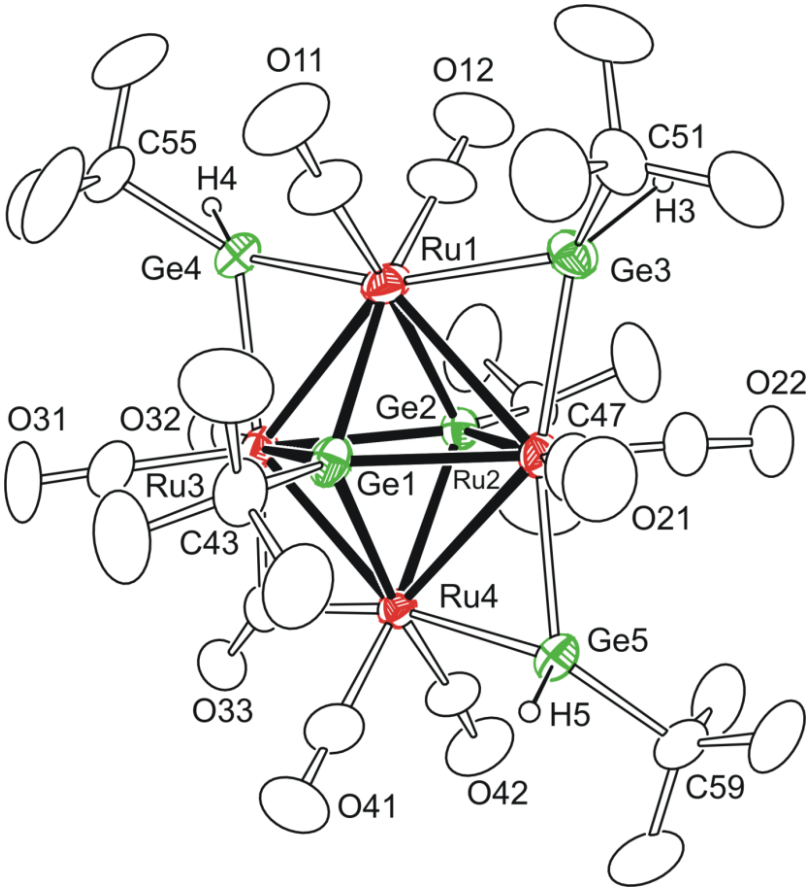

Figure 4.7. An ORTEP diagram of the molecular structure of $Ru_4(CO)_9(\mu_4\text{-}GeBu^t)_2(\mu_2\text{-}GeBu^tH)_3$, **4.7**, showing 30% thermal ellipsoid probability.

4.3. Conclusions

A summary of the reaction system described in this report is presented in Scheme 4.1. The reaction of $Ru_3(CO)_{12}$ with Bu^tGeH_3 has resulted in a number of products which include both fragmented as well as condensed products. The yields of the new complexes remain low due to considerable decomposition of the reaction system. When the reaction time was increased from 45 min to 12 h, a slight increase in yield for compounds **4.1**, **4.5** and **4.6** was observed. When excess (10 equivalents) Bu^tGeH_3 was reacted with $Ru_3(CO)_{12}$ for 45 min, complex **4.2** was obtained in a slightly higher yield (18 %) along with low amounts of **4.4**, in addition to minor amounts of a new compound which we

have not characterized. The Ru_3 triangle remains only in complex **4.1**, where elimination of CO and H_2 affords two $GeBu^t$ caps to form a trigonal bipyramidal structure. One product is a result of cluster fragmentation which yields the symmetric Ru_2Ge_3 complex **4.2**. Four other higher nuclearity Ru-Ge clusters were also isolated due to cluster condensation. Two of these products contain four Ru atoms as seen in compounds **4.3** and **4.4**. In compound **4.3**, the Ru atoms are in a square arrangement while in compound **4.4**, the four Ru atoms are in a butterfly arrangement. In both structures the Ru_4Ge_2 octahedral core is completed with two $GeBu^t$ groups. In compound **4.5**, five Ru atoms are held together in a square pyramidal geometry and then in compound **4.6**, six of these form a Ru_6 octahedron. When one equivalent of tertiary butyl germane was added to the compound **4.3**, another new Ru-Ge cluster compound **4.7** was formed, see Scheme 4.2. This study reveals a variety of different structural motifs of interest to cluster chemistry.

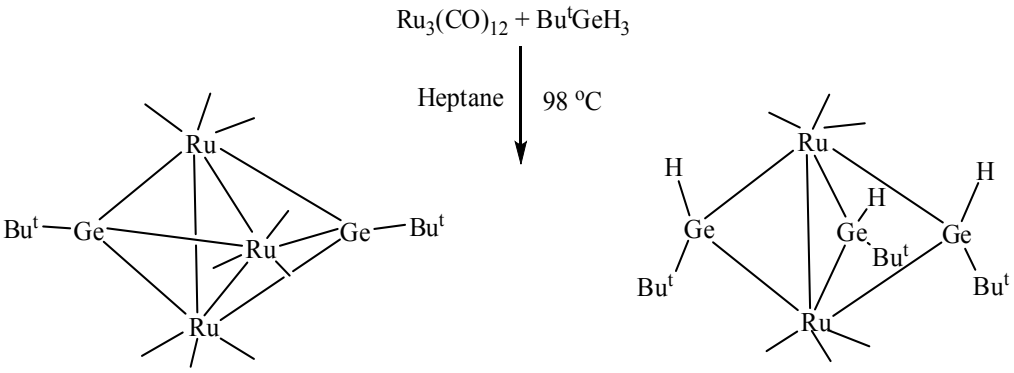

$Ru_3(CO)_9(\mu_3\text{-}GeBu^t)_2$, **4.1**

$Ru_2(CO)_6(\mu\text{-}GeBu^tH)_3$, **4.2**

$Ru_4(CO)_{10}(\mu_4\text{-}Ge_2Bu^t{}_2)(\mu\text{-}GeBu^tH)_2$, **4.3**

$Ru_4(CO)_{10}(\mu_4\text{-}Ge_2Bu^t{}_2)(\mu\text{-}GeBu^tH)_2(\mu_3\text{-}GeBu^t)(H)$, **4.4**

$Ru_5(CO)_{12}(\mu_3\text{-}GeBu^t)_2(\mu_4\text{-}GeBu^t)(H)$, **4.5**

$Ru_6(CO)_{12}(\mu_3\text{-}GeBu^t)_4(H)_2$, **4.6**

Scheme 4.1

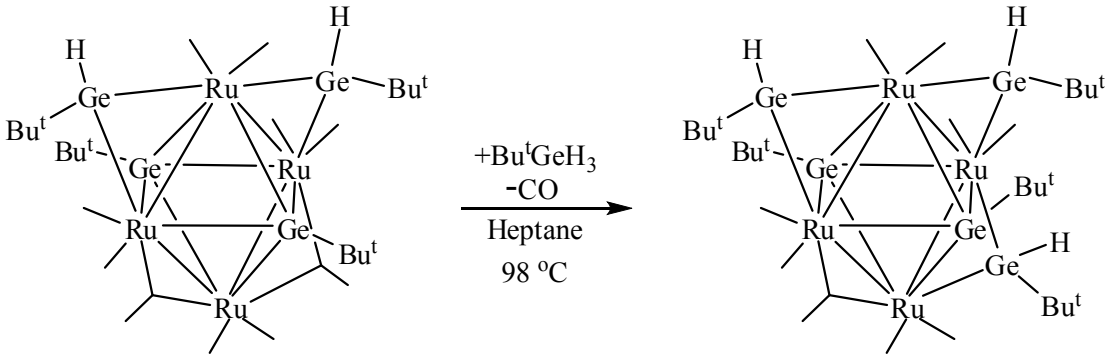

$Ru_4(CO)_{10}(\mu_4\text{-}GeBu^t)_2(\mu\text{-}GeBu^tH)_2$, **4.3**

$Ru_4(CO)_9(\mu_4\text{-}GeBu^t)_2(\mu\text{-}GeBu^tH)_3$, **4.7**

Scheme 4.2

4.4. Experimental section

General data

Unless indicated otherwise, all reactions were performed under an atmosphere of Argon. Reagent grade solvents were dried by the standard procedures and were freshly distilled prior to use. Infrared spectra were recorded on a Nicolet 380 FT-IR spectrophotometer. ^{1}H NMR were recorded on a Bruker 400 spectrometer operating at 399.993 MHz. Mass spectrometric measurements performed by direct–exposure probe using electron impact ionization (EI) were made on a VG 70S instrument at the University of South Carolina, Columbia, SC. $Ru_3(CO)_{12}$ was purchased from Alfa Aesar and was used without further purification. Tertiary butyl germane, Bu^tGeH_3, was purchased from Gelest Inc. and was used without further purification. Product separations were performed by TLC in air on Analtech silica gel GF 250 or 500 μm glass plates. Florisil (F100-500, 60-100 mesh) used for product purifications was purchased from Fisher Scientific.

Reaction of $Ru_3(CO)_{12}$ with Bu^tGeH_3 (4eq.) in heptane solvent for 45 min.

A 50 mg (0.08 mmol) amount of $Ru_3(CO)_{12}$ and 43 mg (0.32 mmol) amount of Bu^tGeH_3 were dissolved in 20 mL of heptane in a 50 mL 3-neck round-bottom flask equipped with a reflux condenser. The solution was then heated to reflux with stirring for 45 minutes. During this time the orange colored solution turned to dark brown and IR showed complete consumption of the starting material $Ru_3(CO)_{12}$. After cooling, the solvent was removed in vacuo and the products were separated by TLC by using a pure hexane solvent to yield in order of elution: 5.2 mg (9% yield) of light yellow $Ru_2(CO)_6(\mu\text{-}GeBu^tH)_3$, **4.2**; 7.8 mg (12% yield) of deep yellow $Ru_3(CO)_9(\mu_3\text{-}GeBu^t)_2$, **4.1**; 1.7 mg (2% yield) of red $Ru_4(CO)_8(\mu_4\text{-}Ge_2Bu^t_2)(\mu\text{-}GeBu^tH)_2(\mu_3\text{-}GeBu^t)(H)$, **4.4**; 2.0 mg (2% yield) of purple $Ru_4(CO)_{10}(\mu_4\text{-}Ge_2Bu^t_2)(\mu\text{-}GeBu^tH)_2$, **4.3**; 1.1 mg (1% yield) of green $Ru_5(CO)_{12}(\mu_3\text{-}GeBu^t)_2(\mu_4\text{-}GeBu^t)(H)$, **4.5** and 1.2 mg (1% yield) of brown $Ru_6(CO)_{12}(\mu_3\text{-}GeBu^t)_4(H)_2$, **4.6**. Spectral data for **4.2**: IR ν_{CO} (cm^{-1} in hexane): 2034 (s), 2001 (s). ^1H NMR (C_6D_6 in ppm): δ = 7.92 (s, 3 H, Ge-H), 1.25 (s, 27 H, CH_3). EI/MS: *m/z* 764 (M^+). The isotope distribution pattern is consistent with the presence of two ruthenium atoms and three germanium atoms. Spectral data for **4.1**: IR ν_{CO} (cm^{-1} in hexane): 2034 (s), 1988 (m). ^1H NMR (C_6D_6 in ppm): δ = 1.71 (s, 18 H, CH_3). EI/MS: *m/z* 816 (M^+), 788(M^+- CO), 760 (M^+- 2CO). The isotope distribution pattern is consistent with the presence of three ruthenium atoms and two germanium atoms. Spectral data for **4.4**: IR ν_{CO} (cm^{-1} in hexane): 2033(m), 2014 (s), 1991 (vs), 1979 (w), 1959 (w), 1939 (m). ^1H NMR (C_6D_6 in ppm): δ = 9.56 (s, 2 H, Ge-H), 1.89 (s, 9 H, CH_3), 1.66 (s, 18 H, CH_3), 1.25 (s, 18 H, CH_3), -20.84 (s, 1 H, hydride). EI/MS: *m/z* 1280 (M^+). The isotope distribution pattern is consistent with the presence of four ruthenium atoms and five

germanium atoms. Spectral data for **4.3**: IR ν_{CO} (cm^{-1} in hexane): 2060 (m), 2026 (s), 2005 (m), 1989 (m), 1970 (w, br), 1860 (m), 1839 (m). ^1H NMR (C_6D_6 in ppm): δ = 8.40 (s, 2 H, Ge-H), 1.45 (s, 18 H, CH_3), 0.85 (s, 18 H, CH_3). EI/MS: *m/z* 1149 (M^+-Bu^t). The isotope distribution pattern is consistent with the presence of four ruthenium atoms and four germanium atoms. Spectral data for **4.5**: IR ν_{CO} (cm^{-1} in hexane): 2062 (vw), 2031 (s), 2013 (s), 1994 (w, br), 1982 (vw), 1967 (w), 1867 (w, br). ^1H NMR (C_6D_6 in ppm): δ = 1.47 (s, 18 H, CH_3), 1.27 (s, 9 H, CH_3), -22.77 (s, 1 H, hydride). EI/MS: *m/z* 1233 (M^+), 1205(M^+- CO). The isotope distribution pattern is consistent with the presence of five ruthenium atoms and three germanium atoms. Spectral data for **4.6**: IR ν_{CO} (cm^{-1} in hexane): 2050 (vw), 2025 (s), 2018 (vs), 2009 (vs), 1995 (m), 1984 (vw), 1975 (w), 1963 (w), 1947 (vw). ^1H NMR (C_6D_6 in ppm): δ = 1.55 (s, 36 H, CH_3), -26.77 (s, 2 H, hydride). EI/MS: *m/z* 1463 (M^+), 1407(M^+- 2CO). The isotope distribution pattern is consistent with the presence of six ruthenium atoms and four germanium atoms.

Note: The IR and NMR of compound **4.2** (light yellow) was impure. Thus pure crystals (6.0 mg) were obtained by dissolving 32.0 mg of compound **4.2** in acetonitrile solvent at -25 ^oC. We were unable to determine the identity of the other product.

Reaction of $Ru_4(CO)_{10}(\mu_4\text{-}GeBu^t)_2(\mu\text{-}GeBu^tH)_2$, 3 with Bu^tGeH_3 (2eq.)

A 12 mg (0.01 mmol) amount of **4.3** and 2 mg (0.02 mmol) amount of Bu^tGeH_3 were dissolved in 10 mL of heptane in a 50 mL 3-neck round-bottom flask equipped with a reflux condenser. The solution was then heated to reflux with stirring for 2 hours. During this time the IR showed complete consumption of the starting material **4.3**. After cooling, the solvent was removed in vacuo and the products were separated by TLC by using a pure hexane solvent to yield in order of elution: 5.0 mg (38% yield) of

purple $Ru_4(CO)_9(\mu_4\text{-}GeBu^t)_2(\mu\text{-}GeBu^tH)_3$, **4.7** and 5.0 mg (42% yield) of purple $Ru_4(CO)_{10}(\mu_4\text{-}GeBu^t)_2(\mu\text{-}GeBu^tH)_2$, **4.3**. Spectral data for **4.7**: IR ν_{CO} (cm^{-1} in hexane): 2044 (m), 2022 (s), 2009 (s), 1998 (m), 1989 (vs), 1869 (w), 1845 (m). ^1H NMR (C_6D_6 in ppm): δ = 8.75 (s, 2 H, H), 8.65 (s, 1 H, H), 1.56 (s, 9 H, CH_3), 1.53 (s, 9 H, CH_3), 1.51 (s, 9 H, CH_3), 0.85 (s, 9 H, CH_3), 0.76 (s, 9 H, CH_3). EI/MS: *m/z* 1309 (M^+), 1251 (M^+-Bu^tH). The isotope distribution pattern is consistent with the presence of four ruthenium atoms and five germanium atoms.

Reaction of $Ru_3(CO)_{12}$ with Bu^tGeH_3 (4eq.) in heptane solvent for 12hr.

A 50 mg (0.08 mmol) amount of $Ru_3(CO)_{12}$ and 43 mg (0.32 mmol) amount of Bu^tGeH_3 were dissolved in 20 mL of heptane in a 50 mL 3-neck round-bottom flask equipped with a reflux condenser. The solution was then heated to reflux with stirring for 12 hours. During this time the orange colored solution turned to dark brown and IR showed complete consumption of the starting material $Ru_3(CO)_{12}$. After cooling, the solvent was removed in vacuo and the products were separated by TLC by using a pure hexane solvent to yield in order of elution: 12.1 mg (19% yield) of deep yellow $Ru_3(CO)_9(\mu_3\text{-}GeBu^t)_2$, **4.1**; 2.9 mg (3% yield) of green $Ru_5(CO)_{12}(\mu_3\text{-}GeBu^t)_2(\mu_4\text{-}GeBu^t)(H)$, **4.5** and 7.5 mg (7% yield) of brown $Ru_6(CO)_{12}(\mu_3\text{-}GeBu^t)_4(H)_2$, **4.6**.

Reaction of $Ru_3(CO)_{12}$ with Bu^tGeH_3 (4eq.) in heptane solvent for 24hr.

A 50 mg (0.08 mmol) amount of $Ru_3(CO)_{12}$ and 43 mg (0.32 mmol) amount of Bu^tGeH_3 were dissolved in 20 mL of heptane in a 50 mL 3-neck round-bottom flask equipped with a reflux condenser. The solution was then heated to reflux with stirring for 24 hours. During this time the orange colored solution turned to dark brown and IR showed complete consumption of the starting material $Ru_3(CO)_{12}$. After cooling, the

solvent was removed in vacuo and the products were separated by TLC by using a pure hexane solvent to yield in order of elution: 4.8 mg (8% yield) of deep yellow $Ru_3(CO)_9(\mu_3\text{-}GeBu^t)_2$, **4.1**; 0.7 mg (1% yield) of green $Ru_5(CO)_{12}(\mu_3\text{-}GeBu^t)_2(\mu_4\text{-}GeBu^t)(H)$, **4.5** and 5.5 mg (5% yield) of brown $Ru_6(CO)_{12}(\mu_3\text{-}GeBu^t)_4(H)_2$, **4.6**.

Reaction of $Ru_3(CO)_{12}$ with Bu^tGeH_3 (10eq.) in heptane solvent for 45 min.

A 50 mg (0.08 mmol) amount of $Ru_3(CO)_{12}$ and 104 mg (0.8 mmol) amount of Bu^tGeH_3 were dissolved in 20 mL of heptane in a 50 mL 3-neck round-bottom flask equipped with a reflux condenser. The solution was then heated to reflux with stirring for 45 minutes. During this time the orange colored solution turned to light red and IR showed complete consumption of the starting material $Ru_3(CO)_{12}$. After cooling, the solvent was removed in vacuo and the products were separated by TLC by using a pure hexane solvent to yield in order of elution: 11 mg (18% yield) of light yellow $Ru_2(CO)_6(\mu\text{-}GeBu^tH)_3$, **4.2**; 2.4 mg (2% yield) of red $Ru_4(CO)_8(\mu_4\text{-}GeBu^t)_2(\mu\text{-}GeBu^tH)_2(\mu_3\text{-}GeBu^t)(H)$, **4.4**.

Reaction of $Ru_3(CO)_{12}$ with Bu^tGeH_3 (10eq.) in toluene solvent for 3hr.

A 50 mg (0.08 mmol) amount of $Ru_3(CO)_{12}$ and 104 mg (0.8 mmol) amount of Bu^tGeH_3 were dissolved in 20 mL of toluene in a 50 mL 3-neck round-bottom flask equipped with a reflux condenser. The solution was then heated to reflux with stirring for 3 hours. During this time the orange colored solution turned to dark brown and IR showed complete consumption of the starting material $Ru_3(CO)_{12}$. After cooling, the solvent was removed in vacuo and the products were separated by TLC by using a pure hexane solvent to yield in order of elution: 4 mg (7% yield) of *impure* light yellow

$Ru_2(CO)_6(\mu\text{-}GeBu^tH)_3$, **4.2**; 1.3 mg (2% yield) of deep yellow $Ru_3(CO)_9(\mu_3\text{-}GeBu^t)_2$, **4.1**; 1.0 mg (1% yield) of purple $Ru_4(CO)_9(\mu_4\text{-}GeBu^t)_2(\mu\text{-}GeBu^tH)_3$, **4.7**.

Reaction of $Ru_3(CO)_{12}$ with Bu^tGeH_3 (10eq.) in heptane solvent for 10hr.

A 50 mg (0.08 mmol) amount of $Ru_3(CO)_{12}$ and 104 mg (0.8 mmol) amount of Bu^tGeH_3 were dissolved in 20 mL of heptane in a 50 mL 3-neck round-bottom flask equipped with a reflux condenser. The solution was then heated to reflux with stirring for 10 hours. During this time the orange colored solution turned to dark brown and IR showed complete consumption of the starting material $Ru_3(CO)_{12}$. After cooling, the solvent was removed in vacuo and the products were separated by TLC by using a pure hexane solvent to yield in order of elution: 5 mg (8% yield) of *impure* light yellow $Ru_2(CO)_6(\mu\text{-}GeBu^tH)_3$, **4.2**; 1.6 mg (3% yield) of deep yellow $Ru_3(CO)_9(\mu_3\text{-}GeBu^t)_2$, **4.1**; 2.0 mg (2% yield) of purple $Ru_4(CO)_9(\mu_4\text{-}GeBu^t)_2(\mu\text{-}GeBu^tH)_3$, **4.7**.

4.5. Crystallographic analyses

Single crystals of **4.1**, **4.3**, **4.4** and **4.7** suitable for diffraction analysis were all grown by slow evaporation of solvent from solutions in ether solvent at – 25 °C. Single crystals of **4.2**, **4.5** and **4.6** suitable for diffraction analysis were all grown by slow evaporation of solvent from solutions in hexane/methylene chloride solvent mixture at – 25 °C. The data crystals for **4.1**, **4.3, 4.4, 4.5**, **4.6** and **4.7** were glued onto the end of a thin glass fiber. For **4.2** the crystal was mounted onto the end of a thin glass fiber using Paratone-N for data collection at 100 K under flow of N_2. X-ray intensity data were measured by using a Bruker SMART APEX2 CCD-based diffractometer using Mo Kα radiation (λ = 0.71073 Å).[50] The raw data frames were integrated with the SAINT+ program by using a narrow-frame integration algorithm.[50] Corrections for Lorentz and

polarization effects were also applied with SAINT+. An empirical absorption correction based on the multiple measurement of equivalent reflections was applied using the program SADABS. All structures were solved by a combination of direct methods and difference Fourier syntheses, and refined by full-matrix least-squares on F^2, by using the SHELXTL software package.[51] All non-hydrogen atoms were refined with anisotropic displacement parameters. Hydrogen atoms were placed in geometrically idealized positions and included as standard riding atoms during the least-squares refinements. Crystal data, data collection parameters, and results of the analyses are listed in Tables C.1, C.2 and C.3.

Compounds **4.1** and **4.3** crystallized in the monoclinic crystal system. For compound **4.1** the systematic absences in the intensity data were consistent with the unique space group $P2_1/c$. For **4.3** the systematic absences in the intensity data were consistent with either space group $P2/n$ or space group Pn. The former space group was chosen and confirmed by the successful solution and refinement of the structure. With Z = 2, the molecule has crystallographic two fold symmetry. The Ge2 atom is disordered over two orientations and was refined in a 90:10 ratio. Compound **4.2** crystallized in the hexagonal crystal system. The systematic absences in the intensity data were consistent with the unique space group $P\bar{6}2c$. With Z = 2, the molecule resides about a site of $\bar{6}$ symmetry. The GeBu^{t}H group is disordered over two orientations and was refined in the ratio 80:20. Compounds **4.4**, **4.5**, and **4.6** crystallized in the orthorhombic crystal system. For compounds **4.4** and **4.5** the systematic absences in the intensity data were consistent with either of the space groups $Pnma$ or $Pna2_1$. The formed space group was chosen in both cases and confirmed by the successful solution and refinement of the structure. For

both compounds, half a formula equivalent of the complex is present in the asymmetric crystal unit possessing crystallographic mirror symmetry. The hydrido ligands in **4.4** and **4.5** were located and refined successfully with isotropic thermal parameters. For compound **4.6**, the systematic absences in the intensity data were consistent with the unique space group $Cmc2_1$. With half a molecule present in the asymmetric crystal unit the complex has crystallographic mirror symmetry. The hydride ligand in **4.6** was located and refined successfully with isotropic thermal parameters. Compound **4.7** crystallized in the triclinic crystal system. For compound **4.7** the systematic absences in the intensity data were consistent with the unique space group $P\ \bar{1}$.

Chapter 5: Synthesis and structural characterization of ruthenium carbonyl cluster complexes containing platinum with a bulky N-heterocyclic carbene ligand

5.1. Background

To synthesize more bulky bimetallic cluster complexes we directed our research to a new avenue. We wanted to incorporate the bulky N-heterocyclic carbene ligand into transition metal clusters. Thus we synthesized the known Pt-NHC complex and started to investigate the reactivity of bulky N-heterocyclic carbene ligand with transition metal complexes.

In 1994, Arduengo synthesized and characterized low-coordinate NHC complexes of nickel(0) and platinum(0).[99] Ever since this report, the synthesis of N-heterocyclic carbenes (NHCs), as well as the use of NHCs as ligands in coordination chemistry has attracted significant attention.[100] With the use of novel NHC-metal complexes, many important reactions, such as olefin metathesis,[101] Pd-catalyzed cross-coupling reactions,[102] and hydrogenation reactions,[103] have shown noticeable improvements. The strong electron donating properties of NHCs often give their metal complexes increased stability.[104] As a result of their electronic properties, NHCs provide a versatile alternative to phosphine ligands. They also provide an equally variable steric environment which is quite different than that of phosphines. Thus, substitution of a phosphine ligand with an NHC can lead to dramatic increase in catalytic activity and stability.[104,105] The synthesis of novel NHC–Pt(0) complexes has been previously reported and their efficiency in the hydrosilylation of a broad range of alkenes was demonstrated.[106] NHC–Pt(alkene)$_2$ complexes were also shown to be used as hydrosilylation catalysts.[107]

While there has been considerable work done with mono nuclear-NHCs; metal clusters with NHC have been less than studied. Mixed-metal cluster complexes have been

shown to be good precursors for the preparation of supported bimetallic nanoparticles.[108] It has been shown that certain bimetallic catalysts have both higher activity and better product selectivity than their monometallic counterparts.[109] Supported platinum–ruthenium clusters have been shown to exhibit high activity for catalytic hydrogenation reactions when immobilized on mesoporous silica.[21,110,111] The use of NHCs in metal cluster chemistry is still relatively limited. To the best of our knowledge, bimetallic Ru–Pt–NHC cluster complexes have not yet been investigated.

Thus, we have now studied the reaction of $Ru_3(CO)_{12}$ and $Ru(CO)_5$ with 2,2'-Bis(1,3-dimesitylimidazol-2-ylidene)platinum(0), $Pt(IMes)_2$ to yield four new Ru–Pt–NHC cluster complexes. Furthermore, we also investigated the reaction of hydrogen with some of these complexes. The synthesis and structural characterization of these new bimetallic N-heterocyclic carbene compounds is presented in this report.

5.2. Results and discussion

The reaction of triruthenium dodecacarbonyl, $Ru_3(CO)_{12}$ with 2,2'-Bis(1,3-dimesitylimidazol-2-ylidene)platinum(0), $Pt(IMes)_2$ in benzene solvent at room temperature afforded two new bimetallic cluster complexes, the monoplatinum–triruthenium cluster complex $Ru_3Pt(IMes)_2(CO)_{11}$, **5.1** in 21 % yield and the diplatinum–triruthenium cluster complex $Ru_3Pt_2(IMes)_2(CO)_{12}$, **5.2** in 26 % yield. Both compounds **5.1** and **5.2** were structurally characterized by a combination of IR, ^1H NMR, mass spectrometry and single-crystal X-ray diffraction analyses. An ORTEP depicting the molecular structure of **5.1** is shown in Figure 5.1, and selected intramolecular distances and angles are listed in Table D.4.

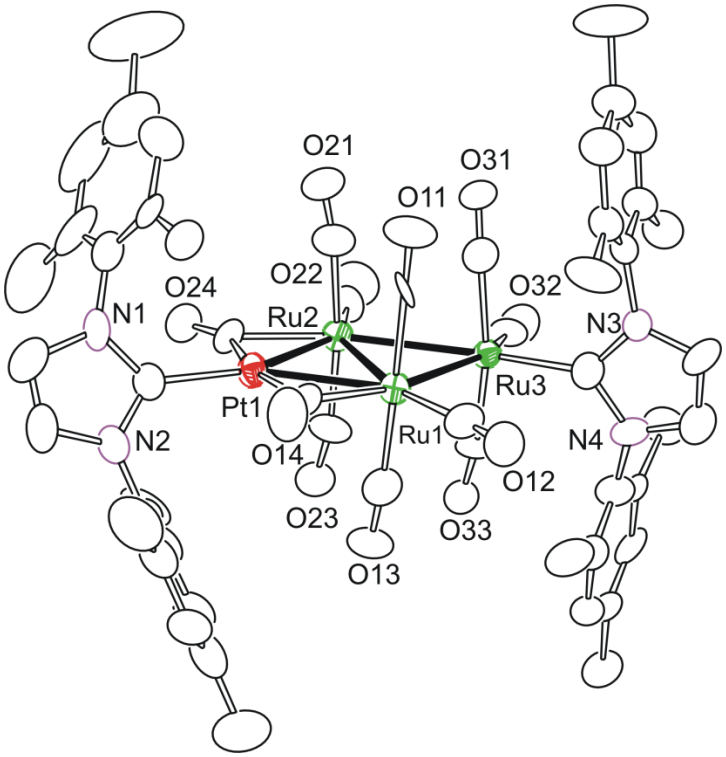

Figure 5.1. An ORTEP showing the molecular structure of $Ru_3Pt(IMes)_2(CO)_{11}$, **5.1** at 30% thermal ellipsoid probability.

Compound **5.1** consists of a square plane with three ruthenium atoms and one platinum atom, and can be viewed as two triangles that share an edge formed by a Ru–Ru single bond, Ru1–Ru2 = 2.892(3) Å. The Pt(IMes) group is an edge bridging on the Ru_3 triangle. There is also an IMes group that is coordinated to atom Ru3 opposite the Pt atom. There are two bridging carbonyl groups that bridge the ruthenium– platinum bonds. The IMes group on Ru3 lies perpendicularly to the Ru_3 triangular plane. Cabeza et. al. have previously reported the reaction of $Ru_3(CO)_{12}$ with N,N'-dimesitylimidazol-2-ylidene (Mes_2Im), which afforded the trinuclear NHC substituted complex [$Ru_3(Mes_2Im)(CO)_{11}$], where one ruthenium atom is bonded with the IMes group.[113] For the formation of **5.1**, dissociation of an IMes group from the starting $Pt(IMes)_2$ reagent

must occur to give the reactive electron deficient "Pt(IMes)" fragment that is able to add across an Ru–Ru bond. The free IMes group is now available to undergo CO ligand substitution, and due to sterics of the bulky NHC group, prefers to coordinate to Ru3 which is furthest away from the Pt(IMes) grouping. Generation of the reactive "Pt(IMes)" fragment in course of this reaction may also yield other various Ru–Pt products, and subsequently we were able to isolate a Ru_3Pt_2 cluster complex, **5.2**.

The structure of complex **5.2** in the solid state is given in Figure 5.2 and selected intramolecular distances and angles are listed in Table D.5.

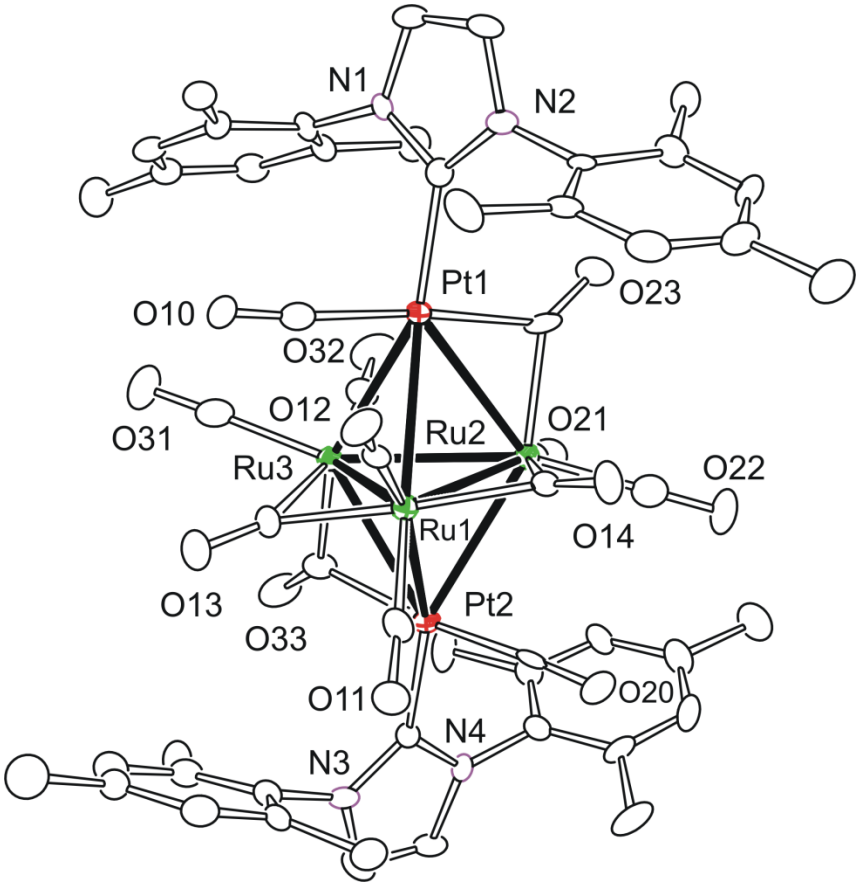

Figure 5.2. An ORTEP showing the molecular structure of $Ru_3Pt_2(IMes)_2(CO)_{12}$, **5.2** at 50% thermal ellipsoid probability.

Compound **5.2** has a trigonal bipyramidal geometry of three ruthenium atoms and two platinum atoms. The Ru atoms occupy the equatorial plane while the Pt atoms occupy the apical positions of the trigonal bipyramid. With no loss of CO ligands, compound **5.2** can be viewed as an adduct of $Ru_3(CO)_{12}$, where two Pt(IMes) groups cap the Ru_3 triangle. The two carbonyl ligands coordinated to each of the Pt atoms are edge bridging and slightly semi-bridging in nature, Pt1–C10–O10 = 172.6(10)° and Pt2–C20–O20 = 172.9(12)°. Adams et al. has prepared the pentanuclear platinum-osmium compound $Pt_2Os_3(CO)_{10}(P^tBu_3)_2$,[114] which has a similar structure to compound **5.2** however contains two less CO ligands. The previously reported reactions of $Ru_3(CO)_{12}$ with $Pd(P^tBu_3)_2$,[115] and $Os_3(CO)_{12}$ with $Pd(P^tBu_3)_2$[116] or $Pt(P^tBu_3)_2$,[117] similar products were obtained where the $Pd(P^tBu_3)$ or $Pt(P^tBu_3)$ groups add across the metal-metal bonds in these reactions to form edge bridging raft-like complexes, such as shown in Figure 5.3.

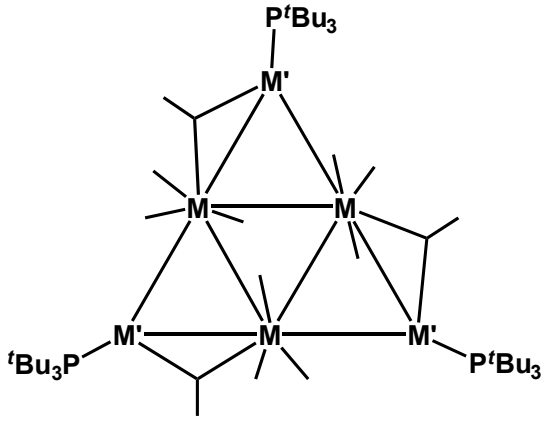

Figure 5.3. Structure of $M(CO)_{12}[M'(P^tBu_3)]_3$ where M = Ru and M' = Pd, M = Os and M' = Pd or Pt

It is interesting to note that in our reaction only two Pt(IMes) groups were able to add to $Ru_3(CO)_{12}$ to give **5.2**, indicating the steric differences between the IMes and P^tBu_3. The

complex $Pt_2Os_3(CO)_{10}(P^tBu_3)_2$ instead was obtained from $Os_3(CO)_{10}(NCMe)_2$ and $Pt(P^tBu_3)_2$.[114]

Another product $Ru_2Pt(IMes)(CO)_9$, **5.3** was also obtained as a result of this reaction, however in lower yields, due to fragmentation of the $Ru_3(CO)_{12}$ reagent. Thus, one could obtain this complex directly from $Ru_2(CO)_9$ and $Pt(IMes)_2$. However, due to high instability of $Ru_2(CO)_9$, it was not possible to perform this reaction.[118] Instead we carried out the reaction of $Ru(CO)_5$ with $Pt(IMes)_2$. $Ru(CO)_5$ reacts with $Pt(IMes)_2$ in benzene solvent at 0 ^oC to afford the bimetallic trinuclear cluster complexes, $Ru_2Pt(IMes)(CO)_9$, **5.3** (15 % yield), and $RuPt_2(IMes)_2(CO)_6$, **5.4** (21 % yield). Both compounds **5.3** and **5.4** were also characterized crystallographically.

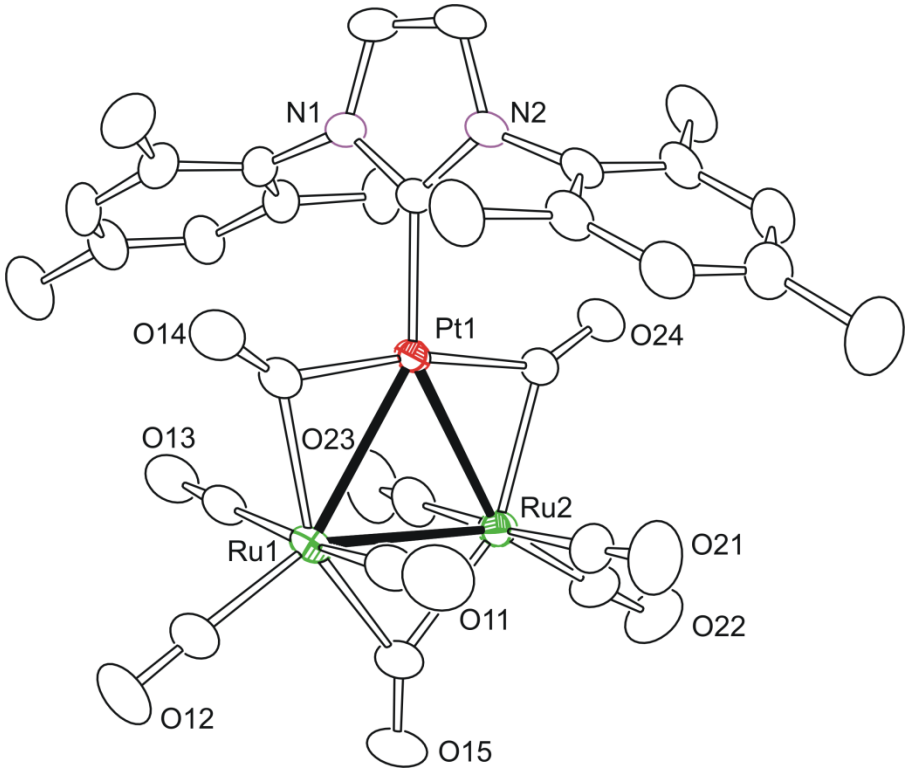

Figure 5.4. An ORTEP showing the molecular structure of $Ru_2Pt(IMes)(CO)_9$, **5.3** at 30% thermal ellipsoid probability.

As shown in Figure 5.4, compound **5.3** contains a triangle of three metal atoms of which two are ruthenium atoms and one is a platinum atom. There are three bridging carbonyl ligands which bridge each of the Pt–Ru bonds and a Ru–Ru bond. With nine CO ligands, this compound can be viewed as a monoplatinum adduct of $Ru_2(CO)_9$. As expected the Ru–Ru bond distance (2.8658 Å) is very close to the Ru1–Ru2 bond length in **5.1** (2.892(3) Å), due to similar donation of electrons from the Ru1–Ru2 bond to the platinum atom. Complex **5.2** is similar in structure to $PtRu_2(CO)_9(PBu^t_3)$,[119] which was obtained from the reaction of $Ru(CO)_5$ with $Pt(P^tBu_3)_2$.

Compound **5.4** is another trinuclear cluster complex that was furnished in this reaction but contains two platinum atoms and one ruthenium atom. Its structure in the solid state (see Figure 5.5) consists of a $RuPt_2$ triangle with the IMes groups located on the platinum atoms.

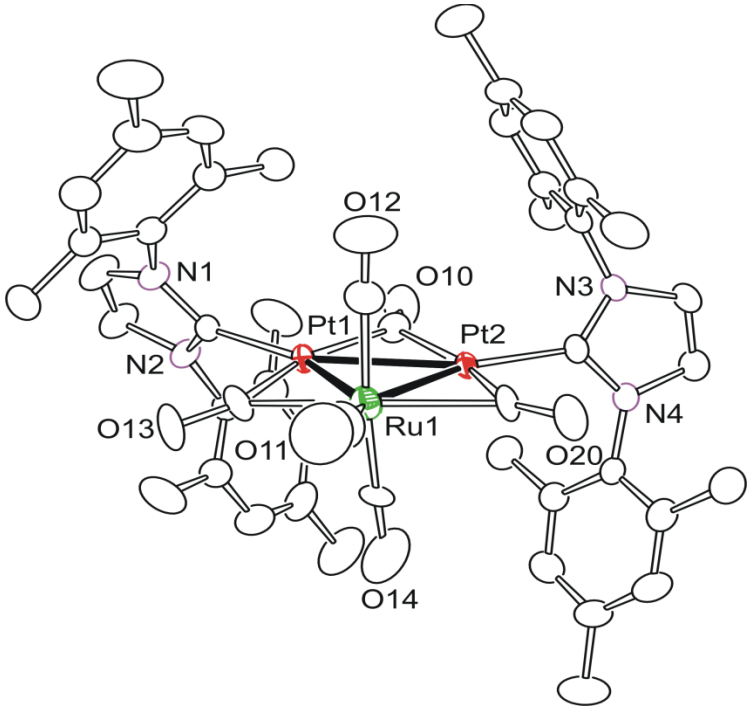

Figure 5.5. An ORTEP showing the molecular structure of $RuPt_2(IMes)_2(CO)_6$, **5.4** at 30% thermal ellipsoid probability.

Interestingly, the ruthenium atom just as in **5.3**, have five carbonyl ligands, two of which bridge to the neighboring Pt atoms and other three carbonyl ligands are terminally coordinated. The sixth carbonyl ligand bridges the two platinum atoms, Pt1 and Pt2. The Pt–Pt bond distance (2.6477 Å) is shorter than the Ru–Pt bond distances (Av. 2.7091 Å).

A comprehensive study of the chemistry of bimetallic cluster complexes containing the bulky Pd(P^tBu_3) or Pt(P^tBu_3) groups has shown interesting reactivity, especially with hydrogen gas.[120] Thus, we investigated the reaction of compound **5.2** with H_2, which afforded the tetrahydrido–tetraruthenium complex $Ru_4(IMes)(CO)_{11}(\mu\text{-}H)_4$, **5.5** (12 % yield) and the dihydride–diruthenium–diplatinum complex $Ru_2Pt_2(IMes)_2(CO)_8(\mu\text{-}H)_2$, **5.6** (36 % yield), at 80 °C. Both compounds **5.5** and **5.6** were structurally characterized by single-crystal X-ray diffraction analyses. Compound **5.5** consists of a Ru_4 tetrahedron with an IMes ligand on Ru1, see Figure 5.6. There are four hydride ligands which bridge four of the ruthenium bonds. These four hydride ligands (located and refined crystallographically) are equivalent and appear as one high-field resonance, at -17.67 ppm, in the ^1H NMR spectrum of the compound. An ORTEP diagram of the molecular structure of compound **5.5** is shown in Figure 5.6 and selected intramolecular distances and angles are listed in Table D.8.

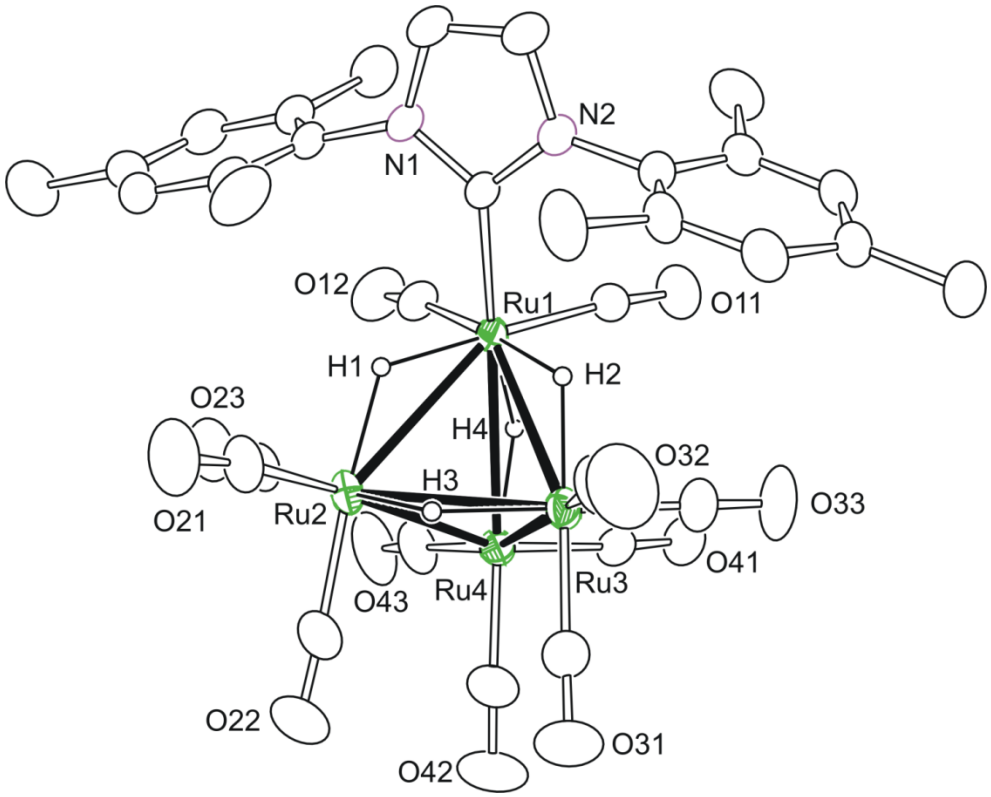

Figure 5.6. An ORTEP showing the molecular structure of $Ru_4(IMes)(CO)_{11}(\mu\text{-}H)_4$, **5.5** at 30% thermal ellipsoid probability.

This compound is isostructural with $Os_4H_4(CO)_{11}(IMes)$[121] and $Ru_4H_4(CO)_{11}(PPh_3)$[122]. Few years ago, Cooke et al. reported the synthesis of compound **5.5** by the treatment of $Ru_4(\mu\text{-}H)_4(CO)_{12}$ with Me_3NO and [(IMes)AgCl].[123] After that Cabeza et al. prepared the same compound using $Ru_4(\mu\text{-}H)_4(CO)_{12}$, potassium *tert*-butoxide and 1,3-dimesitylimidazolium chloride.[124] Its structure was formulated accurately based on IR, ^1H NMR, mass spectrometry and elemental analyses. We have now obtained a crystal structure for compound **5.5** which is shown in Figure 5.6.

Compound **5.6** was obtained as a major product from this reaction. As can be seen in Figure 5.7, the structure of this compound has a butterfly geometry, containing two

ruthenium and two platinum atoms. Both the platinum atoms contain IMes groups which are present at the "wing-tips" of the butterfly, see Figure 5.7.

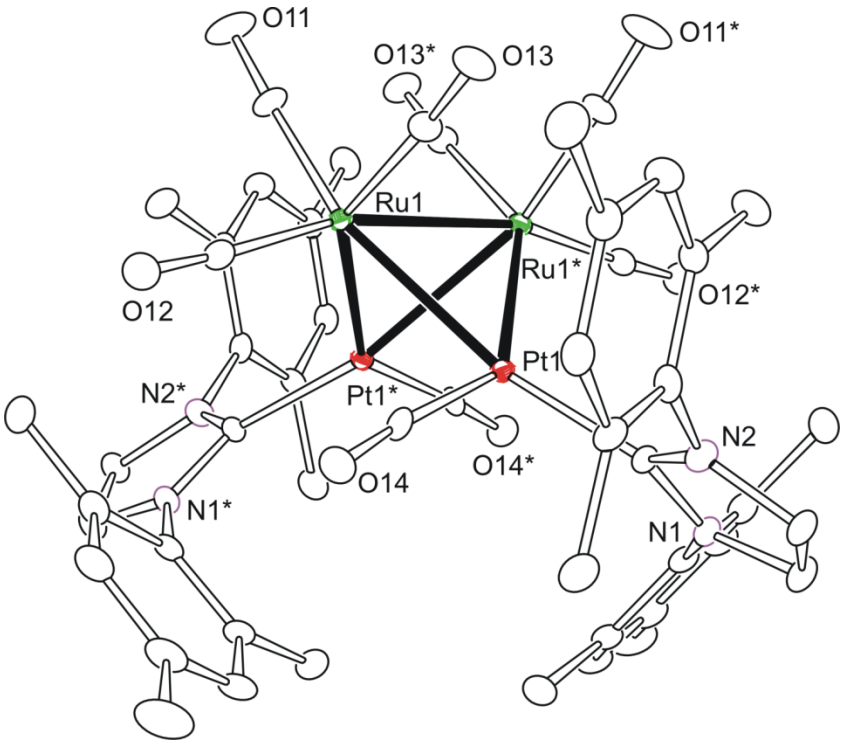

Figure 5.7. An ORTEP showing the molecular structure of $Ru_2Pt_2(IMes)_2(CO)_8(\mu\text{-}H)_2$, **5.6** at 30% thermal ellipsoid probability. Hydride ligands are not shown.

This dihydride–diruthenium–diplatinum compound contains two ruthenium atoms joined by a Ru–Ru single bond, Ru1–Ru1* = 2.7695(8) Å. Each ruthenium atom is bonded with two Pt(IMes) groups and contains three terminally coordinated carbonyl ligands. The platinum atoms, Pt1 and Pt1* both has one carbonyl ligand which is terminally coordinated. There are no bridging carbonyl ligands present in this compound. Appropriately, the complex contains two hydride ligands which bridge two of the Ru–Pt bonds. The presence of two hydride ligands was not located crystallographically, but they appear as one high-field resonance, in the ^{1}H NMR spectrum of the compound. These

two hydride ligands are equivalent and appear at -9.89 ppm, in the ^{1}H NMR spectrum of the compound, showing one and two bond coupling to platinum, $^{1}J_{Pt\text{-}H}$ = 560 Hz, $^{2}J_{Pt\text{-}H}$ = 40 Hz. The hydride-bridged Ru–Pt bond lengths, Ru1–Pt1* = 2.8356(5) Å and Ru1*–Pt1 = 2.8357(5) Å, are significantly longer than the unbridged Ru–Pt bond lengths, Ru1–Pt1 = 2.7136(5) Å and Ru1*–Pt1* = 2.7136(5) Å, as expected due to the bond lengthening effects of bridging hydride ligands.[125] Compound **5.6** is similar in structure to the tetranuclear metal complexes $Pt_2Ru_2(CO)_8(P^tBu_3)_2(\mu\text{-}H)_2$, 7,[119] $Pt_2Ru_2(CO)_8(PPh_3)_2(\mu\text{-}H)_2$, **5.8**,[126] and $Pt_2Ru_2(CO)_9(Sn^tBu_3)_2(\mu\text{-}H)_2$, **5.9**[127]. For complex **5.6**, the Pt-Pt bond distance is 3.2507(3) Å which is a long Pt-Pt bond. In complexes **5.7** and **5.8** the Pt-Pt bond distances are 3.1462(5) Å and 3.137(1) Å respectively, and can be considered as weak Pt-Pt interactions. In **5.9** the Pt-Pt distance is short at 2.8105(2) Å. Thus complex **5.6** may be interpreted as a butterfly rather than a tetrahedron, with two 16 electron Pt atoms, with a total count of 58 electrons and no Pt – Pt bond.

The formation of compound **5.6** prompted us to explore the possibility if **5.6** could eliminate its hydride ligands to yield the unsaturated complex $Ru_2Pt_2(IMes)_2(CO)_8$, **5.10**. When compound **5.6** was heated in both benzene and toluene solution, no reaction was observed. Alternatively, compound **5.10** could be obtained by reaction of **5.3** with one equivalent of $Pt(IMes)_2$. However, the reaction of **5.3** in presence of 1 eq. of $Pt(IMes)_2$ for an hour, gave 38% of compound **5.4** and 6% of compound **5.2**. Also there was no reaction when H_2 was purged through solutions of **5.4**, both at room temperature and at 80 ^{o}C.

5.3. Conclusions

A goal of this work was to compare the reactivity of the bis-NHC complex $Pt(IMes)_2$ to that reported previously for the bis phosphine complexes $Pt(PR_3)_2$. It has been shown that $Pt(IMes)_2$ just like $Pd(P^tBu_3)_2$ and $Pt(P^tBu_3)_2$ is able to add its Pt(IMes) grouping across Ru-Ru bonds in ruthenium carbonyl cluster complexes. However, the different steric and electronic profile presented by the NHC versus PR_3 ligands has allowed isolation of new and different Ru–Pt–IMes bimetallic cluster compounds which have been prepared in reasonable yields. One major difference in reactivity is that whereas mononuclear complexes of Ru could not be obtained from the reaction of $Ru(CO)_5$ with $Pd(P^tBu_3)_2$ or $Pt(P^tBu_3)_2$ that picture changed in the successful preparation of complex **5.4**. In addition, possibly due to increased steric pressure, the bicapped structure presented by $Ru_3Pt_2(IMes)_2(CO)_{12}$ (**5.2**) differs from analogous reactions of the phosphine substituted complexes where edge bridging raft-like complexes are formed. The propensity of $Pt(IMes)_2$ to react with ruthenium carbonyl cluster complexes, represents a start for the incorporation of Pt-NHC groups into transition metal carbonyl cluster complexes. Additional studies to investigate the differing reactivities, particularly towards small molecule activation, of these and related complexes are in progress.

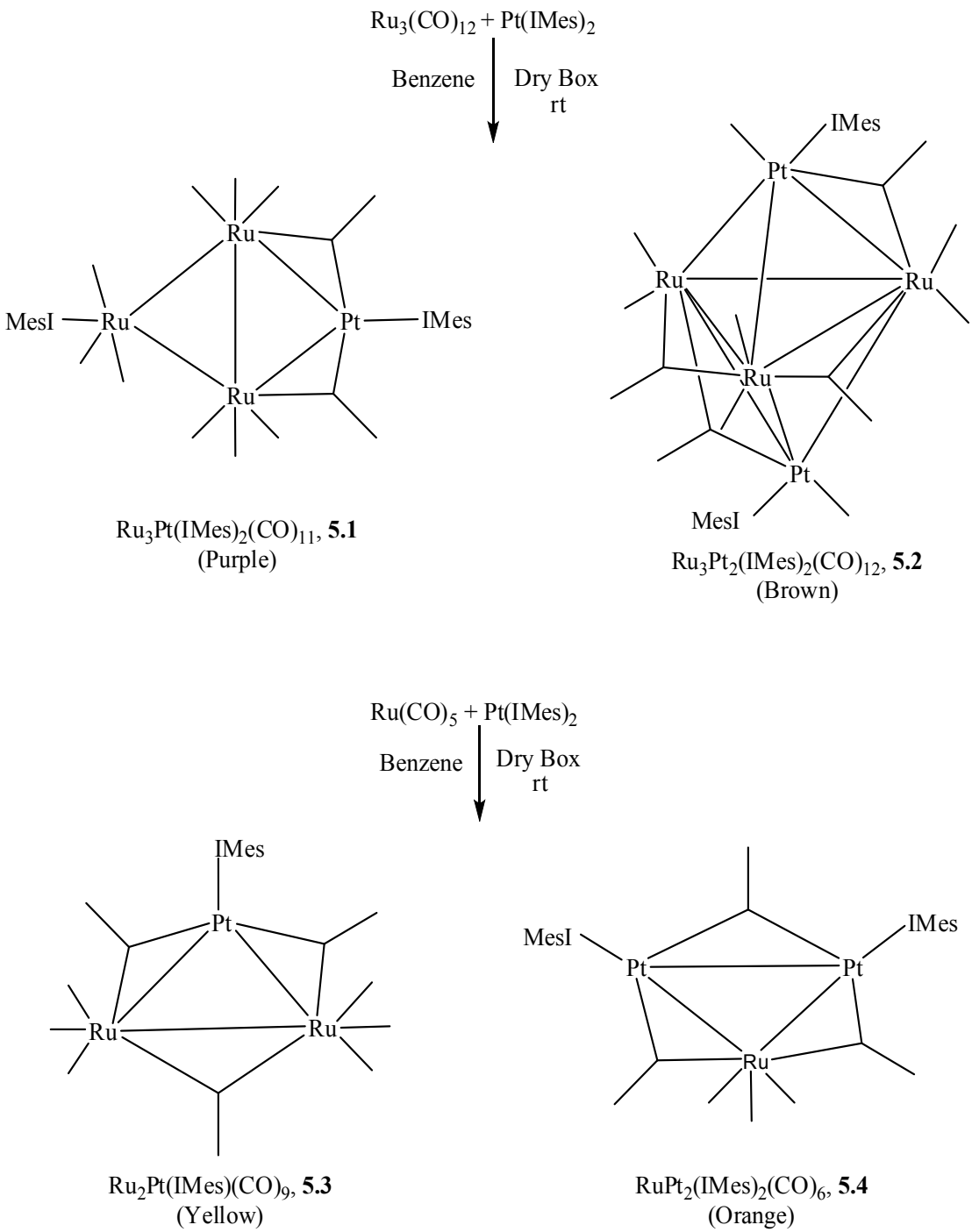
Ru3(CO)12 + Pt(IMes)2
Benzene
Dry Box
rt
Ru
MesI
Ru
Pt
IMes
Ru
Ru3Pt(IMes)2(CO)11, 5.1
(Purple)
IMes
Pt
Ru
Ru
Ru
Pt
MesI
Ru3Pt2(IMes)2(CO)12, 5.2
(Brown)
Ru(CO)5 + Pt(IMes)2
Benzene
Dry Box
rt
IMes
Pt
Ru
Ru
Ru2Pt(IMes)(CO)9, 5.3
(Yellow)
MesI
IMes
Pt
Pt
Ru
RuPt2(IMes)2(CO)6, 5.4
(Orange)

Scheme 5.1

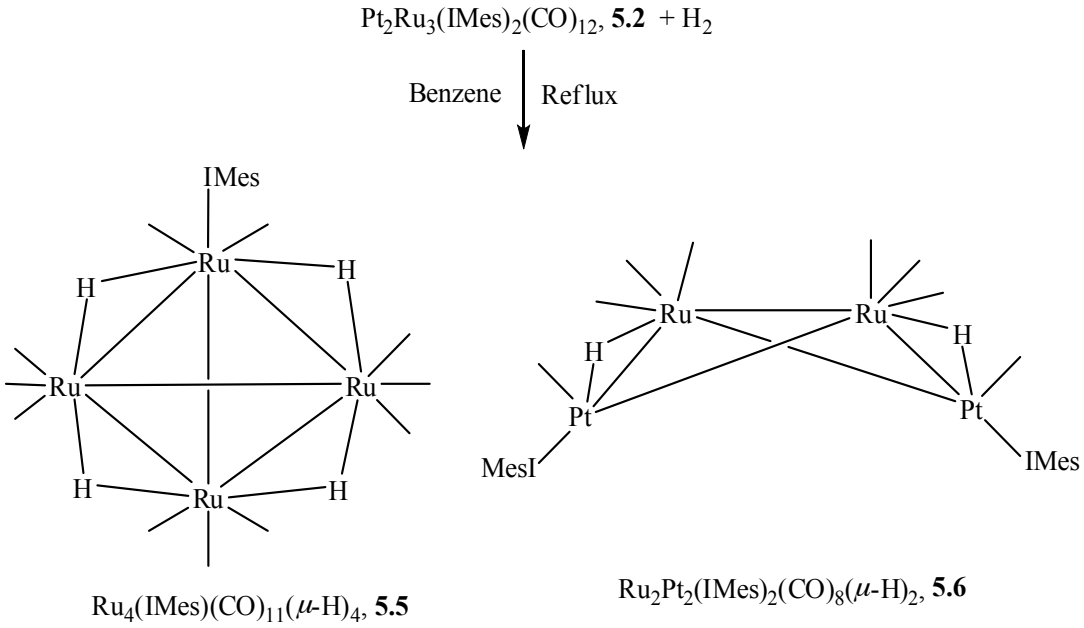

$Ru_4(IMes)(CO)_{11}(\mu\text{-}H)_4$, **5.5**

$Ru_2Pt_2(IMes)_2(CO)_8(\mu\text{-}H)_2$, **5.6**

Scheme 5.2

5.4. Experimental section

General data

Unless indicated otherwise, all reactions were performed under an atmosphere of Argon. Reagent grade solvents were dried by the standard procedures and were freshly distilled prior to use. Infrared spectra were recorded on a Nicolet 380 FT-IR spectrophotometer. ^{1}H NMR were recorded on a Bruker 400 and 500 spectrometer operating at 399.993 MHz and 500.06 MHz, respectively. Electrospray mass spectrometric measurements were obtained on a Bruker microTOF-Q II at the University of Miami, Coral Gables, FL, and mass spectrometric measurements performed by direct–exposure probe using electron impact ionization (EI) were made on a VG 70S instrument at the University of South Carolina, Columbia, SC. $Ru_3(CO)_{12}$ was purchased from Alfa Aesar and was used without further purification. 2,2'-Bis(1,3-dimesitylimidazol-2-ylidene)platinum(0), $Pt(IMes)_2$ was prepared according to the previously published

procedure,[99] and stored and handled in a dry box. Product separations were performed by TLC in air on Analtech silica gel GF 250 or 500 μm glass plates. Silica gel (60-200μm, 70-230 mesh) used for chromatographic separations was purchased from Silicycle. Florisil (F100-500, 60-100 mesh) used for product purifications was purchased from Fisher Scientific.

Reaction of $Ru_3(CO)_{12}$ with $Pt(IMes)_2$

A 20 mg (0.03 mmol) amount of $Ru_3(CO)_{12}$ and 84 mg (0.10 mmol) amount of $Pt(IMes)_2$ were dissolved in 20 mL of benzene in a 50 mL schlenk tube in a dry box. The solution was then stirred at room temperature for 5 min. at which time IR showed complete consumption of the starting $Ru_3(CO)_{12}$. The solvent was removed *in vacuo* and the product was separated by TLC on silica gel by using 2:1 hexane/methylene chloride solvent mixture to yield 9.2 mg (21%) of purple $Ru_3Pt(IMes)_2(CO)_{11}$, **5.1** and 13.4 mg (26%) of brown $Ru_3Pt_2(IMes)_2(CO)_{12}$, **5.2** and 3.5 mg (12%) of yellow $Ru_2Pt(IMes)(CO)_9$, **5.3**. Spectral data for **5.1**: IR ν_{CO} (cm^{-1} in hexane): 2076 (w), 2023 (m), 2001 (s), 1980 (w), 1957 (m), 1844 (m), 1795 (m). ^1H NMR (CD_2Cl_2 in ppm, 400 MHz): δ = 7.14 (s, 2 H, NCH), 7.11 (s, 4 H, *m*-H), 6.94 (s, 4 H, *m*-H), 6.78 (s, 2 H, NCH), 2.46 (s, 6 H, *p*-CH_3), 2.31 (s, 6 H, *p*-CH_3), 2.01 (s, 12 H, *o*-CH_3), 1.98 (s, 12 H, *o*-CH_3). ESI: *m/z* 1417 (M^+). The isotope distribution pattern is consistent with the presence of one platinum atom and three ruthenium atoms. Spectral data for **5.2**: IR ν_{CO} (cm^{-1} in methylene chloride): 2051 (w), 2012 (s), 1988 (m), 1963 (w), 1943 (m), 1869 (w), 1815 (m), 1743 (m). ^1H NMR (CD_2Cl_2 in ppm, 400 MHz): δ = 7.09 (s, 4 H, NCH), 6.87 (s, 8 H, *m*-H), 2.28 (s, 12 H, *p*-CH_3), 1.91 (s, 24 H, *o*-CH_3). ESI: *m/z* 1661 (M^+ + Na). The isotope distribution pattern is consistent with the presence of two platinum atoms and

three ruthenium atoms. Spectral data for **5.3**: IR ν_{CO} (cm^{-1} in methylene chloride): 2102 (w), 2084 (w), 2066 (m), 2025 (s), 1975 (m), 1836 (m), 1816 (m). ^1H NMR (C_6D_6 in ppm, 400 MHz): δ = 6.59 (s, 4 H, *m*-H), 6.26 (s, 2 H, NCH), 2.05 (s, 12 H, *o*-CH_3), 1.94 (s, 6 H, *p*-CH_3). ESI: *m/z* 977 (M^+ + Na). The isotope distribution pattern is consistent with the presence of one platinum atom and two ruthenium atoms.

Reaction of $Ru(CO)_5$ with $Pt(IMes)_2$

A solution of $Ru(CO)_5$ was prepared and used *in situ* as follows.[112] A 40 mg (0.06 mmol) amount of $Ru_3(CO)_{12}$ was dissolved in 120 mL of hexane in a 250 mL three-neck flask. The solution was placed in an ice-bath and was irradiated using a high-pressure mercury 1000 W UV lamp (American Ultraviolet Co.) at the 125 watts per inch setting while CO gas was bubbled through it for 15 min. During this time the orange colored solution turned colorless and IR showed the formation of $Ru(CO)_5$. The reaction flask was then evacuated and filled with argon several times to remove the excess CO gas. A 150 mg (0.19 mmol) amount of $Pt(IMes)_2$ was dissolved in 20 mL of benzene in a 50 mL schlenk tube in a dry box and then added to the $Ru(CO)_5$ solution at 0 ^oC via a cannula. The solution was then allowed to warm to room temperature and stirred for 10 min. at which time IR showed complete consumption of the starting $Ru(CO)_5$. The solvent was removed *in vacuo* and the product was separated by TLC on silica gel by using hexane solvent to yield 8.1 mg (15%) of yellow $Ru_2Pt(IMes)(CO)_9$, **5.3** and 14.0 mg (21%) of orange $RuPt_2(IMes)_2(CO)_6$, **5.4**. Spectral data for **5.4**: IR ν_{CO} (cm^{-1} in hexane): 2071 (m), 1999 (vs), 1970 (vs), 1808 (vs), 1781 (s). ^1H NMR (C_6D_6 in ppm, 400 MHz): δ = 6.65 (s, 8 H, *m*-H), 6.40 (s, 4 H, NCH), 2.16 (s, 24 H, *o*-CH_3), 2.08 (s, 12 H, *p*-CH_3). ESI: *m/z*

1291 (M^+ + Na). The isotope distribution pattern is consistent with the presence of two platinum atoms and one ruthenium atom.

Reaction of $Ru_3Pt_2(IMes)_2(CO)_{12}$, 5.2 with H_2

A 20 mg (0.03 mmol) amount of $Ru_3Pt_2(IMes)_2(CO)_{12}$, **5.2** was dissolved in benzene in a 50 mL 3-neck round-bottom flask equipped with a reflux condenser, stir bar and gas inlet. The solution was then purged with hydrogen (1 atm) for 15 min at 80 ^oC at which time IR showed complete consumption of the starting material, **5.2**. The solvent was removed *in vacuo* and the product was separated by TLC on silica gel by using 1:1 hexane/methylene chloride solvent mixture to yield 1.5 mg (12%) of yellow $Ru_4(IMes)(CO)_{11}(\mu\text{-}H)_4$, **5.5** and 6.2 mg (36%) of orange $Ru_2Pt_2(IMes)_2(CO)_8(\mu\text{-}H)_2$, **5.6**. Spectral data for **5.5**: IR ν_{CO} (cm^{-1} in hexane): 2083 (m), 2061 (w), 2048 (vs), 2028 (s), 2002 (m), 1986 (m), 1967 (w). ^1H NMR (C_6D_6 in ppm): δ = 6.78 (s, 4 H, m-H), 5.87 (s, 2 H, NCH), 2.09 (s, 6 H, p-CH_3), 1.92 (s, 12 H, o-CH_3), -17.67 (s, 4 H, hydride). EI/MS: *m/z* 1022 (M^+), 994 (M^+- CO). The isotope distribution pattern is consistent with the presence of four ruthenium atoms. Spectral data for **5.6**: IR ν_{CO} (cm^{-1} in hexane): 2046 (m), 2013 (vs), 2002 (w), 1988 (w), 1972 (s), 1950 (w), 1936 (m). ^1H NMR (CD_2Cl_2 in ppm, 500 MHz): δ = 7.00 (s, 4 H, NCH), 6.91 (s, 4 H, *m*-H), 6.84 (s, 4 H, *m*-H), 2.27 (s, 12 H, *p*-CH_3), 2.01 (s, 12 H, *o*-CH_3), 1.83 (s, 12 H, *o*-CH_3), -9.89 (s, 2 H, $^1J_{Pt\text{-}H}$ = 560 Hz, $^2J_{Pt\text{-}H}$ = 40 Hz ,hydride). ESI: *m/z* 1428 (M^+). The isotope distribution pattern is consistent with the presence of two platinum atoms and two ruthenium atoms.

Reaction of $Ru_2Pt(IMes)(CO)_9$, 5.3 with $Pt(IMes)_2$

A 20 mg (0.02 mmol) amount of $Ru_2Pt(IMes)(CO)_9$, **5.3** was dissolved in 20 mL of benzene in a 50 mL 3-neck round-bottom flask equipped with a reflux condenser. A 17

mg (0.02 mmol) amount of $Pt(IMes)_2$ was dissolved in 10 mL of benzene in a 25 mL schlenk tube in a dry box and added to the solution of compound **5.3** through cannula. The solution was then refluxed at 80 ^oC for 60 min. at which time IR showed complete consumption of the starting material, **5.3**. The solvent was removed *in vacuo* and the product was separated by TLC on silica gel by using 2:1 hexane/methylene chloride solvent mixture to yield 10.0 mg (38%) of orange $RuPt_2(IMes)_2(CO)_6$, **5.4** and 2.0 mg (6%) of brown $Ru_3Pt_2(IMes)_2(CO)_{12}$, **5.2**.

Note: Same result was obtained when trimethyl amine N-oxide, Me_3NO, was added to a benzene solution of $Ru_2Pt(IMes)(CO)_9$, **5.3** and $Pt(IMes)_2$.

Reaction of $RuPt_2(IMes)_2(CO)_6$, 5.4 with $Ru(CO)_5$

A solution of $Ru(CO)_5$ was prepared and used *in situ* as follows.[112] A 20 mg (0.03 mmol) amount of $Ru_3(CO)_{12}$ was dissolved in 20 mL of hexane in 50 mL three-neck flask equipped with a reflux condenser. The solution was placed in an ice-bath and was irradiated using a high-pressure mercury 1000 W UV lamp (American Ultraviolet Co.) at the 125 wpi setting while CO gas was bubbled through it for 10 min. During this time the orange colored solution turned colorless and $Ru(CO)_5$ was formed. The reaction flask was then evacuated and filled with argon to remove the excess CO gas. A 40 mg (0.03 mmol) amount of $RuPt_2(IMes)_2(CO)_6$, **5.4** was dissolved in 10 mL of benzene in a 25 mL schlenk tube and added to the $Ru(CO)_5$ solution through cannula. The solution was then refluxed at 80 ^oC for 60 min. at which time IR showed complete consumption of the starting material, **5.4**. The solvent was removed *in vacuo* and the product was separated by TLC on silica gel by using 2:1 hexane/methylene chloride solvent mixture to yield

26.2 mg (87%) of yellow $Ru_2Pt(IMes)(CO)_9$, **5.3** and 4.7 mg (9%) of brown $Ru_3Pt_2(IMes)_2(CO)_{12}$, **5.2**.

5.5. Crystallographic analyses

Single crystals of **5.1**, **5.3** and **5.6** suitable for diffraction analysis were all grown by slow evaporation of solvent from solutions in methylene chloride/hexane solvent mixture at -25 °C. Single crystals of compound **5.2** and **5.5** suitable for diffraction analysis were grown by slow evaporation of solvent from solutions in methylene chloride/toluene/octane and ether solvent mixture respectively at -25 °C. Single crystals of compound **5.4** suitable for diffraction analysis were grown by slow evaporation of solvent from solutions in benzene/octane solvent mixture at 5 °C. The data crystals for **5.1**, **5.3, 5.4** and **5.5** were glued onto the end of a thin glass fiber. The data crystals for **5.2** and **5.6** were mounted onto the end of a thin glass fiber using Paratone-N. X-ray intensity data were measured by using a Bruker SMART APEX2 CCD-based diffractometer using Mo Kα radiation (λ = 0.71073 Å).[50] The raw data frames were integrated with the SAINT+ program by using a narrow-frame integration algorithm.[50] Corrections for Lorentz and polarization effects were also applied with SAINT+. An empirical absorption correction based on the multiple measurement of equivalent reflections was applied using the program SADABS. All structures were solved by a combination of direct methods and difference Fourier syntheses, and refined by full-matrix least-squares on F^2, by using the SHELXTL software package.[51] All non-hydrogen atoms were refined with anisotropic displacement parameters. Hydrogen atoms were placed in geometrically idealized positions and included as standard riding atoms during the least-squares

refinements. Crystal data, data collection parameters, and results of the analyses are listed in Tables D.1, D.2 and D.3.

Compounds **5.1, 5.2, 5.4** and **5.6** crystallized in the monoclinic crystal system. For compounds **5.1** and **5.4**, the systematic absences in the intensity data were consistent with the unique space group $P2_1/c$. For compound **5.1**, with Z = 8 there are two formula equivalents of the complex in the asymmetric crystal unit. The R value is high because of poor data quality and the large number of parameters. Low temperature data set at 100 K also gave results with high R values. Several attempts were made to obtain "better" quality crystals from various different solvents, however, only thin tiny plates were obtained, or large blocks of crystals which were severely twinned. Other characterization data (provided above) is consistent with the solved structure. For compound **5.4**, the largest peak in the difference map of 7.935 e^- / $Å^3$, is located 0.79 Å from Ru1 and 0.84 Å from C14. However, final refinement gave low R values (4.97 %) and its structure is in agreement with other characterization data provided above. For compound **5.2**, the systematic absences in the intensity data were consistent with the unique space group $P2_1/n$. For compound **5.2**, a chemically reasonable starting solution provided good positions for all Pt, Ru, and most O, N and C atoms, but yielded negative thermal parameters for some of the non-heavy metal atoms, high R factors (R1 ~ 25 %), some large electron density peaks which are chemically unreasonable, a systematic pattern of Fobs >> Fcalc, and all attempts to solve the structure in the orthorhombic crystal system were unsuccessful considering the beta angle was very close to 90 °, which is indicative of some form of crystal twinning. The appropriate twin law common for a monoclinic system with the beta angle close to 90 ° is a 2-fold rotation about the [100] direction. The

corresponding twin law is, by rows, {1 0 0/0 $\bar{1}$ 0/0 0 $\bar{1}$}. This twin law was implemented in the final refinement stages to give low R factors (R1 = 4.85%) and good thermal parameters. The highest peak in the final difference Fourier map was 3.970 e^- / $Å^3$, located 0.99 Å from atom Pt(1). The final refined batch scale factor indicated the crystal to be composed of two twin domains of percentage 0.5209(4)/0.4791(4). For compound **5.6**, the systematic absences in the intensity data were consistent with the space groups *C*2, *C*2/*m* or *Cm*. The structure could only be solved in the space group *C*2. Hydrides in this structure were not located crystallographically but their presence was confirmed by ^{1}H NMR. Two molecules of CH_2Cl_2 from the crystallization solvent co-crystalized with the complex, and were included in the crystal analysis.

Compounds **5.3** and **5.5** crystallized in the triclinic crystal system. The space groups $P\ \bar{1}$ was chosen for both and confirmed by the successful solution and refinement of the structure. The hydride ligands in **5.5** were located and refined successfully with isotropic thermal parameters. Atoms H1 and H4 were refined with a fixed isotropic thermal parameter.

References

1. (a) Hieber, W.; Schulten, H. *Z. Anorg. Allg. Chem.* **1937**, *232*, 17. (b) Hieber, W.; Fischer, E. O.; Bockly, E. *Z. Anorg. Allg. Chem.* **1952**, *269*, 308.

2. Adams, R. D.; Captain, B. *J. Organomet. Chem.* **2004**, *689*, 4521.

3. (a) Coffey, E. C.; Lewis, J.; Nyholm, R. S. *J. Chem. Soc.* **1964**, 1741. (b) Kasenally, A. S.; Nyholm, R. S.; O'Brien, R. J.; Stiddard, M. H. B. *Nature* **1964**, 871.

4. Abel, E. W.; Singh, A.; Wilkinson, G. *J. Chem. Soc.* **1960**, 1321.

5. King, R. B.; Treichel, P. M.; Stone, F. G. A. *Chem. Ind. (London)* **1961**, 747.

6. Tilney-Bassett, J. F. *Proc. Chem. Soc.* **1960**, 419.

7. Madach, T.; Vahrenkamp, H. *Chem. Ber.* **1980**, *113*, 2675.

8. (a) Chini, P.; Colli, L.; Peraldo, M. *Gazz. Chim. Ital.* **1960**, *90*, 1005. (b) Chini, P. *Inorg. Chim. Acta Rev.* **1968**, *2*, 31.

9. Ceriotti, A.; Demartin, F.; Longoni, G.; Manassero, M.; Marchionna, M.; Piva, G.; Sansoni, M. *Angew. Chem., Int. Ed. Engl.* **1985**, *24*, 697.

10. Demartin, F.; Femoni, C.; Carmela Iapalucci, M.; Longoni, G.; Macci, P. *Angew. Chem., Int. Ed. Engl.* **1999**, *38*, 531.

11. Zhang, J. M.; Dahl, L. F. *J. Chem. Soc., Dalton Trans.* **2002**, 1269.

12. Doyle, G.; Eriksen, K. A.; Van Engen, D. *J. Am. Chem. Soc.* **1986**, *108*, 445.

13. Chetcuti, M. J.; Gordon, J. C.; Fanwick, P. E. *Inorg. Chem.* **1990**, *29*, 3781.

14. Adams, R. D.; Barnard, T. S.; Li, Z.; Wu, W.; Yamamoto, J. *Organometallics* **1994**, *13*, 2357.

15. Adams, R. D.; Captain, B.; Fu, W. *J. Clust. Sci.* **2001**, *12*, 303.

16. (a) Sinfelt, J. H. Bimetallic Catalysts. Discoveries, Concepts and Applications, Wiley, New York, **1983.** (b) Sinfelt, J. H. *Adv. Chem. Eng.* **1964**, *5*, 37. (c) Sinfelt, J. H. *Sci. Am.* **1985**, *253*, 90. (d) Sinfelt, J. H. *Acc. Chem. Res.* **1977**, *10*, 15. (e) Sachtler, W. M. H. *J. Mol. Catal.* **1984**, *25*, 1. (f) Guczi, L. *J. Mol. Catal.* **1984**, *25*, 13. (g) Sachtler, W. M. H.; van Santen, R. A. *Adv. Catal.* **1977**, *26*, 69.

17. (a) Oh, S. H.; Carpenter, J. E. *J. Catal.* **1986**, *98*, 178. (b) Wang, T.; Schmidt, L. D. *J. Catal.* **1981**, *71*, 411. (c) Barbier Jr., J.; Duprez, D. *Appl. Catal. B Environ.* **1994**, *4*, 105.

18. (a) Desai, S.; Neurock, M. *Electrochim. Acta* **2003**, *48*, 3759. (b) Steigerwalt, E. S.; Deluga, G. A.; Cliffel, D. E.; Lukehart, C. M. *J. Phys. Chem. B* **2001**, *105*, 8097. (c) Rolison, D. R.; Hagans, P. L.; Swider, K. E.; Long, J. W. *Langmuir* **1999**, *15*, 774. (d) Hogarth, M. P.; Hards, G. A. *Platinum Met. Rev.* **1996**, *40*, 150.

19. Raja, R.; Sankar, G.; Hermans, S.; Shephard, D. S.; Bromley, S. T.; Thomas, J. M.; Maschmeyer, T.; Johnson, B. F. G. *Chem. Commun.* **1999**, 1571.

20. (a) Thomas, J. M.; Raja, R.; Sankar, G.; Johnson, B. F. G.; Lewis, D. W. *Chem. Eur. J.* **2001**, *7*, 2973-2978. (b) Thomas, J. M.; Raja, R.; Sankar, G.; Bell, R. G.; Lewis, D. W. *Pure Appl. Chem.* **2001**, *73*, 1087-1101.

21. Thomas, J. M.; Johnson, B. F. G.; Raja, R.; Sankar, G.; Midgley, P. A. *Acc. Chem. Res.* **2003,** *36*, 20.

22. Klooster, W. T.; Koetzle, T. F. *J. Am. Chem. Soc.* **1994**, *116*, 7677.

23. Koetzle, T.; Schultz, A. *Top. Catal.* **2005**, *32*, 251.

24. Kubas, G. J. *J. Organomet. Chem.* **2009**, *694*, 2648.

25. Kubas, G. J. *Science* **2006**, *314*, 1096.

26. Adams, R. D.; Captain, B. *Angew. Chem. Int. Ed.* **2008**, *47*, 252.

27. Xiao, J.; Kristof, E.; Vittal, J. J.; Puddephatt, R. J. *J. Organomet. Chem.* **1995**, *490*, 1.

28. Church, M. J.; Mays, M. J.; Simpson, R. N. F.; Stefanini, F. P. *J. Chem. Soc. (A)* **1970**, 2909.

29. Lee, J. C.; Peris, E.; Rheingold, A. L.; Crabtree, R. H. *J. Am. Chem. Soc.* **1994**, *116*, 11014.

30. Weller, A. S.; McIndoe, J. S. *Eur. J. Inorg. Chem.* **2007**, *2007*, 4411.

31. Otsuka, S.; Yoshida, T.; Matsumoto, M.; Nakatsu, K. *J. Am. Chem. Soc.* **1976**, *98*, 5850.

32. Gandolfi, C.; Heckenroth, M.; Neels, A.; Laurenczy, G. b.; Albrecht, M. *Organometallics* **2009**, *28*, 5112.

33. Samantaray, M. K.; Shaikh, M. M.; Ghosh, P. *Organometallics* **2009**, *28*, 2267.

34. Zenkina, O. V.; Keske, E. C.; Wang, R.; Crudden, C. M. *Organometallics* **2011**, *30*, 6423.

35. Jia, G.; Meek, D. W. *Inorg. Chem.* **1991**, *30*, 1953.

36. Arnold, P. L.; Cloke, F. G. N.; Geldbach, T.; Hitchcock, P. B. *Organometallics* **1999**, *18*, 3228.

37. Turculet, L.; Feldman, J. D.; Tilley, T. D. *Organometallics* **2003**, *22*, 4627.

38. (a) Armor, J. N. *Catal. Lett.* **2005**, *101*, 131-135. (b) Thomas, J. M.; Raja, R.; Johnson, B. F. G.; Hermans, S.; Jones, M. D.; Khimyak, T. *Ind. Eng. Chem. Res.* **2003**, *42*, 1563-1570.

39. (a) Collman, J. P.; Hegedus, L. S.; Norton, J. R.; Finke, R. G. Principles and Applications of Organotransition Metal Chemistry, University Science Books, Mill Valley, **1987**, chap. 10. (b) "Catalysis by Metals and Alloys": Ponec, V.; Bond, G. C.; *Stud. Surf. Sci. Catal.* **1995**, 95.

40. Farrugia, L. J.; Green, M.; Hankey, D. R.; Orpen, A. G.; Stone, F. G. A. *J. Chem. Soc. Chem. Commun.* **1983**, 310-312.

41. (a) Adams, R. D.; Captain, B.; Beddie, C.; Hall, M. B. *J. Am. Chem. Soc.* **2007**, *129*, 986-1000. (b) Adams, R. D.; Captain, B. *Angew. Chem.* **2005**, *117*, 2587-2589; *Angew. Chem. Int. Ed.* **2005**, *44*, 2531-2533.

42. (a) Adams, R. D.; Captain, B.; Smith, M. D.; Beddie, C.; Hall, M. B. *J. Am. Chem. Soc.* **2007**, *129*, 5981-5991. (b) Adams, R. D.; Captain, B.; Smith, M. D. *Angew. Chem.* **2006**, *118*, 1127-1130; *Angew. Chem. Int. Ed.* **2006**, *45*, 1109-1112.

43. (a) Thomas, J. M.; Johnson, B. F. G.; Raja, R.; Sankar, G.; Midgley, P. A. *Acc. Chem. Res.* **2003**, *36*, 20-30. (b) Hermans, S.; Raja, R.; Thomas, J. M.; Johnson, B. F. G.; Sankar, G.; Gleeson, D. *Angew. Chem., Int. Ed.* **2001**, *40*, 1211-1215. (c) Johnson, B. F. G.; Raynor, S. A.; Brown, D. B.; Shephard, D. S.; Mashmeyer, T.; Thomas, J. M.; Hermans, S.; Raja, R.; Sankar, G. *J. Mol. Catal. A: Chem* **2002**, *182-183*, 89-97. (d) Johnson, B. F. G. *Coord. Chem. Rev.* **1999**, *190-192*, 1269-1285. (e) Hungria, A. B.; Raja, R.; Adams, R. D.; Captain, B.; Thomas, J. M.; Midgley, P. A.; Golvenko, V.; Johnson, B. F. G. *Angew. Chem. Int. Ed.* **2006**, *45*, 4782-4785. (f) Adams, R. D.; Blom, D. A.; Captain, B.; Raja, R.; Thomas, J. M.; Trufan, E. *Langmuir* **2008**, *24*, 9223-9226. (g) Siani, A.; Alexeev, O. S.; Captain, B.; Lafaye, G.; Marécot, P., Adams, R. D.; Amiridis, M. D. *J. Catal.* **2008**, *255*, 162-179.

44. (a) Sinfelt, J. H., *Bimetallic Catalysts. Discoveries, Concepts and Applications*; Wiley: New York, **1983**. (b) Sachtler, W. M. H. *J. Mol. Catal.* **1984**, *25*, 1-12.
45. (a) Goodman, D. W.; Houston, J. E. *Science* **1987**, *236*, 403-409. (b) Ichikawa, M. *Adv. Catal.* **1992**, *38*, 283-400.

46. (a) Kustov, A. L.; Frey, A. M.; Larsen, K. E.; Johannessen T.; Nørskov, J. K.; Christensen, C. H. *Appl. Catal., A* **2007**, *320*, 98-104. (b) Ishihara, T.; Eguchi, K.; Arai, H. *Appl. Catal.* **1987**, *30*, 225-238. (c) Tee, Y-H; Grulke, E.; Bhattacharyya, D. *Ind. Eng. Chem. Res.* **2005**, *44*, 7062-7070. (d) Schrick, B.; Blough, J. L.; Jones, A. D.; Mallaouk, T. E. *Chem. Mater.* **2002**, *14*, 5140-5147. (e) Park, C.; Baker, R. T. K. *J. Catal.* **2000**, *190*, 104-117. (f) Kibria, A. K. M. F.; Mo, Y. H.; Nahm K. S. Catal. Lett. **2001**, *71*, 229-236. (g) Kumbhar, P. S.; Kharkar, M. R.; Yadav, G. D.; Rajadhyaksha, R. A. *J. Chem. Soc., Chem. Commun.* **1992**, 584-586.

47. Pergola, R. D.; Fumagalli, A.; Garlaschelli, L.; Manassero, C.; Manassero, M.; Sansoni, M.; Sironi, A. *Inorg. Chim. Acta* **2008**, *361*, 1763-1769.

48. (a) Braye, E. H.; Dahl, L. H.; Hübel, W.; Wampler, D. L. *J. Am. Chem. Soc.* **1962**, *84*, 4633-4639. (b) Tachikawa, M.; Geerts, R. L.; Muetterties, E. L. *J. Organometal. Chem.* **1981**, *213*, 11-24. (c) Hriljac, J. A.; Harris, S.; Shriver, D.F. *Inorg. Chem.* **1988**, *27*, 816-821.

49. Yempally, V.; Zhu, L.; Captain, B. *J. Cluster Sci.* **2009**, *20*, 695-705.

50. Apex2 Version 2.2-0 and SAINT+ Version 7.46A; Bruker Analytical X-ray System, Inc., Madison, Wisconsin, USA, **2007**.

51. (a) Sheldrick, G. M. SHELXTL Version 6.1; Bruker Analytical X-ray Systems, Inc., Madison, Wisconsin, USA, **2000**. (b) Sheldrick, G. M. *Acta Cryst*. **2008**, *A64*, 112–122.

52. Bogdan, P. L.; Sabat, M.; Sunshine, S. A.; Woodcock, C.; Shriver, D. F. *Inorg. Chem.* **1988**, *27*, 1904-1910.

53. (a) Mingos, D. M. P. *Acc. Chem. Res.* **1984**, *17*, 311-319. (b) Mingos, D. M. P. *Introduction to Cluster Chemistry*; Prentice Hall: Engelwood Cliffs, NJ, **1990**; Chapter. 2.

54. Adams, R. D.; Wu, W. *J. Cluster Sci.* **1991**, *2*, 271-290.

55. (a) Kovacs, A.; Frenking, G. *Organometallics* **2001**, *20*, 2510-2524. (b) Varshavsky, Y.S.; Galding, M.R.; Cherkasova, T.G.; Smirnov, S.N.; Khrustalev. V.N. *J. Organometal. Chem.*, **2007**, *692,* 5788-5794.

56. (a) Kukushkin, Y. N.; Aleksandrova, E. A.; Pakhomova, T. B.; Vlasova, R. A. *Zh. Obshch. Khim.* **1994**, *64*, 70507. (b) Intini, F. P.; Pellicani, R. Z.; Boccarelli, A.; Sasanelli, R.; Coluccia, M.; Natile, G. *Eur. J. Inorg. Chem.* **2008**, 4555-4561.

57. (a) Jesson, J. P.; Muetterties, E. L. In *Dynamic Nuclear Magnetic Resonance Spectroscopy*; Jackman, L., Cotton, F. A., Eds.; Academic Press: New York, **1975**; Chapter 8. (b) Adams, R. D.; Cotton, F. A. In *Dynamic Nuclear Magnetic Resonance Spectroscopy*; Jackman, L., Cotton, F. A., Eds.; Academic Press: New York, **1975**; Chapter 12. (c) Johnson, B. F. G.; Benfield, R. E. In *Transition Metal Clusters*; Johnson, B. F. G., Ed.; Wiley, Chichester, U.K., **1980**; Chapter 7. (d) Muetterties, E. L.; Band, E. *Chem. Re*v. **1978**, *78*, 639-658. (e) Aime, S.; Dastru, W.; Gobetto, R.; Krause, J.; Violano, L. *Inorg. Chim. Acta* **1995**, *235*, 357-366. (f) Adams, R.D.; Captain, B.; Fu, W. *J. Cluster Sci.* **2001**, *12*, 303-312.

58. (a) Johnson, B. F. G.; Lewis, J.; Nicholls, J. N.; Oxton, I. A.; Raithby, P. J.; Rosales, M. J. *Chem. Commun.* **1982**, 289-290. (b) Dyson, P. J. *Adv. Organomet. Chem.* **1998**, *43*, 43-124.

59. Raja, R.; Khimyak, T.; Thomas, J. M.; Hermans, S.; Johnson, B. F. G. *Angew. Chem. Int. Ed. Engl.* **2001**, 4638–4642.

60. Raja, R.; Sankar, G.; Hermans, S.; Shephard, D. S.; Bromley, S.; Thomas, J. M.; Johnson, B. F. G.; Maschmeyer, T. *Chem. Commun.* **1999**, *16*, 1571–1572.

61. Castiglioni, M.; Giordano, R.; Sappa, E. *J. Mol. Catal.* **1987**, *40*, 65-69.

62. Das, P. C.; Pradhan, N. C.; Dalai, A. K.; bakshi, N. N. *Fuel Processing Technology* **2004**, *85*, 1487-1501.

63. Rangan, M.; Yung, M. M. *Catal. Lett.* **2012**, *142*, 718-727.

64. Khimyak, T.; Johnson, B. F. G. *J. Cluster Sci.* **2004**, *15*, 543-558.

65. Lanfranchi, M.; Tiripicchio, A.; Sappa, E.; Carty, A. J. *J. Chem. Soc. Dalton Trans.* **1986**, 2737-2740.

66. Brivio, E.; Ceriotti, A.; Della Pergola, R.; Garlaschelli, L.; Manassero, M.; Sansoni, M. *J. Cluster Sci.* **1995**, *6*, 271-287.

67. Saha, S.; Zhu, L.; Captain, B. *Inorg. Chem.* **2010**, *49*, 3465-3472.

68. Nicholls, J. N.; Vargas, M. D.; Hriljac, J.; Sailor, M. *Inorg. Synth*. **1989**, *26*, 283.

69. (a) Johnson, B. F. G.; Lewis, J.; Williams, I. G. *J. Chem. Soc. (A)* **1968**, 2865. (b) Eady, C. R.; Johnson, B. F. G.; Lewis, J. *J. Chem. Soc. Dalton Trans.* **1975**, 2606. (c) Braga, D.; Grepioni, F.; Righi, S.; Dyson, P. J.; Johnson, B. F. G.; Bailey, P.

J.; Lewis, J. *Organometallics* **1992**, *11*, 4042-4048. (d) Dyson, P. J.; Johnson, B. F. G.; Reed, D.; Braga, D.; Grepioni, F.; Parisini, E. *J. Chem. Soc. Dalton Trans.* **1993**, 2817-2815. (e) Dyson, P. J.; Johnson, B. F. G.; Lewis, J.; Martinelli, M.; Braga, D.; Grepioni, F. *J. Am. Chem. Soc.* **1993**, *115*, 9062-9068. (f) Braga, D.; Grepioni, F.; Sabatino, P.; Dyson, P. J.; Johnson, B. F. G.; Lewis, J.; Bailey, P. J.; Raithby, P. R.; Stalke, D. *J. Chem. Soc. Dalton Trans.***1993**, 985-992. (g) Bailey, P. J.; Braga, D.; Dyson, P. J.; Grepioni, F.; Johnson, B. F. G.; Lewis, J.; Sabatino, P. *Chem. Commun.* **1992**, 177-178. (h) Wing-Sze Hui, J.; Wong, W-T *J. Organomet. Chem.* **1996**, *524*, 211-217. (i) Mallors, R. L.; Blake, A. J.; Parsons, S.; Johnson, B. F. G.; Dyson, P. J.; Braga, D.; Grepioni, F.; Parisini, E. *J. Organomet. Chem.* **1997**, *532*, 133-142.

70. (a) Adams, R. D.; Wu, W. *Polyhedron* **1992**, *11*, 2123-2124. (b) Gomez-Sal, M. P.; Johnson, B. F. G.; Lewis, J.; Raithby, P. R.; Wright, A. H. *Chem. Commun.* **1985**, 1682-1684. (c) Dyson, P. J.; Johnson, B. F. G.; Lewis, J.; Braga, D.; Sabatino, P. *Chem. Commun*. **1993**, 301-302. (d) Braga, D.; Sabatino, P.; Dyson, P. J.; Blake, A. J.; Johnson, B. F. G. *J. Chem. Soc. Dalton Trans.* **1994**, 393-399.

71. (a) Adams, R. D.; Captain, B.; Pellechia, P. J.; Zhu, L. *Inorg. Chem.* **2004**, *43*, 7243-7249. (b) Adams, R. D.; Captain, B.; Fu, W.; Hall, M. B.; Manson, J.; Smith, M. D.; Webster, C. E. *J. Am. Chem. Soc.* **2004**, *126*, 5253-5267.

72. (a) Farrugia, L. J. *Acta Crystallogr., Sect.C: Cryst. Struct. Commun.* **1988**, *44*, 997-998. (b) Dyson, P. J.; Johnson, B. F. G.; Braga, D.; Grepioni, F.; Martin, C. M.; Parisini, E. *Inorg. Chim. Acta* **1995**, *235*, 413-420. (c) Braga, D.; Grepioni, F.; Parisini, E.; Dyson, P. J.; Johnson, B. F. G.; Reed, D.; Shepherd, D. S.; Bailey, P. J.; Lewis, J. *J. Organomet. Chem.* **1993**, *462*, 301-308.

73. (a) Lafaye, G.; Micheaud-Especel, C.; Montassier, C.; Marecot, P.; *Appl. Catal. A* **2002**, *230*, 19. (b) Didillon, B.; Candy, J. P.; Lepepetier, F.; Ferretti, O. A.; Basset, J. M. *Stud. Surf. Sci. Catal.* **1993**, *78*, 147. (c) Lafaye, G.; Mihut, C.; Especel, C.; Marecot, P.; Amiridis, M. D. *Langmuir* **2004**, *20*, 10612.

74. Bodnar, Z.; Mallat, T.; Bakos, I.; Szabo, S.; Zsoldos, Z.; Schay, Z. *Appl. Catal. A* **1993**, *102*, 105-123.

75. (a) Hermans, S.; Johnson, B. F. G. *Chem. Commun.* **2000**, 1955. (b) Raja, R.; Khimyak, T.; Thomas, J. M.; Hermans, S.; Johnson, B. F. G. *Angew. Chem., Int. Ed.* **2001**, *40*, 4638. (c) Tijani, A.; Coq, B.; Figueras, F. *Appl. Catal.* **1991**, *76*, 255. (d) Sanchez-Sierra, M. C.; Garcı´a-Ruiz, J.; Proietti, M. G.; Blasco, J. *J. Mol. Catal. A* **1996**, *108*, 95.

76. Adams, R. D.; Captain, B.; Fu, W. *J. Organomet. Chem.* **2003**, *671*, 158-165.

77. Adams, R. D.; Captain, B.; Fu, W. *Inorg. Chem.* **2003**, *42*, 1328-1333.

78. Adams, R. D.; Captain, B.; Zhu, L. *Inorg. Chem.* **2005**, *44*, 6623-6631.

79. Adams, R. D.; Captain, B.; Trufan, E. *J. Cluster Sci.* **2007**, *18*, 642-659.

80. Adams, R. D.; Boswell, E.M.; Captain, B.; Patel, M. A. *Inorg. Chem.* **2007**, *46*, 533-540.

81. Adams, R. D.; Kan, Y.; Rassolov, V.; Zhang, W. *J. Organomet. Chem.* **2013**, *730*, 20-31.

82. Kawano, Y.; Sugawara, K.; Tobita, H.; Ogino, H. *Chem. Lett.* **1994**, *2*, 293-296.

83. Gusbeth, P.; Vahrenkamp, H. *Chem. Ber. 1985*, *118*, 1746-1757.

84. Gusbeth, P.; Vahrenkamp, H. *Chem. Ber. 1985*, *118*, 1770-1781.

85. Anema, S. G.; Mackay, K. M.; Nicholson, B. K.; Tiel, M. V. *Organometallics* **1990**, *9*, 2436-2442.

86. Mobarok, Md H.; McDonald, R.; Ferguson, M. J.; Cowie, M. *Inorg. Chem.* **2012**, *51*, 4020-4034.

87. Elder, M.; Hall, D. *Inorg. Chem.* **1969**, *8*, 1424-1427.

88. Leong, W. K.; Einstein, F. W. B.; Pomeroy, R. K. *Organometallics* **1996**, *15*, 1589-1596.

89. Du, V. A.; Stipicic, G. N.; Bendova, M.; Schubert, U. *Monatsh. Chem.* **2010**, *141*, 671-675.

90. (a) Mingos, D. M. P. *Acc. Chem. Res.* **1984**, *17*, 311-319. (b) Cotton, F. A. *Chemical Applications of Group Theory*; John Wiley & Sons, Inc., NY, **1990**; Third Edition, Chapter 8.

91. Adams, R. D.; Boswell, E. M.; Captain, B.; Hungria, A. B.; Midgley, P. A.; Raja, R.; Thomas, J. M. *Angew. Chem., Int. Ed.* **2007**, *46*, 8182-8185.

92. Draeger, V. M.; Ross, L. *Z. anorg. allg. Chem.* **1980**, *469*, 115-122.

93. Amadoruge, M. L.; Rheingold, A. L.; Weinert, C. S. *Acta Cryst.* **2009**, *E65*, o2186.

94. Arii, H.; Nanjo, M.; Mochida, K. *Organometallics* **2008**, *27*, 4147-4151.

95. Zirngast, M.; Flock, M.; Baumgartner, J.; Marschner, C. *J. Am. Chem. Soc.* **2009**, *131*, 15952-15962.

96. Adams, R. D.; Captain, B.; Fu, W.; Smith, M. D. *Inorg. Chem.* **2002**, *41*, 5593-5601.

97. (a) Bau, R.; Drabnis, M. H. *Inorg. Chim. Acta* **1997**, *259*, 27-50. (b) Teller, R. G.; Bau, R. *Struc. Bonding* **1981**, *41*, 1-82.

98. Hermans, S.; Johnson, B. F. G. *Chem. Commun.* **2000**, *19*, 1955-1956.

99. Arduengo, A. J., III; Gamper, S. F.; Calabrese, J. C.; Davidson, F. J. Am. Chem. Soc. 1994, 116, 4391-4394.

100. (a) Nolan, S. P., Ed. N-Heterocyclic Carbenes in Synthesis; Wiley-VCH: Weinheim, Germany, 2006. (b) Glorius, F. N-Heterocyclic Carbenes in Transition Metal Catalysis; Springer: Berlin, 2007.

101. (a) Weskamp, T.; Schattenmann, W. C.; Spiegler, M.; Herrmann, W. A. *Angew. Chem., Int. Ed.* **1998**, *37*, 2490-2493. (b) Huang, J.; Stevens, E. D.; Nolan, S. P.; Petersen, J. L. *J. Am. Chem. Soc.* **1999**, *121*, 2674-2678. (c) Scholl, M.; Ding, S.; Lee, C. W.; Grubbs, R. H. *Org. Lett.* **1999**, *1*, 953-956. (d) Huang, J.; Stevens, E. D.; Nolan, S. P. *Organometallics* **2000**, *19*, 1194-1197. (e) Choi, T. L.; Grubbs, R. H. *Angew. Chem., Int. Ed.* **2003**, *42*, 1743-1746.

102. (a) Grasa, G. A.; Viciu, M. S.; Huang, J.; Nolan, S. P. *J. Org. Chem.* **2001**, *66*, 7729-7737. (b) Grasa, G. A.; Viciu, M. S.; Huang, J.; Zhang, C.; Trudell, M. L.; Nolan, S. P. *Organometallics* **2002**, *21*, 2866-2873. (c) Navarro, O.; Kelly, R. A., III; Nolan, S. P. *J. Am. Chem. Soc.* **2003**, *125*, 16194-16195. (d) Marion, N.; Navarro, O.; Mei, J.; Stevens, E. D.; Scott, N. M.; Nolan, S. P. *J. Am. Chem. Soc.* **2006**, *128*, 4101-4111. (e) Navarro, O.; Marion, N.; Mei, J. Nolan, S. P. *Chem. Eur. J.* **2006**, *12*, 5142-5148. (f) Lock, J. A.; Albrecht, M.; Peris, E.; Mata, J.; Faller, J. W.; Crabtree, R. H. *Organometallics* **2002**, *21*, 700-706. (g) Peris, E.; Loch, J. A.; Mata, J.; Crabtree, R. H. *Chem. Commun.* **2001**, 201-202.

103. (a) Hillier, A. C.; Lee, H. M.; Stevens, E. D.; Nolan, S. P. *Organometallics* **2001**, *20*, 4246-4252. (b) Vasquez-Serrano, L. D.; Owens, B. T.; Buriak, J. M. *Chem. Commun.* **2002**, 2518-2519. (c) Sprengers, J. W.; Wassenaar, J.; Clément, N. D.; Cavell, K. J.; Elsevier, C. J. *Angew. Chem., Int. Ed.* **2005**, *44*, 2026-2029. (d) Dharmasena, U. L.; Foucault, H. M.; Dos Santos, E. N.; Fogg, D. E.; Nolan, S. P. *Organometallics* **2005**, *24*, 1056-1058. (e) Albrecht, M.; Crabtree, R. H.; Mata, J.; Peris, E. *Chem. Commun.* **2002**, 32-33. (f) Albrecht, M.; Miecznikowski, J. R.; Samuel, A.; Faller, J. W.; Crabtree, R. H. *Organometallics* **2002**, *21*, 3596-3604.

104. (a) Lappert, M. F. *J. Organomet. Chem.* **1988**, *358*, 185-214. (b) Herrmann, W. A.; Köcher, C. *Angew. Chem., Int. Ed. Engl.* **1997**, *36*, 2162-2187. (c) Weskamp, T.; Böhm, V. P. W.; Herrmann, W. A. *J. Organomet. Chem.* **2000**, *600*, 12-22. (d) Bourissou, D.; Guerret, O.; Gabbaï, F. P.; Bertrand, G. *Chem. Rev.* **2000**, *100*, 39-91. (e) Herrmann, W. A. *Angew. Chem., Int. Ed.* **2002**, *41*, 1290-1309.

105. (a) Trnka, T. M.; Grubbs, R. H. *Acc. Chem. Res.* **2001**, *34*, 18-29. (b) Sanford, M. S.; Love, J. A.; Grubbs, R. H. *J. Am. Chem. Soc.* **2001**, *123*, 6543-6554. (c) Huang, J.; Schanz, H. J.; Stevens, E. D.; Nolan, S. P. *Organometallics* **1999**, *18*, 5375-5380.

106. (a) Markó, I. E.; Stérin, S.; Buisine, O.; Mignani, G.; Branlard, P.; Tinant, B.; Declercq, J. P. *Science* **2002**, *298*, 204-207. (b) Markó, I. E.; Michaud, G.; Berthon-Gelloz, G.; Buisine, O.; Stérin, S. *Adv. Synth. Catal.* **2004**, 1429-1434. (c) Buisine, O.; Berthon-Gelloz, G.; Brière, J. F.; Stérin, S.; Mignani, G.; Branlard, P.; Tinant, B.; Declercq, J. P.; Markó, I. E. *Chem. Commun.* **2005**, 3856-3868.

107. (a) Duin, M. A.; Clement, N. D.; Cavell, K. J.; Elsevier, C. J. *Chem. Commun.* **2003**, 400-401. (b) Sprengers, J. W.; Mars, M. J.; Duin, M. A.; Cavell, K. J.; Elsevier, C. J. *J. Organomet. Chem.* **2003**, *679*, 149-152.

108. (a)Toshima, N.; Yonezawa, T. *New J. Chem.* **1998**, 1179-1201. (b) Johnson, B. F. G. *Coord. Chem. Rev.* **1999**, *192*, 1269-1285. (c) Midgley, P. A.; Weyland, M.; Thomas, J. M.; Johnson, B. F. G. *Chem. Commun.* **2001**, 907-908. (d) Nashner, M. S.; Frenkel, A. I.; Somerville, D.; Hills, C. W.; Shapley, J. R.; Nuzzo, R. G. *J. Am. Chem. Soc.* **1998**, *120*, 8093-8101. (e) Nashner, M. S.; Frenkel, A. I.; Adler, D. L.; Shapley, J. R.; Nuzzo, R. G. *J. Am. Chem. Soc.* **1997**, *119*, 7760-7771. (f) Shephard, D. S.; Maschmeyer, T.; Johnson, B. F. G.; Thomas, J. M.; Sankar, G.; Ozkaya, D.; Zhou, W.; Oldroyd, R. D.; Bell, R. G. *Angew. Chem., Int. Ed. Engl.* **1997**, *36*, 2242-2245. (g) Shephard, D. S.; Maschmeyer, T.; Sankar, G.; Thomas, J. M.; Ozkaya, D.; Johnson, B. F. G.; Raja, R.; Oldroyd, R. D.; Bell, R. G. *Chem. Eur. J.* **1998**, *4*, 1214-1224.

109. (a) Raja, R.; Sankar, G.; Hermans, S.; Shephard, D. S.; Bromley, S.; Thomas, J. M.; Johnson, B. F. G. *Chem. Commun.* **1999**, 1571-1572. (b) Alexeev, O. S.; Gates, B. C. *Ind. Eng. Chem. Res.* **2003**, *42*, 1571-1587. (c) Goodman, D. W.; Houston, J. E. *Science*, **1987**, *236*, 403-409. (d) Ichikawa, M. *Adv. Catal.*, **1992**, *38*, 283-400.

110. Braunstein, P.; Rose, J. In *Catalysis by Di- and Polynuclear Metal Cluster Complexes*; Adams, R. D., Cotton, F. A., Eds.; VCH: New York, 1998; Chapter 13, p 443.

111. (a) Raja, R.; Khimyak, T.; Thomas, J. M.; Hermans, S.; Johnson, B. F. G. *Angew. Chem., Int. Ed.* **2001**, *40*, 4638-4642. (b) Hermans, S.; Raja, R.; Thomas, J. M.; Johnson, B. F. G.; Sankar, G.; Gleeson, D. *Angew. Chem., Int. Ed.* **2001**, *40*, 1211-1215. (c) Raja, R.; Sankar, G.; Hermans, S.; Shephard, D. S.; Bromley, S.; Thomas, J. M.; Johnson, B. F. G.; Maschemeyer, T. *Chem. Commun.* **1999**, 1571-1572.

112. Huq, R.; Poe, A. J.; Chawla, S. *Inorg. Chim. Acta* **1980**, *38*, 121-125.

113. Cabeza, J. A.; del Rio, I.; Miguel, D.; Perez-Carreno, E.; Sanchez-Vega, M. G. *Organometallics* **2008**, *27*, 211-217.

114. Adams, R. D.; Captain, B.; Zhu, L. *J. Am. Chem. Soc.* **2007**, *129*, 2454-2455.

115. (a) Adams, R. D.; Captain, B.; Fu, W.; Smith, M. D. *J. Am. Chem. Soc.* **2002**, *124*, 5628-5629. (b) Adams, R. D.; Captain, B.; Fu, W.; Hall, M. B.; Manson, J.; Smith, M. D.; Webster, C. E. *J. Am. Chem. Soc.* ***2004****, 126,* 5253-5267.

116. Adams, R. D.; Captain, B.; Fu, W.; Smith, M. D.; Zhu, L. *J. Cluster Sci.* **2006**, *17*, 87-95.

117. Adams, R. D.; Captain, B.; Zhu, L. *Inorg. Chem.* **2006**, *45*, 430-436.

118. Moss, J. R.; Graham, W. A. G. *J. Chem. Soc., Dalton Trans.* **1977**, 95-99.

119. Adams, R. D.; Captain, B.; Fu, W.; Hall, M. B.; Smith, M. D.; Webster, C. E. *Inorg. Chem.* **2004**, *43*, 3921-3929.

120. Adams, R. D.; Captain, B. *Acc. Chem. Res.***2009**, *42*, 409-418.

121. Cooke, C. E.; Jennings, M. C.; Pomeroy, R. K.; Clyburne, J. A. C. *Organometallics* **2007**, *26*, 6059-6062.

122. Haerkoenen, A. U.; Ahlgren, M.; Pakkanen, T. A.; Pursiainen, J. *J. Organomet. Chem.* **1997**, *530*, 191-197.

123. Cooke, C. E.; Jennings, M. C.; Katz, M. J.; Pomeroy, R. K.; Clyburne, J. A. C. *Organometallics* **2008**, *27*, 5777-5799.

124. Cabeza, J. A.; del Río, I.; Fernández-Colinas, J. M.; Pérez-Carreño, E.; Sánchez-Vega, M. Gabriela; Vázquez-García, D. *Organometallics* **2009**, *28*, 1832-1837.

125. Teller, R. G.; Bau, R. *Struct. Bonding* **1981**, *41*, 1.

126. Adams, R. D.; Bunz, U.; Captain, B.; Fu, W.; Steffen, W. *J.Organomet.Chem.* **2000**, 6*14*, 75-82.

127. Manzoli, M.; Shetti, V. N.; Blaine, J. A. L.; Zhu, L.; Isrow, D.; Yempally, V.; Captain, B.; Coluccia, S.; Raja, R.; Gianotti, E. *Daltan Trans.* **2012**, *41*, 982-989.

128. (a) Chapter 2 is adapted from Saha, S.; Zhu, L.; Captain, B. "Synthesis and characterization of bimetallic iron-nickel carbido cluster complexes." *Inorg. Chem.* **2010**, *49*, 3465-3472. (b) Chapter 3 is adapted from Saha, S.; Zhu, L.; Captain, B. "Bimetallic octahedral ruthenium-nickel carbido cluster complexes. synthesis and structural characterization." *Inorg. Chem.* **2013**, *52*, 2526-2532. (c) Chapter 4 is adapted from Saha, S.; Isrow, D.; Captain, B. "Build-up of a Ru_6 octahedral cluster core stabilized by tert-butyl germyl ligands." *J. Organomet. Chem.* **2013**, *in press*. (d) Chapter 5 is adapted from Saha, S.; Captain, B. "Synthesis and structural characterization of ruthenium carbonyl cluster complexes containing platinum with a bulky N-heterocyclic carbene ligand." *Inorg. Chem.* **2013**, *submitted*.

Appendix A: Supporting information for chapter 2

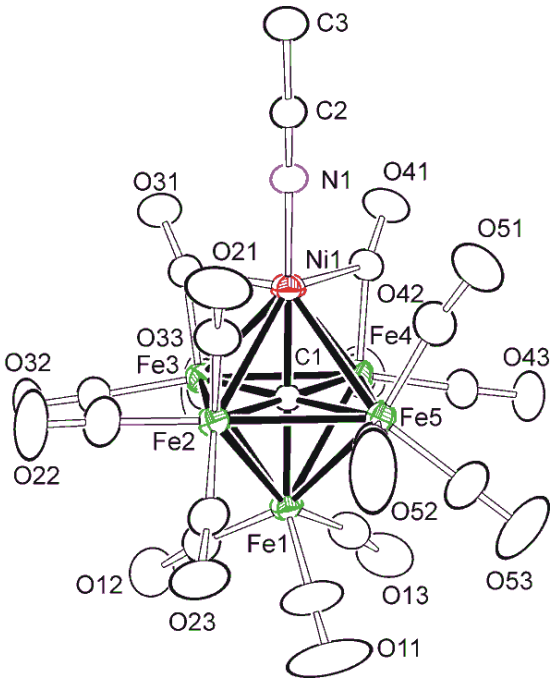

Figure A.1. The molecular structure of $Fe_5Ni(NCMe)(CO)_{15}(\mu_6\text{-}C)$, **2.3**.

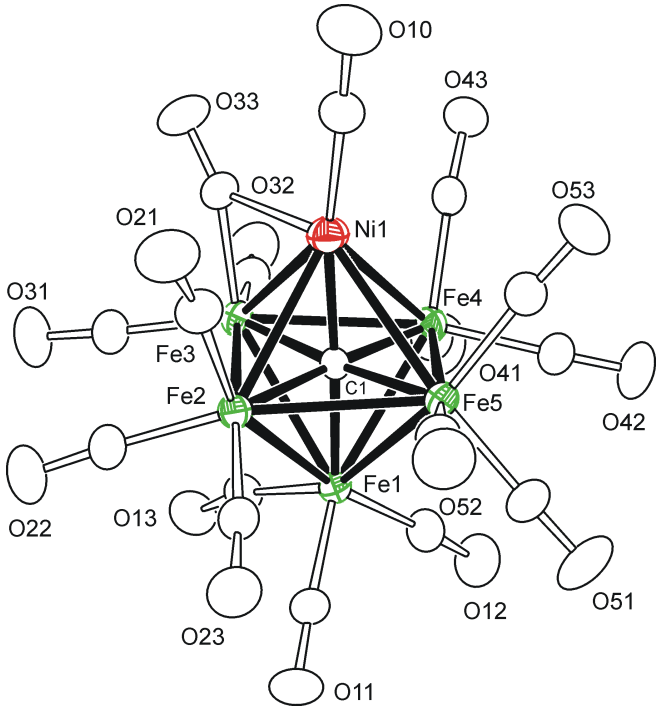

Figure A.2. The molecular structure of $Fe_5Ni(CO)_{16}(\mu_6\text{-}C)$, **2.4**.

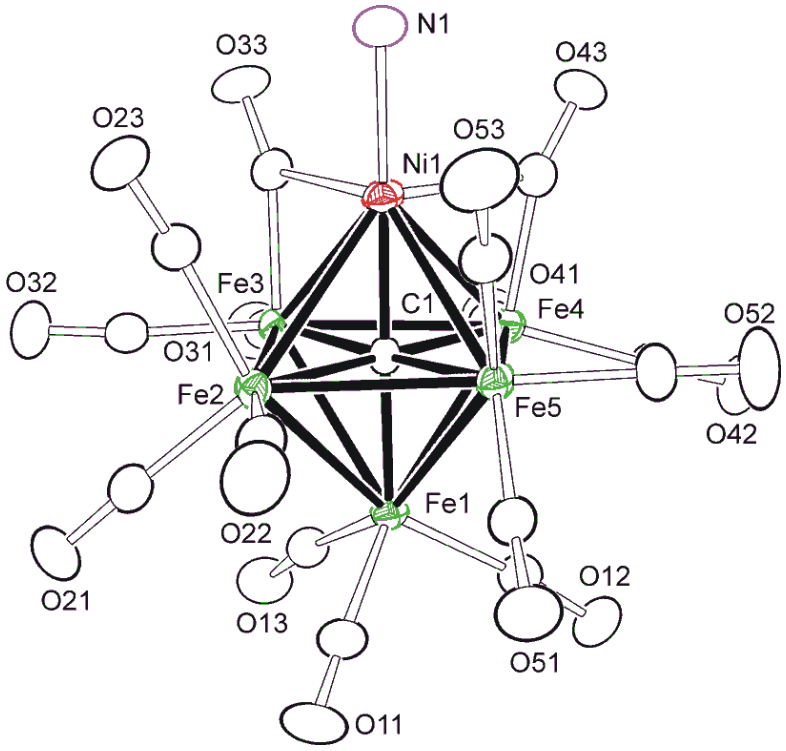

Figure A.3. The molecular structure of $Fe_5Ni(NH_3)(CO)_{15}(\mu_6\text{-}C)$, **2.6**.

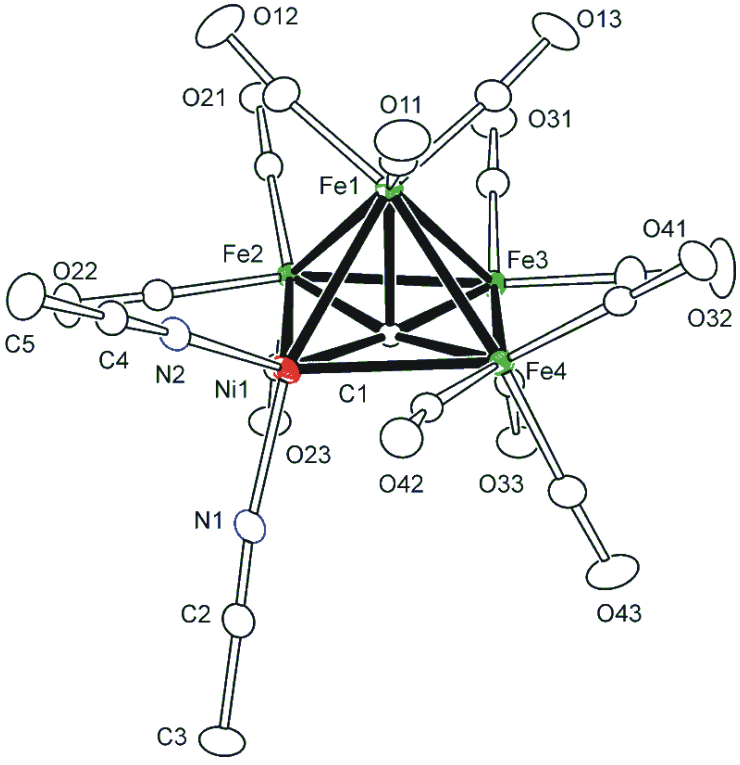

Figure A.4. The molecular structure of $Fe_4Ni(NCMe)_2(CO)_{12}(\mu_5\text{-}C)$, **2.7**.

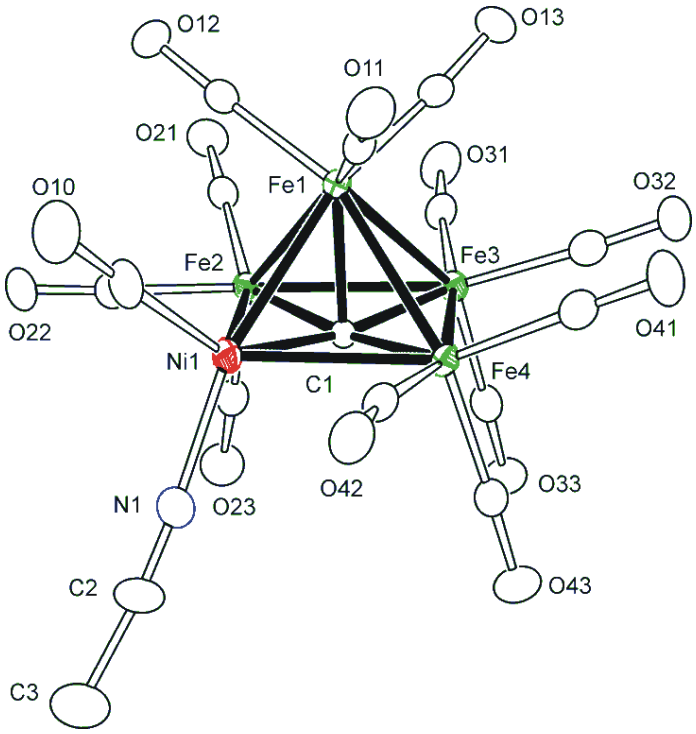

Figure A.5. The molecular structure of $Fe_4Ni(NCMe)(CO)_{13}(\mu_5\text{-}C)$, **2.8**.

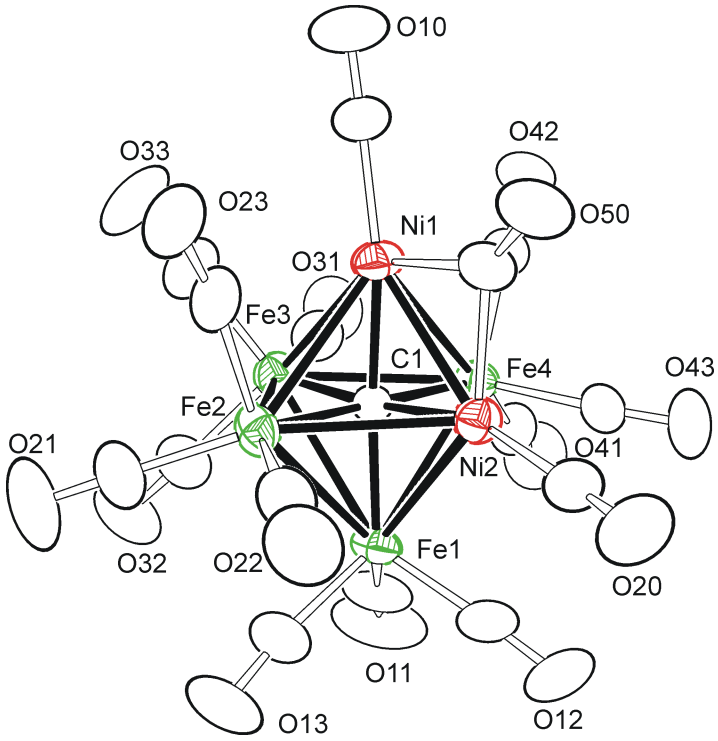

Figure A.6. The molecular structure of $Fe_4Ni_2(CO)_{15}(\mu_6\text{-}C)$, **2.9**.

Table A.1. Crystallographic data for compounds $Fe_5Ni(NCMe)(CO)_{15}(\mu_6\text{-}C)$, 2.3, $Fe_5Ni(CO)_{16}(\mu_6\text{-}C)$, 2.4 and $Fe_5Ni(NH_3)(CO)_{15}(\mu_6\text{-}C)$, 2.6.

Compound	**2.3**	**2.4**	**2.6**
Empirical formula	$NiFe_5O_{15}NC_{18}H_3$	$NiFe_5O_{16}C_{17}$	$NiFe_5O_{15}NC_{16}H_3$
Formula weight	811.17	798.13	787.15
Crystal system	Orthorhombic	Triclinic	Orthorhombic
Lattice parameters			
a (Å)	17.3484(6)	9.0290(5)	20.8118(11)
b (Å)	9.2771(3)	9.5672(5)	10.3605(5)
c (Å)	15.7591(5)	15.5994(8)	10.7284(6)
α (deg)	90	85.381(1)	90
β (deg)	90	83.673(1)	90
γ (deg)	90	63.223(1)	90
V ($Å^3$)	2536.31(14)	1194.96(11)	2313.3(2)
Space group	$Pna2_1$ (# 33)	$P\bar{1}$ (# 2)	$Pna2_1$ (# 33)
Z value	4	2	4
ρ_{calc} (g / cm^3)	2.124	2.218	2.260
μ (Mo Kα) (mm^{-1})	3.586	3.805	3.927
Temperature (K)	296	296	296
$2\Theta_{max}$ (°)	56.00	58.00	51.98
No. Obs. ($I > 2\sigma(I)$)	5301	4679	4301
No. Parameters	363	352	344
Goodness of fit	1.066	1.038	1.004
Max. shift in cycle	0.001	0.000	0.001
Residuals*:R1; wR2	0.0304; 0.0670	0.0380; 0.1091	0.0333; 0.0786
Absorption Correction, Max/min	Multi-scan 0.7461/ 0.5169	Multi-scan 0.9278/0.4882	Multi-scan 0.6948/0.5072
Largest peak in Final Diff. Map (e^- / $Å^3$)	0.593	0.617	0.681

*$R = \Sigma_{hkl}(\,|\,|F_{obs}| - |F_{calc}|\,|)/\Sigma_{hkl}|F_{obs}|$; $R_w = [\Sigma_{hkl}w(|F_{obs}| - |F_{calc}|)^2/\Sigma_{hkl}wF_{obs}^2]^{1/2}$, $w = 1/\sigma^2(F_{obs})$; $GOF = [\Sigma_{hkl}w(|F_{obs}| - |F_{calc}|)^2/(n_{data} - n_{vari})]^{1/2}$.

Table A.2. Crystallographic data for compounds $Fe_4Ni(NCMe)_2(CO)_{12}(\mu_5\text{-}C)$, 2.7, $Fe_4Ni(NCMe)(CO)_{13}(\mu_5\text{-}C)$, 2.8 and $Fe_4Ni_2(CO)_{15}(\mu_6\text{-}C)$, 2.9.

Compound	**2.7**	**2.8**	**2.9**
Empirical formula	$NiFe_4O_{12}N_2C_{17}H_6$	$NiFe_4O_{13}NC_{16}H_3$	$Ni_2Fe_4O_{15}C_{16}$
Formula weight	712.35	699.30	772.98
Crystal system	Monoclinic	Monoclinic	Monoclinic
Lattice parameters			
a (Å)	9.6040(3)	9.5977(5)	10.5011(7)
b (Å)	15.3859(6)	15.5438(8)	10.9743(8)
c (Å)	16.0687(6)	14.7267(8)	20.5591(14)
α (deg)	90	90	90
β (deg)	106.2706(5)	91.1432(9)	90.551(1)
γ (deg)	90	90	90
V ($Å^3$)	2279.31(14)	2196.6(2)	2369.2(3)
Space group	$P\,2_1/c$ (# 14)	$P\,2_1/n$ (# 14)	$P\,2_1/c$ (# 14)
Z value	4	4	4
ρ_{calc} (g / cm^3)	2.076	2.115	2.167
μ (Mo Kα) (mm^{-1})	3.362	3.489	4.013
Temperature (K)	100	100	296
$2\Theta_{max}$ (°)	62.00	63.00	52.90
No. Obs. (I > 2σ(I))	6821	5286	3226
No. Parameters	327	317	334
Goodness of fit	1.107	1.008	1.056
Max. shift in cycle	0.004	0.001	0.000
Residuals*:R1; wR2	0.0197; 0.0485	0.0364; 0.0755	0.0499; 0.1158
Absorption Correction, Max/min	Multi-scan 0.8773/ 0.3774	Multi-scan 0.9659/0.4417	Multi-scan 0.9240/0.5007
Largest peak in Final Diff. Map (e^- / $Å^3$)	0.443	0.951	1.563

*$R = \Sigma_{hkl}(\,|\,|F_{obs}| - |F_{calc}|\,|)/\Sigma_{hkl}|F_{obs}|$; $R_w = [\Sigma_{hkl}w(|F_{obs}| - |F_{calc}|)^2/\Sigma_{hkl}wF_{obs}^2]^{1/2}$, $w = 1/\sigma^2(F_{obs})$; $GOF = [\Sigma_{hkl}w(|F_{obs}| - |F_{calc}|)^2/(n_{data} - n_{vari})]^{1/2}$.

Table A.3. Selected intramolecular distances and angles for compounds $Fe_5Ni(NCMe)(CO)_{15}(\mu_6\text{-}C)$, 2.3 and $Fe_5Ni(NH_3)(CO)_{15}(\mu_6\text{-}C)$, 2.6.[a]

(a) Distances

atom	atom	distance (Å) **2.3**	distance (Å) **2.6**	atom	atom	distance (Å) **2.3**	distance (Å) **2.6**
Ni(1)	Fe(2)	2.7149(7)	2.7666(9)	Fe(1)	Fe(4)	2.6880(7)	2.7055(9)
Ni(1)	Fe(3)	2.5653(7)	2.5361(8)	Fe(1)	Fe(5)	2.6875(7)	2.6847(8)
Ni(1)	Fe(4)	2.5424(7)	2.5365(8)	Fe(2)	Fe(3)	2.7214(7)	2.6655(8)
Ni(1)	Fe(5)	2.7233(7)	2.6911(8)	Fe(2)	Fe(5)	2.6671(7)	2.6717(8)
Fe(1)	Fe(2)	2.7009(7)	2.6450(8)	Fe(3)	Fe(4)	2.7163(7)	2.7440(8)
Fe(1)	Fe(3)	2.6804(7)	2.7511(9)	Fe(4)	Fe(5)	2.6817(7)	2.7070(9)

(b) Angles

atom	atom	atom	angle (deg) **2.3**	angle (deg) **2.6**
Fe(4)	Ni(1)	Fe(3)	64.25(2)	65.50(2)
Fe(4)	Ni(1)	Fe(2)	92.79(2)	91.84(3)
Fe(3)	Ni(1)	Fe(2)	61.972(19)	60.17(2)
Fe(4)	Ni(1)	Fe(5)	61.117(19)	62.29(2)
Fe(3)	Ni(1)	Fe(5)	92.38(2)	93.63(3)
Fe(2)	Ni(1)	Fe(5)	58.739(19)	58.60(2)
Ni(1)	Fe(2)	Fe(3)	56.314(18)	55.63(2)
Ni(1)	Fe(3)	Fe(4)	57.464(18)	57.26(2)
Ni(1)	Fe(3)	Fe(2)	61.714(19)	64.21(2)
Fe(4)	Fe(3)	Fe(2)	88.92(2)	89.63(2)
Ni(1)	Fe(4)	Fe(5)	62.771(19)	61.66(2)
Ni(1)	Fe(4)	Fe(3)	58.28(2)	57.24(2)
Fe(2)	Fe(5)	Ni(1)	60.473(19)	62.11(2)
Fe(4)	Fe(5)	Ni(1)	56.112(18)	56.05(2)

[a]Estimated standard deviations in the least significant figure are given in parentheses.

Table A.4. Selected intramolecular distances and angles for compound $Fe_5Ni(CO)_{16}(\mu_6\text{-}C)$, 2.4.[a]

(a) Distances

atom	atom	distance (Å)	atom	Atom	distance (Å)
Ni(1)	Fe(2)	2.6613(7)	Fe(1)	Fe(4)	2.6415(7)
Ni(1)	Fe(3)	2.5095(7)	Fe(1)	Fe(5)	2.7354(7)
Ni(1)	Fe(4)	2.6957(8)	Fe(2)	Fe(3)	2.7237(7)
Ni(1)	Fe(5)	2.6705(7)	Fe(2)	Fe(5)	2.6910(7)
Fe(1)	Fe(2)	2.6615(7)	Fe(3)	Fe(4)	2.6957(7)
Fe(1)	Fe(3)	2.7194(7)	Fe(4)	Fe(5)	2.6588(7)

(b) Angles

atom	atom	atom	angle (deg)	atom	atom	atom	angle (deg)
Fe(3)	Ni(1)	Fe(2)	63.49(2)	Ni(1)	Fe(3)	Fe(4)	62.26(2)
Fe(3)	Ni(1)	Fe(5)	94.17(2)	Ni(1)	Fe(3)	Fe(2)	60.97(2)
Fe(2)	Ni(1)	Fe(5)	60.623(19)	Fe(4)	Fe(3)	Fe(2)	89.41(2)
Fe(3)	Ni(1)	Fe(4)	62.26(2)	Fe(5)	Fe(4)	Fe(3)	90.27(2)
Fe(2)	Ni(1)	Fe(4)	90.74(2)	Fe(5)	Fe(4)	Ni(1)	59.827(19)
Fe(5)	Ni(1)	Fe(4)	59.400(19)	Fe(3)	Fe(4)	Ni(1)	55.480(19)
Ni(1)	Fe(2)	Fe(5)	59.857(19)	Fe(4)	Fe(5)	Ni(1)	60.77(2)
Ni(1)	Fe(2)	Fe(3)	55.538(19)	Fe(4)	Fe(5)	Fe(2)	90.89(2)
Fe(5)	Fe(2)	Fe(3)	89.00(2)	Ni(1)	Fe(5)	Fe(2)	59.521(19)

[a]Estimated standard deviations in the least significant figure are given in parentheses.

Table A.5. Selected intramolecular distances and angles for compounds $Fe_4Ni(NCMe)_2(CO)_{12}(\mu_5\text{-}C)$, 2.7 and $Fe_4Ni(NCMe)(CO)_{13}(\mu_5\text{-}C)$, 2.8.[a]

(a) Distances

atom	atom	distance (Å) **2.7**	distance (Å) **2.8**
Ni(1)	Fe(1)	2.5612(2)	2.5129(5)
Ni(1)	Fe(2)	2.6696(2)	2.6467(5)
Ni(1)	Fe(4)	2.5913(2)	2.6077(5)
Fe(1)	Fe(2)	2.5802(2)	2.5948(5)
Fe(1)	Fe(3)	2.6346(2)	2.6144(5)
Fe(1)	Fe(4)	2.5527(2)	2.5879(5)
Fe(2)	Fe(3)	2.6265(2)	2.6399(5)
Fe(3)	Fe(4)	2.6253(2)	2.6323(5)

(b) Angles

atom	atom	atom	angle (deg) **2.7**	angle (deg) **2.8**
Fe(1)	Ni(1)	Fe(4)	59.394(6)	60.681(14)
Fe(1)	Ni(1)	Fe(2)	59.068(6)	60.319(14)
Fe(4)	Ni(1)	Fe(2)	91.320(7)	90.295(16)
Fe(4)	Fe(1)	Ni(1)	60.890(7)	61.471(14)
Ni(1)	Fe(1)	Fe(2)	62.562(7)	62.395(15)
Fe(4)	Fe(1)	Fe(2)	94.295(8)	91.903(17)
Ni(1)	Fe(1)	Fe(3)	89.704(8)	92.924(17)
Fe(4)	Fe(1)	Fe(3)	60.783(7)	60.790(14)
Fe(2)	Fe(1)	Fe(3)	60.473(7)	60.896(14)
Fe(1)	Fe(2)	Fe(3)	60.789(7)	59.919(14)
Fe(1)	Fe(2)	Ni(1)	58.370(6)	57.286(14)
Fe(3)	Fe(2)	Ni(1)	87.572(8)	89.370(16)
Fe(4)	Fe(3)	Fe(1)	58.067(6)	59.107(14)
Fe(2)	Fe(3)	Fe(1)	58.737(6)	59.184(14)
Fe(4)	Fe(3)	Fe(2)	91.538(8)	89.911(16)
Fe(1)	Fe(4)	Ni(1)	59.716(6)	57.848(13)
Ni(1)	Fe(4)	Fe(3)	89.260(8)	90.381(16)

[a]Estimated standard deviations in the least significant figure are given in parentheses.

Table A.6. Selected intramolecular distances and angles for compound $Fe_4Ni_2(CO)_{15}(\mu_6\text{-}C)$, 2.9.[a]

(a) Distances

atom	atom	distance (Å)	atom	atom	distance (Å)
Ni(1)	Ni(2)	2.4642(11)	Ni(2)	Fe(4)	2.6685(11)
Ni(1)	Fe(2)	2.6686(12)	Fe(1)	Fe(2)	2.6707(12)
Ni(1)	Fe(3)	2.6798(11)	Fe(1)	Fe(3)	2.7188(12)
Ni(1)	Fe(4)	2.6857(11)	Fe(1)	Fe(4)	2.6535(11)
Ni(2)	Fe(1)	2.6874(11)	Fe(2)	Fe(3)	2.6530(12)
Ni(2)	Fe(2)	2.6994(12)	Fe(3)	Fe(4)	2.6505(12)

(b) Angles

atom	atom	atom	angle (deg)	atom	atom	atom	angle (deg)
Ni(2)	Ni(1)	Fe(2)	63.31(3)	Fe(4)	Fe(3)	Fe(2)	91.95(4)
Ni(2)	Ni(1)	Fe(3)	92.74(3)	Fe(4)	Fe(3)	Ni(1)	60.51(3)
Fe(2)	Ni(1)	Fe(3)	59.48(3)	Fe(2)	Fe(3)	Ni(1)	60.05(3)
Ni(2)	Ni(1)	Fe(4)	62.24(3)	Fe(3)	Fe(2)	Ni(1)	60.47(3)
Fe(2)	Ni(1)	Fe(4)	90.83(3)	Fe(3)	Fe(2)	Ni(2)	88.24(3)
Fe(3)	Ni(1)	Fe(4)	59.21(3)	Ni(1)	Fe(2)	Ni(2)	54.65(3)
Ni(1)	Ni(2)	Fe(4)	62.95(3)	Fe(4)	Fe(3)	Fe(2)	91.95(4)
Ni(1)	Ni(2)	Fe(2)	62.04(3)	Fe(4)	Fe(3)	Ni(1)	60.51(3)
Fe(4)	Ni(2)	Fe(2)	90.54(4)	Fe(2)	Fe(3)	Ni(1)	60.05(3)
Fe(3)	Fe(2)	Ni(1)	60.47(3)	Fe(3)	Fe(4)	Ni(2)	88.94(3)
Fe(3)	Fe(2)	Ni(2)	88.24(3)	Fe(3)	Fe(4)	Ni(1)	60.29(3)
Ni(1)	Fe(2)	Ni(2)	54.65(3)	Ni(2)	Fe(4)	Ni(1)	54.80(3)

[a]Estimated standard deviations in the least significant figure are given in parentheses.

Appendix B: Supporting information for chapter 3

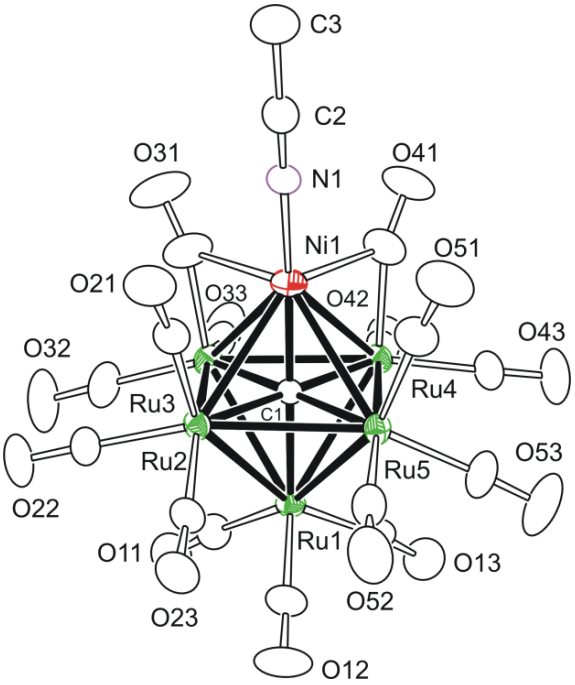

Figure B.1. The molecular structure of $Ru_5Ni(NCMe)(CO)_{15}(\mu_6\text{-}C)$, **3.1**.

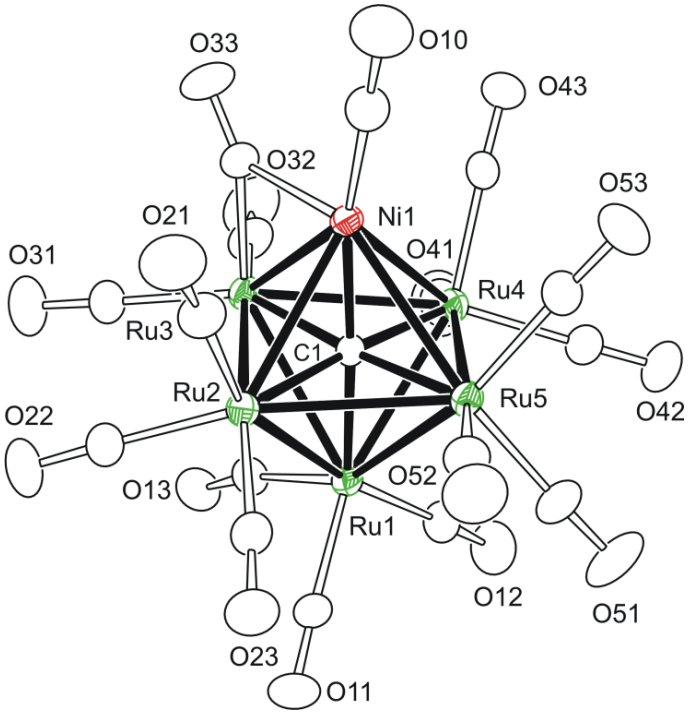

Figure B.2. The molecular structure of $Ru_5Ni(CO)_{16}(\mu_6\text{-}C)$, **3.2**.

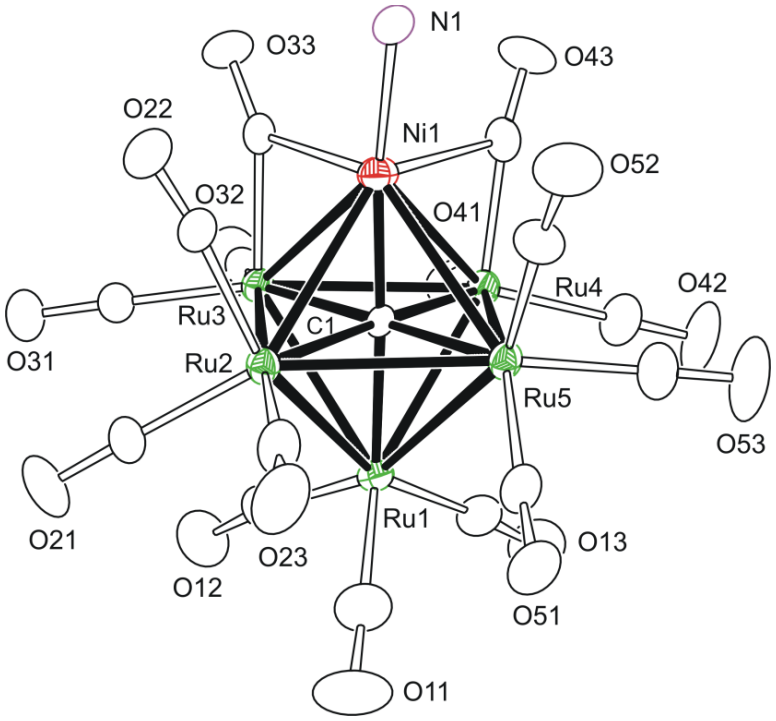

Figure B.3. The molecular structure of $Ru_5Ni(NH_3)(CO)_{15}(\mu_6\text{-}C)$, **3.3**.

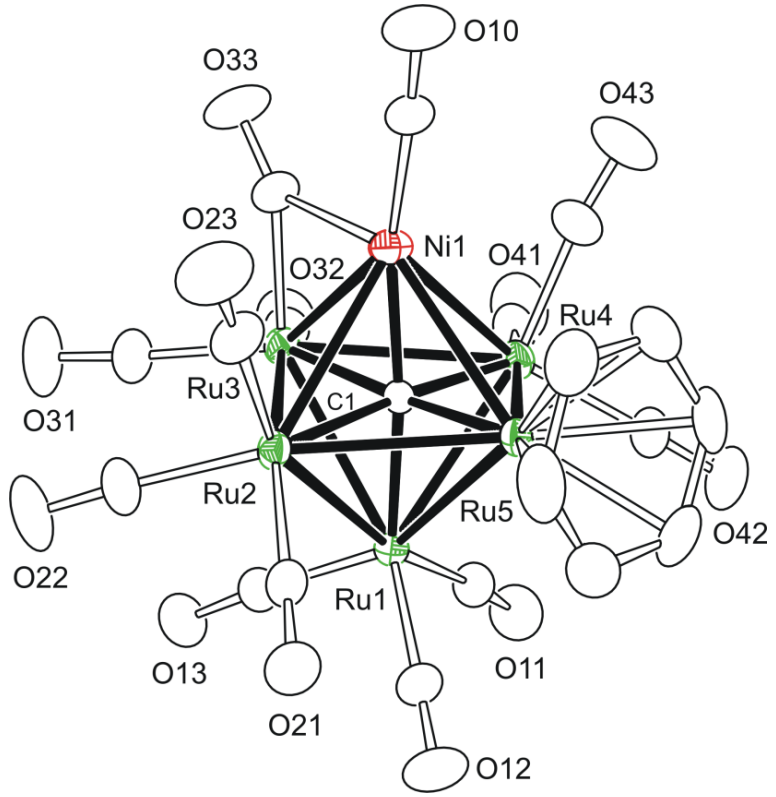

Figure B.4. The molecular structure of $Ru_5Ni(CO)_{13}(\eta^6\text{-}C_6H_6)(\mu_6\text{-}C)$, **3.4**.

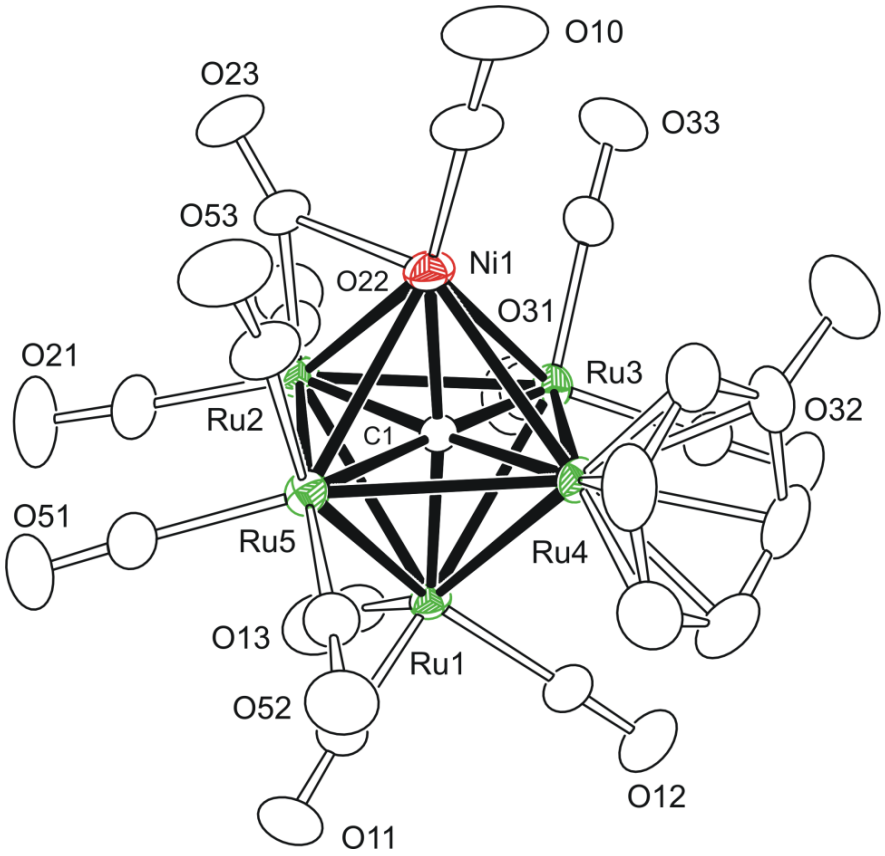

Figure B.5. The molecular structure of $Ru_5Ni(CO)_{13}(\eta^6\text{-}C_7H_8)(\mu_6\text{-}C)$, **3.5**.

Table B.1. Crystallographic data for compounds $Ru_5Ni(NCMe)(CO)_{15}(\mu_6\text{-}C)$, 3.1 $Ru_5Ni(CO)_{16}(\mu_6\text{-}C)$, 3.2 and $Ru_5Ni(NH_3)(CO)_{15}(\mu_6\text{-}C)$, 3.3.

Compound	**3.1**	**3.2**	**3.3**
Empirical formula	$NiRu_5O_{15}NC_{18}H_3$	$NiRu_5O_{16}C_{17}$	$NiRu_5O_{15}NC_{16}H_3$
Formula weight	1037.27	1024.23	1013.25
Crystal system	Orthorhombic	Triclinic	Triclinic
Lattice parameters			
a (Å)	23.7452(11)	9.2207(4)	9.4325(4)
b (Å)	10.6244(5)	9.9312(4)	17.0113(7)
c (Å)	10.9461(5)	16.0529(7)	17.5226(7)
α (deg)	90	85.1360(6)	62.614 (1)
β (deg)	90	83.3197(7)	89.195 (1)
γ (deg)	90	63.3268(6)	89.350(1)
V ($Å^3$)	2761.5(2)	1303.77(10)	2496.27(18)
Space group	$Pna2_1$ (# 33)	$P\bar{1}$ (# 2)	$P\bar{1}$ (# 2)
Z value	4	2	4
ρ_{calc} (g / cm^3)	2.495	2.609	2.696
μ (Mo Kα) (mm^{-1})	3.402	3.603	3.760
Temperature (K)	296	296	296
$2\Theta_{max}$ (°)	62.00	55.00	56.00
No. Obs. ($I > 2\sigma(I)$)	7217	5261	6539
No. Parameters	362	352	685
Goodness of fit	1.010	1.015	1.097
Max. shift in cycle	0.001	0.001	0.001
Residuals*:R1; wR2	0.0296; 0.0670	0.0321; 0.0840	0.0477; 0.0636
Absorption Correction, Max/min	Multi-scan 0.9668/ 0.3431	Multi-scan 0.8693 /0.5327	Multi-scan 0.7465 /0.6478
Largest peak in Final Diff. Map (e^- / $Å^3$)	0.805	1.378	0.881

*$R = \Sigma_{hkl}(\,|\,|F_{obs}|-|F_{calc}|\,|)/\Sigma_{hkl}|F_{obs}|$; $R_w = [\Sigma_{hkl}w(|F_{obs}|-|F_{calc}|)^2/\Sigma_{hkl}wF_{obs}^2]^{1/2}$, $w = 1/\sigma^2(F_{obs})$; $GOF = [\Sigma_{hkl}w(|F_{obs}|-|F_{calc}|)^2/(n_{data} - n_{vari})]^{1/2}$.

Table B.2. Crystallographic data for compounds $Ru_5Ni(CO)_{13}(\eta^6\text{-}C_6H_6)(\mu_6\text{-}C)$, 3.4 and $Ru_5Ni(CO)_{13}(\eta^6\text{-}C_7H_8)(\mu_6\text{-}C)$, 3.5.

Compound	**3.4**	**3.5**
Empirical formula	$NiRu_5O_{13}C_{20}H_6$	$NiRu_5O_{13}C_{21}H_8$
Formula weight	1018.31	1032.33
Crystal system	Orthorhombic	Monoclinic
Lattice parameters		
a (Å)	15.3325(6)	17.4209(8)
b (Å)	16.0776(6)	18.8346(8)
c (Å)	21.1873(8)	18.4782(8)
α (deg)	90	90
β (deg)	90	116.945(1)
γ (deg)	90	90
V (Å^3)	5222.9(3)	5404.8(4)
Space group	*Pbca* (# 61)	$P2_1/n$ (# 14)
Z value	8	8
ρ_{calc} (g / cm^3)	2.590	2.537
μ (Mo Kα) (mm^{-1})	3.588	3.469
Temperature (K)	296	296
$2\Theta_{max}$ (°)	56.00	63.00
No. Obs. (I > 2σ(I))	5653	13559
No. Parameters	353	723
Goodness of fit	1.070	1.036
Max. shift in cycle	0.003	0.002
Residuals*:R1; wR2	0.0212; 0.0510	0.0320; 0.0762
Absorption Correction, Max/min	Multi-scan 0.8698/0.3279	Multi-scan 0.7688 /0.3523
Largest peak in Final Diff. Map (e$^-$ / Å^3)	0.679	1.631

*$R = \Sigma_{hkl}(\,|\,|F_{obs}|-|F_{calc}|\,|)/\Sigma_{hkl}|F_{obs}|$; $R_w = [\Sigma_{hkl}w(|F_{obs}|-|F_{calc}|)^2/\Sigma_{hkl}wF_{obs}^2]^{1/2}$, $w = 1/\sigma^2(F_{obs})$; $GOF = [\Sigma_{hkl}w(|F_{obs}|-|F_{calc}|)^2/(n_{data} - n_{vari})]^{1/2}$.

Table B.3. Selected intramolecular distances and angles for compounds $Ru_5Ni(NCMe)(CO)_{15}(\mu_6\text{-}C)$, 3.1 and $Ru_5Ni(NH_3)(CO)_{15}(\mu_6\text{-}C)$, 3.3.[a]

(a) Distances

atom	atom	distance (Å) **3.1**	distance (Å) **3.3**	atom	atom	distance (Å) **3.1**	distance (Å) **3.3**
Ni(1)	Ru(2)	2.8394(7)	2.881(1)	Ru(1)	Ru(4)	2.9210(5)	2.870(1)
Ni(1)	Ru(3)	2.6914(7)	2.651(1)	Ru(1)	Ru(5)	2.8420(5)	2.891(1)
Ni(1)	Ru(4)	2.6756(7)	2.706(1)	Ru(2)	Ru(3)	2.9008(5)	2.885(1)
Ni(1)	Ru(5)	2.8831(7)	2.864(1)	Ru(2)	Ru(5)	2.8894(5)	2.891(1)
Ru(1)	Ru(2)	2.8718(5)	2.852(1)	Ru(3)	Ru(4)	2.9103(5)	2.919(1)
Ru(1)	Ru(3)	2.8889(5)	2.909(1)	Ru(4)	Ru(5)	2.8922(5)	2.910(1)

(b) Angles

atom	atom	Atom	angle (deg) **3.1**	angle (deg) **3.3**
Ru(2)	Ni(1)	Ru(3)	63.20(2)	62.71(3)
Ru(2)	Ni(1)	Ru(4)	95.93(2)	94.42(4)
Ru(2)	Ni(1)	Ru(5)	60.65(2)	60.43(3)
Ru(3)	Ni(1)	Ru(4)	65.68(2)	66.02(3)
Ru(3)	Ni(1)	Ru(5)	94.60(2)	96.06(4)
Ru(4)	Ni(1)	Ru(5)	62.57(2)	62.91(3)
Ni(1)	Ru(2)	Ru(3)	55.91(2)	54.73(3)
Ni(1)	Ru(3)	Ru(2)	60.89(2)	62.56(3)
Ni(1)	Ru(3)	Ru(4)	56.90(2)	57.90(3)
Ni(1)	Ru(4)	Ru(3)	57.43(2)	56.08(3)
Ni(1)	Ru(4)	Ru(5)	62.23(2)	61.19(3)
Ni(1)	Ru(5)	Ru(2)	58.93(2)	60.09(3)
Ni(1)	Ru(5)	Ru(4)	55.20(2)	55.90(3)

[a]Estimated standard deviations in the least significant figure are given in parentheses.

Table B.4. Selected intramolecular distances and angles for compound $Ru_5Ni(CO)_{16}(\mu_6\text{-}C)$, 3.2.[a]

(a) Distances

atom	atom	distance (Å)	atom	atom	distance (Å)
Ni(1)	Ru(2)	2.8295(6)	Ru(1)	Ru(4)	2.8442(5)
Ni(1)	Ru(3)	2.6624(6)	Ru(1)	Ru(5)	2.9365(5)
Ni(1)	Ru(4)	2.8945(6)	Ru(2)	Ru(3)	2.9384(5)
Ni(1)	Ru(5)	2.8194(6)	Ru(2)	Ru(5)	2.9062(5)
Ru(1)	Ru(2)	2.8541(5)	Ru(3)	Ru(4)	2.9001(5)
Ru(1)	Ru(3)	2.9537(5)	Ru(4)	Ru(5)	2.8682(5)

(b) Angles

atom	atom	atom	angle (deg)	atom	atom	atom	angle (deg)
Ru(3)	Ni(1)	Ru(5)	96.16(2)	Ni(1)	Ru(3)	Ru(4)	62.54(2)
Ru(3)	Ni(1)	Ru(2)	64.61(2)	Ni(1)	Ru(3)	Ru(2)	60.45(2)
Ru(5)	Ni(1)	Ru(2)	61.92(2)	Ru(4)	Ru(3)	Ru(2)	89.74(1)
Ru(3)	Ni(1)	Ru(4)	62.76(2)	Ru(5)	Ru(4)	Ni(1)	58.58(1)
Ru(5)	Ni(1)	Ru(4)	60.24(1)	Ru(5)	Ru(4)	Ru(3)	90.04(1)
Ru(2)	Ni(1)	Ru(4)	92.04(2)	Ru(3)	Ru(4)	Ni(1)	54.71(1)
Ni(1)	Ru(2)	Ru(5)	58.87(1)	Ni(1)	Ru(5)	Ru(4)	61.18(2)
Ni(1)	Ru(2)	Ru(3)	54.94(1)	Ni(1)	Ru(5)	Ru(2)	59.21(1)
Ru(5)	Ru(2)	Ru(3)	88.55(1)	Ru(4)	Ru(5)	Ru(2)	91.01(1)

[a]Estimated standard deviations in the least significant figure are given in parentheses.

Table B.5. Selected intramolecular distances and angles for compounds $Ru_5Ni(CO)_{13}(\eta^6\text{-}C_6H_6)(\mu_6\text{-}C)$, 3.4 and $Ru_5Ni(CO)_{13}(\eta^6\text{-}C_7H_8)(\mu_6\text{-}C)$, 3.5.[a]

(a) Distances

atom	atom	distance (Å) **3.4**	distance (Å) **3.5**
Ni(1)	Ru(2)	2.8522(5)	2.6246(5)
Ni(1)	Ru(3)	2.6032(4)	2.8475(6)
Ni(1)	Ru(4)	2.8260(5)	2.7682(5)
Ni(1)	Ru(5)	2.7746(4)	2.7856(6)
Ru(1)	Ru(2)	2.8243(3)	2.9287(4)
Ru(1)	Ru(3)	2.9050(3)	2.8472(4)
Ru(1)	Ru(4)	2.8686(4)	2.8860(4)
Ru(1)	Ru(5)	2.9212(3)	2.8574(4)
Ru(2)	Ru(3)	2.9320(4)	2.8779(4)
Ru(2)	Ru(5)	2.8224(4)	2.8961(4)
Ru(3)	Ru(4)	2.9392(4)	2.8677(4)
Ru(4)	Ru(5)	2.8135(4)	2.8514(4)

(b) Angles

atom	atom	atom	angle (deg) **3.4**	angle (deg) **3.5**
Ni(1)	Ru(2)	Ru(1)	87.06(1)	89.24(1)
Ni(1)	Ru(2)	Ru(3)	53.473(9)	62.13(1)
Ni(1)	Ru(2)	Ru(5)	58.54(1)	60.37(1)
Ni(1)	Ru(3)	Ru(1)	90.26(1)	86.63(1)
Ni(1)	Ru(3)	Ru(2)	61.69(1)	54.57(1)
Ni(1)	Ru(3)	Ru(4)	60.96(1)	57.94(1)
Ni(1)	Ru(4)	Ru(1)	86.71(1)	87.38(1)
Ni(1)	Ru(4)	Ru(3)	53.64(1)	60.67(1)
Ni(1)	Ru(4)	Ru(5)	58.94(1)	59.41(1)
Ni(1)	Ru(5)	Ru(1)	86.65(1)	87.61(1)
Ni(1)	Ru(5)	Ru(2)	61.27(1)	54.98(1)
Ni(1)	Ru(5)	Ru(4)	60.75(1)	58.81(1)
Ru(2)	Ni(1)	Ru(3)	64.83(1)	63.31(1)
Ru(2)	Ni(1)	Ru(4)	92.96(1)	96.11(1)
Ru(2)	Ni(1)	Ru(5)	60.19(1)	64.65(1)
Ru(3)	Ni(1)	Ru(4)	65.40(1)	61.40(1)
Ru(3)	Ni(1)	Ru(5)	96.23(1)	93.59(1)
Ru(4)	Ni(1)	Ru(5)	60.30(1)	61.78(1)

[a]Estimated standard deviations in the least significant figure are given in parentheses.

Appendix C: Supporting information for chapter 4

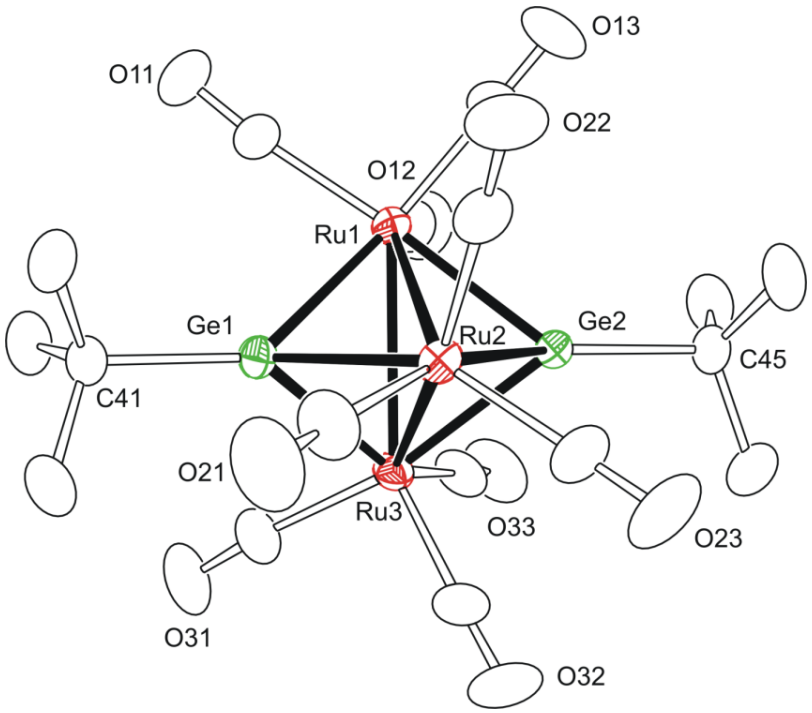

Figure C.1. The molecular structure of $Ru_3(CO)_9(\mu_3\text{-}GeBu^t)_2$, **4.1**.

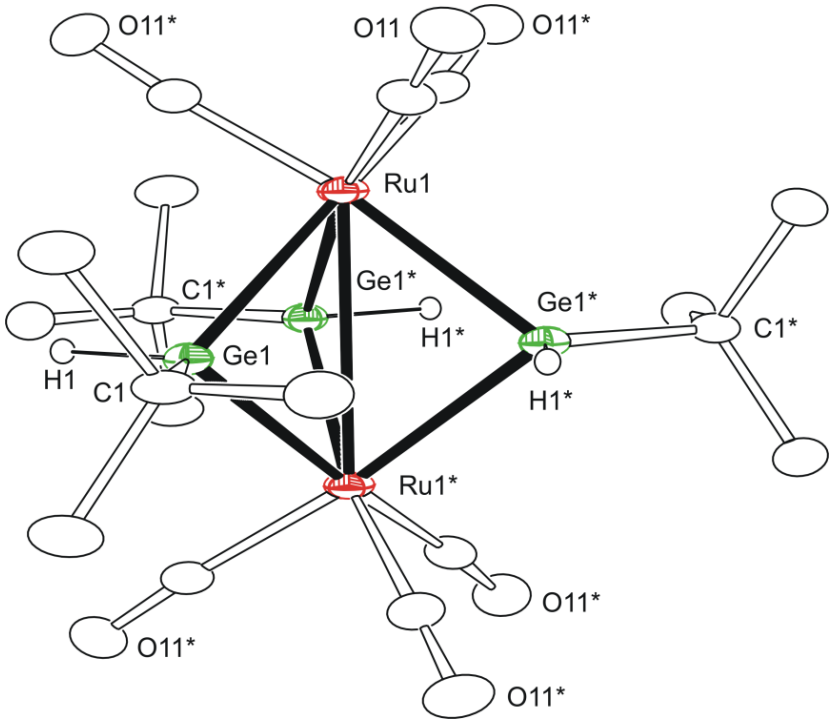

Figure C.2. The molecular structure of $Ru_2(CO)_6(\mu\text{-}GeBu^tH)_3$, **4.2**.

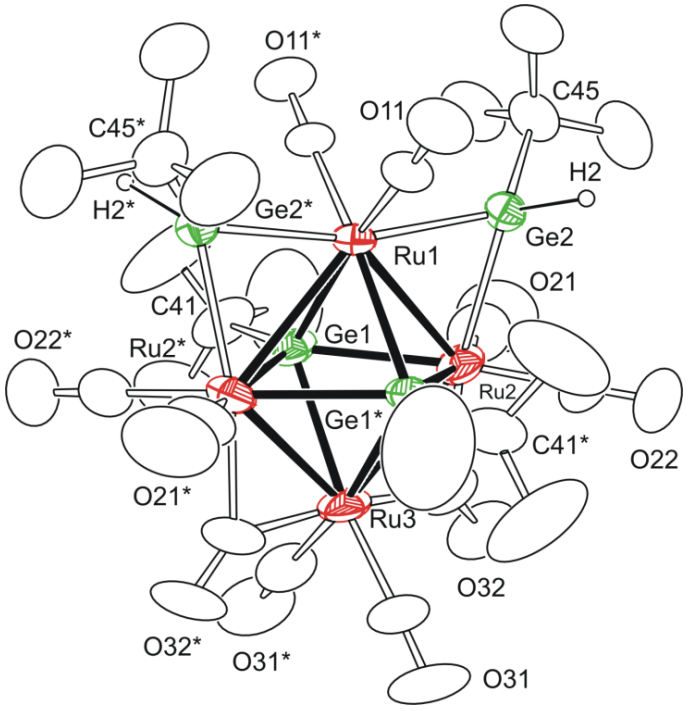

Figure C.3. The molecular structure of $Ru_4(CO)_{10}(\mu_4\text{-}Ge_2Bu^t_2)(\mu\text{-}GeBu^tH)_2$, **4.3**.

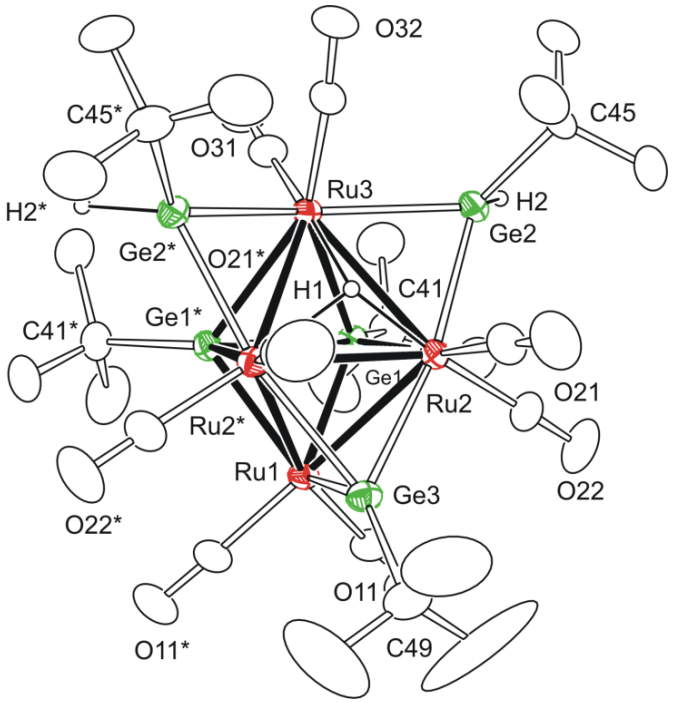

Figure C.4. The molecular structure of $Ru_4(CO)_8(\mu_4\text{-}Ge_2Bu^t_2)(\mu\text{-}GeBu^tH)_2(\mu_3\text{-}GeBu^t)(H)$, **4.4**.

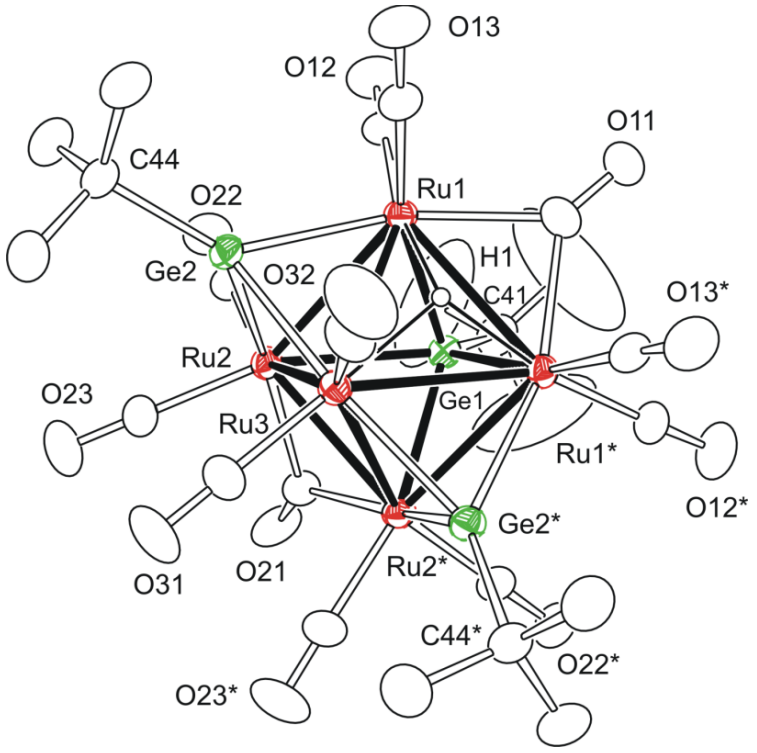

Figure C.5. The molecular structure of $Ru_5(CO)_{12}(\mu_3\text{-}GeBu^t)_2(\mu_4\text{-}GeBu^t)(H)$, **4.5**.

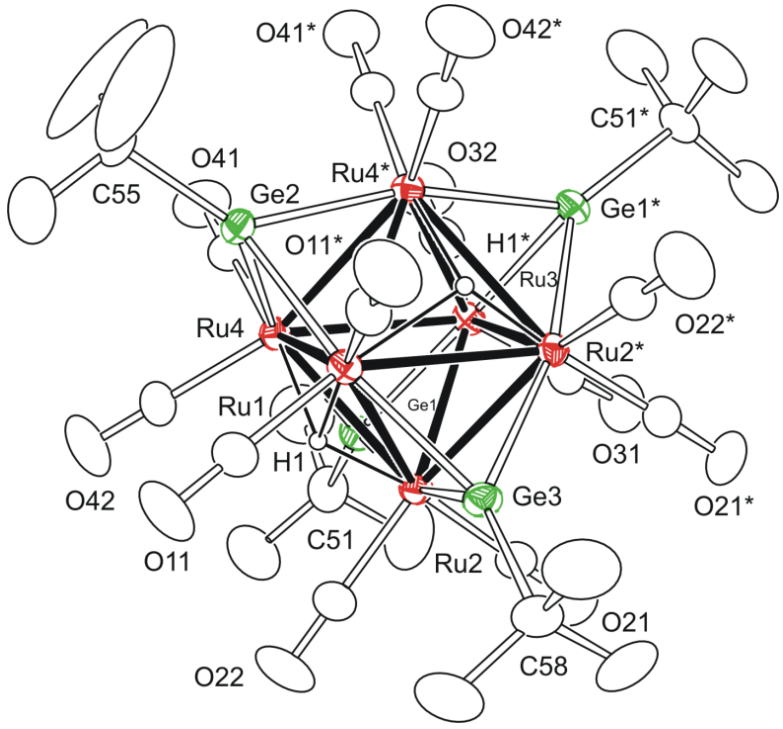

Figure C.6. The molecular structure of $Ru_6(CO)_{12}(\mu_3\text{-}GeBu^t)_4(H)_2$, **4.6**.

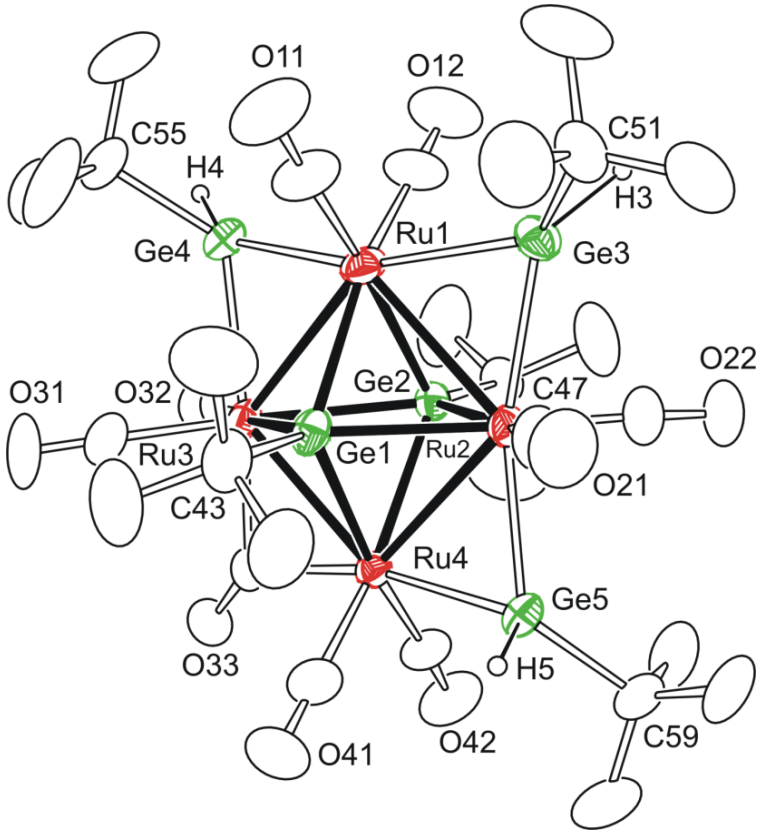

Figure C.7. The molecular structure of $Ru_4(CO)_9(\mu_4\text{-}GeBu^t)_2(\mu_2\text{-}GeBu^tH)_3$, **4.7**.

Table C.1. Crystallographic data for compounds $Ru_3(CO)_9(\mu_3\text{-}GeBu^t)_2$, 4.1, $Ru_2(CO)_6(\mu\text{-}GeBu^tH)_3$, 4.2 and $Ru_4(CO)_{10}(\mu_4\text{-}Ge_2Bu^t{}_2)(\mu\text{-}GeBu^tH)_2$, 4.3.

Compound	**4.1**	**4.2**	**4.3**
Empirical formula	$Ru_3Ge_2O_9C_{17}\ H_{18}$	$Ru_2Ge_3O_6C_{18}\ H_{30}$	$Ru_4Ge_4O_{10}C_{26}\ H_{38}$
Formula weight	814.70	762.33	1205.20
Crystal system	Monoclinic	Hexagonal	Monoclinic
Lattice parameters			
a (Å)	16.5858(7)	11.9763(7)	12.8397(8)
b (Å)	8.9936(4)	11.9763(7)	11.4929(7)
c (Å)	17.1900(7)	13.2176(8)	13.2836(9)
α (deg)	90	90	90
β (deg)	94.260(3)	90	93.2400(10)
γ (deg)	90	120	90
V ($Å^3$)	2557.08(19)	1641.83(17)	1957.1(2)
Space group	$P2_1/c$ (#14)	$P\ \bar{6}2c$ (#190)	$P2/n$ (#13)
Z value	4	2	2
ρ_{calc} (g / cm^3)	2.116	1.542	2.045
μ (Mo Kα) (mm^{-1})	4.095	3.635	4.571
Temperature (K)	296	100	296
$2\Theta_{max}$ (°)	60.00	60.10	50.00
No. Obs. ($I > 2\sigma(I)$)	6068	1487	2325
No. Parameters	286	65	223
Goodness of fit	1.076	1.264	1.037
Max. shift in cycle	0.001	0.000	0.001
Residuals*:R1; wR2	0.0342; 0.0955	0.0335; 0.1016	0.0519; 0.1203
Absorption Correction, Max/min	Multi-scan 0.9226/0.7353	Multi-scan 0.9308/0.5301	Multi-scan 0.7457/0.5367
Largest peak in Final Diff. Map (e^- / $Å^3$)	0.782	0.917	1.733

*$R = \Sigma_{hkl}(\ |\ |F_{obs}|\ -\ |F_{calc}|\ |\ )/\Sigma_{hkl}|F_{obs}|$; $R_w = [\Sigma_{hkl}w(\ |F_{obs}|\ -\ |F_{calc}|\ )^2/\Sigma_{hkl}wF_{obs}{}^2]^{1/2}$, $w = 1/\sigma^2(F_{obs})$; $GOF = [\Sigma_{hkl}w(\ |F_{obs}|\ -\ |F_{calc}|\ )^2/(n_{data} - n_{vari})]^{1/2}$.

Table C.2. Crystallographic data for compounds $Ru_4(CO)_8(\mu_4\text{-}Ge_2Bu^t_2)(\mu\text{-}GeBu^tH)_2(\mu_3\text{-}GeBu^t)(H)$, 4.4, $Ru_5(CO)_{12}(\mu_3\text{-}GeBu^t)_2(\mu_4\text{-}GeBu^t)(H)$, 4.5 and $Ru_6(CO)_{12}(\mu_3\text{-}GeBu^t)_4(H)_2$, 4.6.

	4.4	4.5	4.6
Empirical formula	$Ru_4Ge_5O_8C_{28}H_{48}$	$Ru_5Ge_3O_{12}C_{24}H_{28}$	$Ru_6Ge_4O_{12}C_{28}H_{38}$
Formula weight	1279.89	1231.58	1463.36
Crystal system	Orthorhombic	Orthorhombic	Orthorhombic
Lattice parameters			
a (Å)	12.3846(5)	21.1687(8)	17.9981(8)
b (Å)	18.6904(8)	18.8398(7)	13.0117(6)
c (Å)	18.5242(8)	9.0900(4)	19.5874(9)
α (deg)	90	90	90
β (deg)	90	90	90
γ (deg)	90	90	90
V ($Å^3$)	4287.9(3)	3625.2(2)	4587.1(4)
Space group	*Pnma* (#62)	*Pnma* (#62)	$Cmc2_1$ (#36)
Z value	4	4	4
ρ_{calc} (g / cm^3)	1.983	2.257	2.119
μ (Mo Kα) (mm^{-1})	4.858	4.526	4.543
Temperature (K)	296	296	296
$2\Theta_{max}$ (°)	60.00	60.00	56.00
No. Obs. ($I > 2\sigma(I)$)	4827	4351	5199
No. Parameters	229	223	247
Goodness of fit	1.099	1.027	1.006
Max. shift in cycle	0.002	0.001	0.001
Residuals*:R1; wR2	0.0338; 0.0828	0.0321; 0.0840	0.0261; 0.0556
Absorption Correction, Max/min	Multi-scan 0.7593/0.2597	Multi-scan 0.7729/0.2647	Multi-scan 0.8392/0.6117
Largest peak in Final Diff. Map ($e^- / Å^3$)	1.632	1.611	0.542

*$R = \Sigma_{hkl}(\,|\,|F_{obs}|-|F_{calc}|\,|)/\Sigma_{hkl}|F_{obs}|$; $R_w = [\Sigma_{hkl}w(|F_{obs}|-|F_{calc}|)^2/\Sigma_{hkl}wF_{obs}^2]^{1/2}$,
$w = 1/\sigma^2(F_{obs})$; $GOF = [\Sigma_{hkl}w(|F_{obs}|-|F_{calc}|)^2/(n_{data} - n_{vari})]^{1/2}$.

Table C.3. Crystallographic data for the compound $Ru_4(CO)_9(\mu_4\text{-}GeBu^t)_2(\mu_2\text{-}GeBu^tH)_3$, 4.7.

	4.7
Empirical formula	$Ru_4 Ge_5O_9C_{29} H_{48}$
Formula weight	1307.90
Crystal system	Triclinic
Lattice parameters	
a (Å)	12.0190(9)
b (Å)	12.2865(9)
c (Å)	17.4935(13)
α (deg)	89.7830(10)
β (deg)	87.7630(10)
γ (deg)	63.7860(10)
V ($Å^3$)	2315.6(3)
Space group	$P\ \bar{1}$ (# 2)
Z value	2
ρ_{calc} (g / cm^3)	1.876
μ (Mo Kα) (mm^{-1})	4.501
Temperature (K)	296
$2\Theta_{max}$ (°)	50.00
No. Obs. ($I > 2\sigma(I)$)	5500
No. Parameters	478
Goodness of fit	1.058
Max. shift in cycle	0.001
Residuals*:R1; wR2	0.0614; 0.1776
Absorption Correction, Max/min	Multi-scan 0.7457/0.5326
Largest peak in Final Diff. Map (e^- / $Å^3$)	1.894

*$R = \Sigma_{hkl}(\,|\,|F_{obs}|-|F_{calc}|\,|)/\Sigma_{hkl}|F_{obs}|$; $R_w = [\Sigma_{hkl}w(|F_{obs}|-|F_{calc}|)^2/\Sigma_{hkl}wF_{obs}^2]^{1/2}$, $w = 1/\sigma^2(F_{obs})$; GOF = $[\Sigma_{hkl}w(|F_{obs}|-|F_{calc}|)^2/(n_{data} - n_{vari})]^{1/2}$.

Table C.4. Selected intramolecular distances and angles for compound $Ru_3(CO)_9(\mu_3\text{-}GeBu^t)_2$, 4.1.[a]

(a) Distances

atom	atom	distance (Å)
Ru(1)	Ge(2)	2.4608(6)
Ru(1)	Ge(1)	2.4714(7)
Ru(1)	Ru(2)	2.9556(6)
Ru(1)	Ru(3)	2.9613(6)
Ru(2)	Ge(1)	2.4642(7)
Ru(2)	Ge(2)	2.4691(6)
Ru(2)	Ru(3)	2.9535(6)
Ru(3)	Ge(1)	2.4527(7)
Ru(3)	Ge(2)	2.4650(6)

(b) Angles

atom	atom	atom	angle (deg)
Ge(2)	Ru(1)	Ge(1)	92.178(18)
Ge(2)	Ru(1)	Ru(2)	53.293(15)
Ge(1)	Ru(1)	Ru(2)	53.102(17)
Ge(2)	Ru(1)	Ru(3)	53.111(13)
Ge(1)	Ru(1)	Ru(3)	52.741(17)
Ru(2)	Ru(1)	Ru(3)	59.889(14)
Ge(1)	Ru(2)	Ge(2)	92.151(16)
Ge(1)	Ru(2)	Ru(3)	52.903(15)
Ge(2)	Ru(2)	Ru(3)	53.168(15)
Ge(1)	Ru(2)	Ru(1)	53.326(16)
Ge(2)	Ru(2)	Ru(1)	53.034(13)
Ru(3)	Ru(2)	Ru(1)	60.151(14)
Ge(1)	Ru(3)	Ge(2)	92.530(17)
Ge(1)	Ru(3)	Ru(2)	53.261(18)
Ge(2)	Ru(3)	Ru(2)	53.295(14)
Ge(1)	Ru(3)	Ru(1)	53.321(14)
Ge(2)	Ru(3)	Ru(1)	52.980(15)
Ru(2)	Ru(3)	Ru(1)	59.960(12)
Ru(3)	Ge(1)	Ru(2)	73.837(16)
Ru(3)	Ge(1)	Ru(1)	73.937(16)
Ru(2)	Ge(1)	Ru(1)	73.572(15)
Ru(1)	Ge(2)	Ru(3)	73.909(19)
Ru(1)	Ge(2)	Ru(2)	73.672(17)
Ru(3)	Ge(2)	Ru(2)	73.537(17)

[a] Estimated standard deviations in the least significant figure are given in parentheses.

Table C.5. Selected intramolecular distances and angles for compound $Ru_2(CO)_6(\mu\text{-}GeBu^tH)_3$, 4.2.[a]

(a) Distances

atom	atom	distance (Å)
Ru(1)	Ru(1)*	2.9541(9)
Ru(1)	Ge(1)	2.5114(7)
Ru(1)*	Ge(1)	2.5113(7)

(b) Angles

atom	atom	atom	angle (deg)
Ge(1)	Ru(1)	Ru(1)*	53.973(14)
Ru(1)	Ge(1)	Ru(1)*	72.05(3)

[a] Estimated standard deviations in the least significant figure are given in parentheses.

Table C.6. Selected intramolecular distances and angles for compound $Ru_4(CO)_{10}(\mu_4\text{-}GeBu^t)_2(\mu\text{-}GeBu^tH)_2$, 4.3.[a]

(a) Distances

atom	atom	distance (Å)
Ru(1)	Ge(1)	2.5208(11)
Ru(1)	Ge(1)*	2.5209(11)
Ru(1)	Ru(2)	2.9469(9)
Ru(1)	Ru(2)*	2.9469(9)
Ru(2)	Ge(1)*	2.5655(16)
Ru(2)	Ge(1)	2.5861(14)
Ru(2)	Ru(3)	2.8314(12)
Ru(3)	Ge(1)*	2.6119(12)
Ru(3)	Ge(1)	2.6119(12)
Ru(3)	Ru(2)*	2.8314(12)
Ge(1)	Ru(2)*	2.5655(16)

(b) Angles

atom	atom	atom	angle (deg)
Ge(1)	Ru(1)	Ge(1)*	76.37(5)
Ge(1)	Ru(1)	Ru(2)	55.80(3)
Ge(1)*	Ru(1)	Ru(2)	55.30(4)
Ge(1)	Ru(1)	Ru(2)*	55.31(4)
Ge(1)*	Ru(1)	Ru(2)*	55.80(3)
Ru(2)	Ru(1)	Ru(2)*	87.95(4)
Ge(1)*	Ru(2)	Ge(1)	74.46(4)
Ge(1)*	Ru(2)	Ru(3)	57.64(3)
Ge(1)	Ru(2)	Ru(3)	57.43(3)
Ge(1)*	Ru(2)	Ru(1)	53.89(3)
Ge(1)	Ru(2)	Ru(1)	53.73(3)
Ru(3)	Ru(2)	Ru(1)	89.74(3)
Ge(1)*	Ru(3)	Ge(1)	73.26(5)
Ge(1)*	Ru(3)	Ru(2)	56.06(3)
Ge(1)	Ru(3)	Ru(2)	56.56(3)
Ge(1)	Ru(3)	Ru(2)*	56.07(3)
Ru(2)	Ru(3)	Ru(2)*	92.56(4)
Ru(1)	Ge(1)	Ru(2)*	70.81(3)
Ru(1)	Ge(1)	Ru(2)	70.47(3)
Ru(1)	Ge(1)	Ru(3)	105.19(4)
Ru(2)	Ge(1)	Ru(3)	66.01(3)

[a] Estimated standard deviations in the least significant figure are given in parentheses.

Table C.7. Selected intramolecular distances and angles for compound $Ru_4(CO)_8(\mu_4\text{-}GeBu^t)_2(\mu\text{-}GeBu^tH)_2(\mu_3\text{-}GeBu^t)(H)$, 4.4.[a]

(a) Distances

atom	atom	distance (Å)
Ru(1)	Ge(1)*	2.4976(6)
Ru(1)	Ge(1)	2.4977(6)
Ru(1)	Ru(2)*	2.9299(5)
Ru(1)	Ru(2)	2.9299(5)
Ru(2)	Ge(1)	2.5490(5)
Ru(2)	Ru(2)*	2.9121(6)
Ru(2)	Ru(3)	2.9455(5)
Ru(3)	Ge(1)	2.6517(6)
Ru(3)	Ge(1)*	2.6517(6)
Ru(3)	Ru(2)*	2.9455(5)
Ge(1)	Ge(1)*	2.4490(8)

(b) Angles

atom	atom	atom	angle (deg)
Ge(1)*	Ru(1)	Ge(1)	58.72(2)
Ge(1)*	Ru(1)	Ru(2)*	55.333(14)
Ge(1)	Ru(1)	Ru(2)*	85.324(16)
Ge(1)*	Ru(1)	Ru(2)	85.324(16)
Ge(1)	Ru(1)	Ru(2)	55.331(14)
Ru(2)*	Ru(1)	Ru(2)	59.600(15)
Ge(1)	Ru(2)	Ru(2)*	84.789(11)
Ge(1)	Ru(2)	Ru(1)	53.698(14)
Ru(2)*	Ru(2)	Ru(1)	60.200(7)
Ge(1)	Ru(2)	Ru(3)	57.165(14)
Ru(2)*	Ru(2)	Ru(3)	60.374(8)
Ru(1)	Ru(2)	Ru(3)	87.601(14)
Ge(1)	Ru(3)	Ru(2)*	82.357(16)
Ge(1)	Ru(3)	Ru(2)	53.873(13)
Ge(1)*	Ru(3)	Ru(2)	82.356(16)
Ru(2)*	Ru(3)	Ru(2)	59.253(15)
Ge(1)*	Ge(1)	Ru(1)	60.641(11)
Ge(1)*	Ge(1)	Ru(2)	95.212(11)
Ru(1)	Ge(1)	Ru(2)	70.970(16)
Ru(1)	Ge(1)	Ru(3)	104.281(18)
Ru(2)	Ge(1)	Ru(3)	68.962(16)

[a] Estimated standard deviations in the least significant figure are given in parentheses.

Table C.8. Selected intramolecular distances and angles for compound $Ru_5(CO)_{12}(\mu_3\text{-}GeBu^t)_2(\mu_4\text{-}GeBu^t)(H)$, 4.5.[a]

(a) Distances

atom	atom	distance (Å)
Ru(1)	Ru(1)*	2.8765(5)
Ru(1)	Ru(2)	2.9404(4)
Ru(1)	Ru(3)	2.9424(5)
Ru(1)	Ge(1)	2.5525(5)
Ru(2)	Ru(2)*	2.7997(5)
Ru(2)	Ru(3)	2.9080(5)
Ru(2)	Ge(1)	2.5388(5)
Ru(3)	Ru(1)*	2.9423(5)
Ru(3)	Ru(2)*	2.9080(5)
Ge(1)	Ru(1)*	2.5524(5)
Ge(1)	Ru(2)*	2.5387(5)

(b) Angles

atom	atom	atom	angle (deg)
Ge(1)	Ru(1)	Ru(1)*	55.703(9)
Ge(1)	Ru(1)	Ru(2)	54.505(14)
Ru(1)*	Ru(1)	Ru(2)	89.250(7)
Ge(1)	Ru(1)	Ru(3)	81.849(15)
Ru(1)*	Ru(1)	Ru(3)	60.737(7)
Ru(2)	Ru(1)	Ru(3)	59.250(11)
Ge(1)	Ru(2)	Ru(2)*	56.537(9)
Ge(1)	Ru(2)	Ru(3)	82.769(15)
Ru(2)*	Ru(2)	Ru(3)	61.225(7)
Ge(1)	Ru(2)	Ru(1)	54.941(14)
Ru(2)*	Ru(2)	Ru(1)	90.748(7)
Ru(3)	Ru(2)	Ru(1)	60.410(11)
Ru(2)	Ru(3)	Ru(2)*	57.551(13)
Ru(2)	Ru(3)	Ru(1)*	88.611(14)
Ru(2)	Ru(3)	Ru(1)	60.341(11)
Ru(2)*	Ru(3)	Ru(1)	88.610(14)
Ru(1)	Ru(3)	Ru(1)*	58.524(13)
Ru(2)	Ge(1)	Ru(2)*	66.925(19)
Ru(2)	Ge(1)	Ru(1)*	106.77(2)
Ru(2)	Ge(1)	Ru(1)	70.554(14)
Ru(1)	Ge(1)	Ru(1)*	68.593(19)

[a] Estimated standard deviations in the least significant figure are given in parentheses.

Table C.9. Selected intramolecular distances and angles for compound $Ru_6(CO)_{12}(\mu_3\text{-}GeBu^t)_4(H)_2$, 4.6.[a]

(a) Distances

atom	atom	distance (Å)
Ru(1)	Ru(2)	2.9591(6)
Ru(1)	Ru(2)*	2.9591(6)
Ru(1)	Ru(4)	2.9657(5)
Ru(1)	Ru(4)*	2.9657(5)
Ru(2)	Ru(2)*	2.8863(6)
Ru(2)	Ru(3)	2.8730(5)
Ru(2)	Ru(4)	2.9414(5)
Ru(3)	Ru(2)*	2.8731(5)
Ru(3)	Ru(4)	2.8842(5)
Ru(3)	Ru(4)*	2.8841(5)
Ru(4)	Ru(4)*	2.9290(6)

(b) Angles

atom	atom	atom	angle (deg)
Ru(2)	Ru(1)	Ru(2)*	58.379(16)
Ru(2)	Ru(1)	Ru(4)*	88.542(16)
Ru(2)	Ru(1)	Ru(4)	59.531(12)
Ru(2)*	Ru(1)	Ru(4)	88.545(16)
Ru(4)*	Ru(1)	Ru(4)	59.182(15)
Ru(3)	Ru(2)	Ru(2)*	59.849(8)
Ru(3)	Ru(2)	Ru(4)	59.463(13)
Ru(2)*	Ru(2)	Ru(4)	90.416(9)
Ru(3)	Ru(2)	Ru(1)	89.979(14)
Ru(2)*	Ru(2)	Ru(1)	60.810(8)
Ru(4)	Ru(2)	Ru(1)	60.346(12)
Ru(2)	Ru(3)	Ru(2)*	60.305(16)
Ru(2)	Ru(3)	Ru(4)	61.448(12)
Ru(2)*	Ru(3)	Ru(4)	91.842(17)
Ru(2)	Ru(3)	Ru(4)*	91.842(17)
Ru(4)	Ru(3)	Ru(4)*	61.031(16)
Ru(3)	Ru(4)	Ru(4)*	59.484(8)
Ru(3)	Ru(4)	Ru(2)	59.089(13)
Ru(4)*	Ru(4)	Ru(2)	89.582(9)
Ru(3)	Ru(4)	Ru(1)	89.633(14)
Ru(2)	Ru(4)	Ru(1)	60.123(13)

[a] Estimated standard deviations in the least significant figure are given in parentheses.

Table C.10. Selected intramolecular distances and angles for compound $Ru_4(CO)_9(\mu_4\text{-}GeBu^t)_2(\mu_2\text{-}GeBu^tH)_3$, 4.7.[a]

(a) Distances

atom	atom	distance (Å)
Ru(1)	Ru(2)	2.9567(14)
Ru(1)	Ru(3)	2.9433(14)
Ru(1)	Ge(1)	2.5602(18)
Ru(1)	Ge(2)	2.5450(16)
Ru(2)	Ru(4)	2.9327(13)
Ru(2)	Ge(1)	2.5583(16)
Ru(2)	Ge(2)	2.5515(15)
Ru(3)	Ru(4)	2.8054(13)
Ru(3)	Ge(1)	2.6202(15)
Ru(3)	Ge(2)	2.6045(15)
Ru(4)	Ge(1)	2.6009(15)
Ru(4)	Ge(2)	2.6094(15)

(b) Angles

atom	atom	atom	angle (deg)
Ge(2)	Ru(1)	Ru(3)	56.10(4)
Ge(1)	Ru(1)	Ru(3)	56.35(4)
Ge(2)	Ru(1)	Ru(2)	54.64(4)
Ge(1)	Ru(1)	Ru(2)	54.68(4)
Ru(3)	Ru(1)	Ru(2)	88.58(4)
Ge(2)	Ru(2)	Ru(4)	56.31(4)
Ge(1)	Ru(2)	Ru(4)	56.05(4)
Ge(2)	Ru(2)	Ru(1)	54.44(4)
Ge(1)	Ru(2)	Ru(1)	54.74(4)
Ru(4)	Ru(2)	Ru(1)	88.47(4)
Ge(2)	Ru(3)	Ru(4)	57.53(4)
Ge(1)	Ru(3)	Ru(4)	57.17(4)
Ge(2)	Ru(3)	Ru(1)	54.19(4)
Ge(1)	Ru(3)	Ru(1)	54.42(4)
Ru(4)	Ru(3)	Ru(1)	91.20(4)
Ge(1)	Ru(4)	Ru(3)	57.83(4)
Ge(2)	Ru(4)	Ru(3)	57.36(4)
Ge(1)	Ru(4)	Ru(2)	54.68(4)
Ge(2)	Ru(4)	Ru(2)	54.45(4)
Ru(3)	Ru(4)	Ru(2)	91.75(4)

[a] Estimated standard deviations in the least significant figure are given in parentheses.

Appendix D: Supporting information for chapter 5

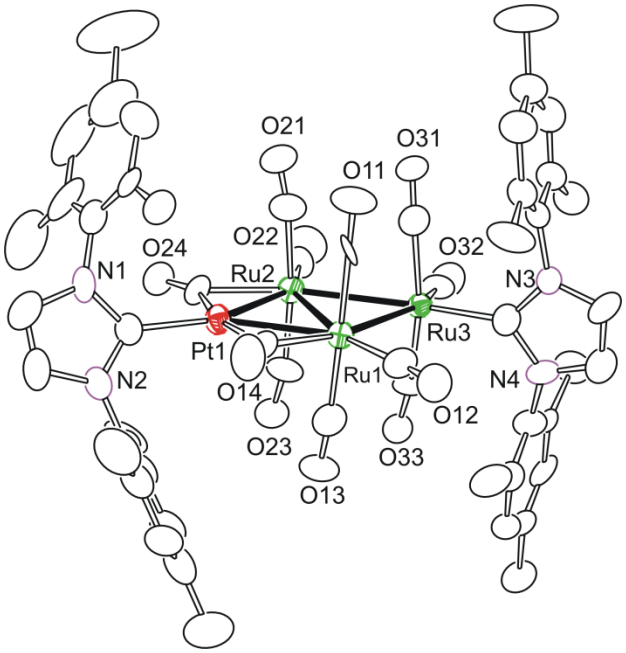

Figure D.1. The molecular structure of $Ru_3Pt(IMes)_2(CO)_{11}$, **5.1**.

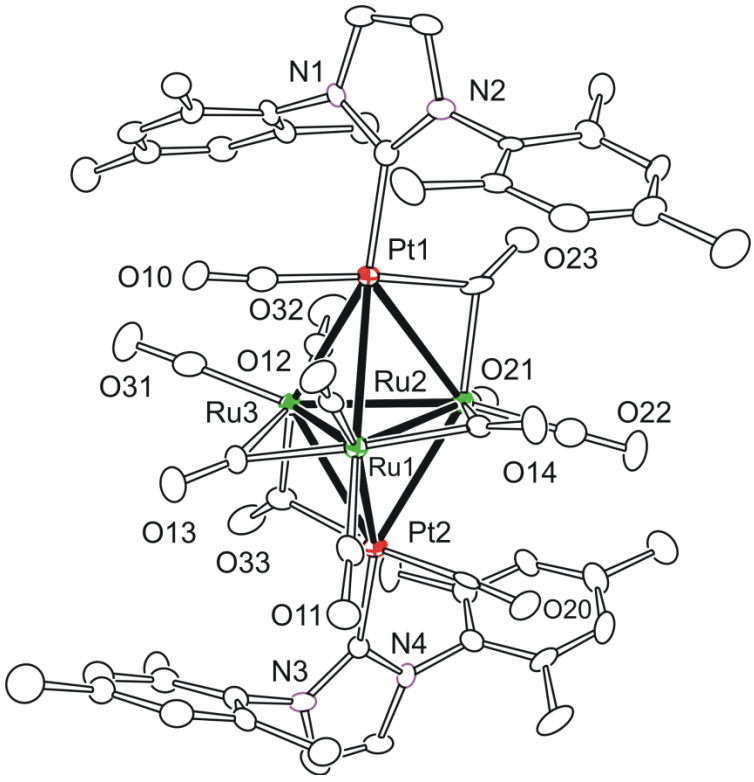

Figure D.2. The molecular structure of $Ru_3Pt_2(IMes)_2(CO)_{12}$, **5.2**.

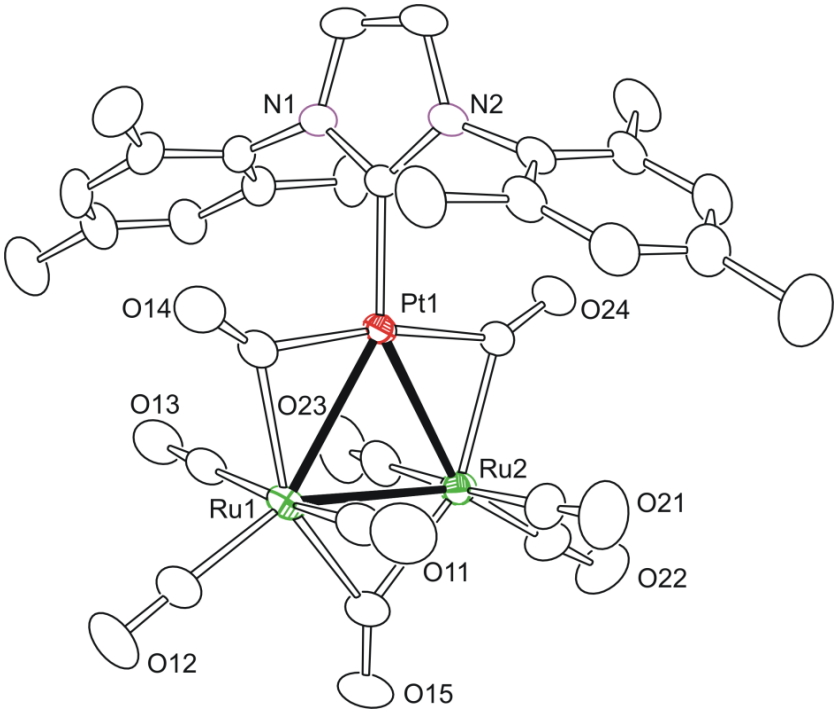

Figure D.3. The molecular structure of $Ru_2Pt(IMes)(CO)_9$, **5.3**.

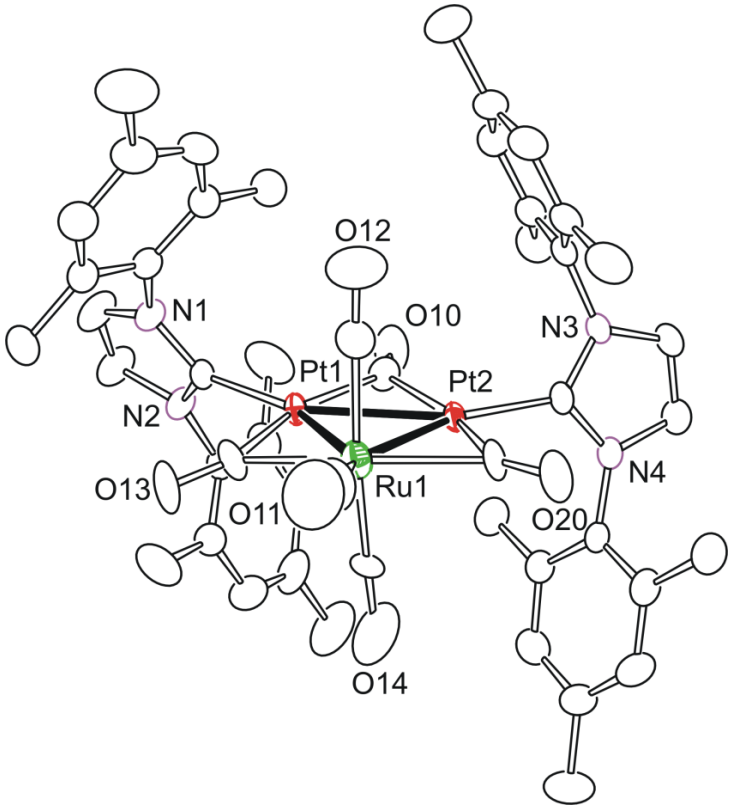

Figure D.4. The molecular structure of $RuPt_2(IMes)_2(CO)_6$, **5.4**.

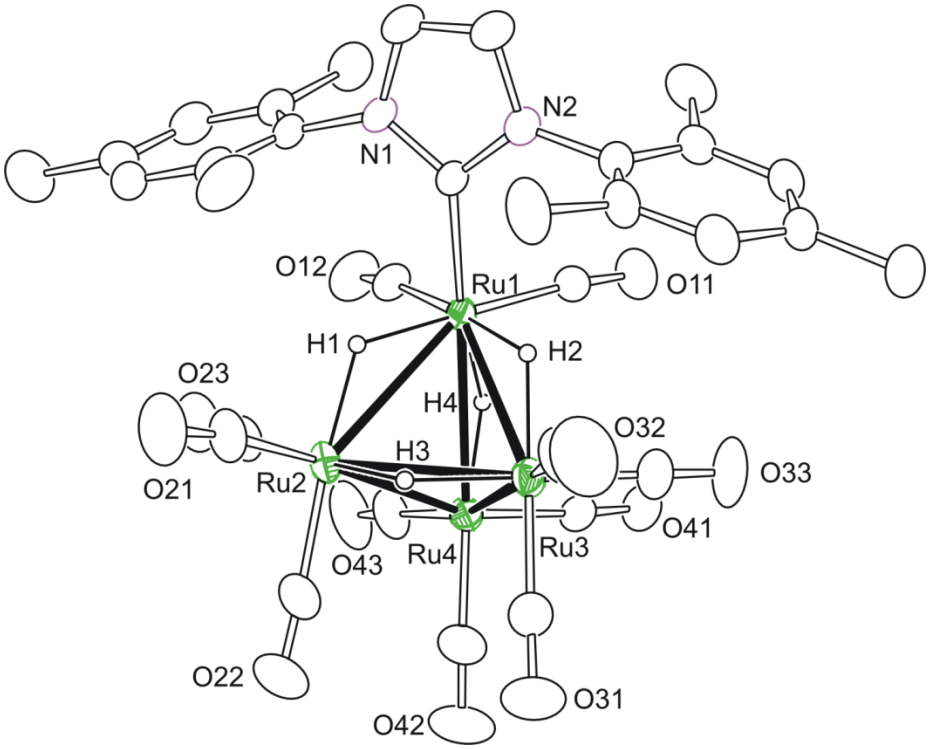

Figure D.5. The molecular structure of $Ru_4(IMes)(CO)_{11}(\mu\text{-}H)_4$, **5.5**.

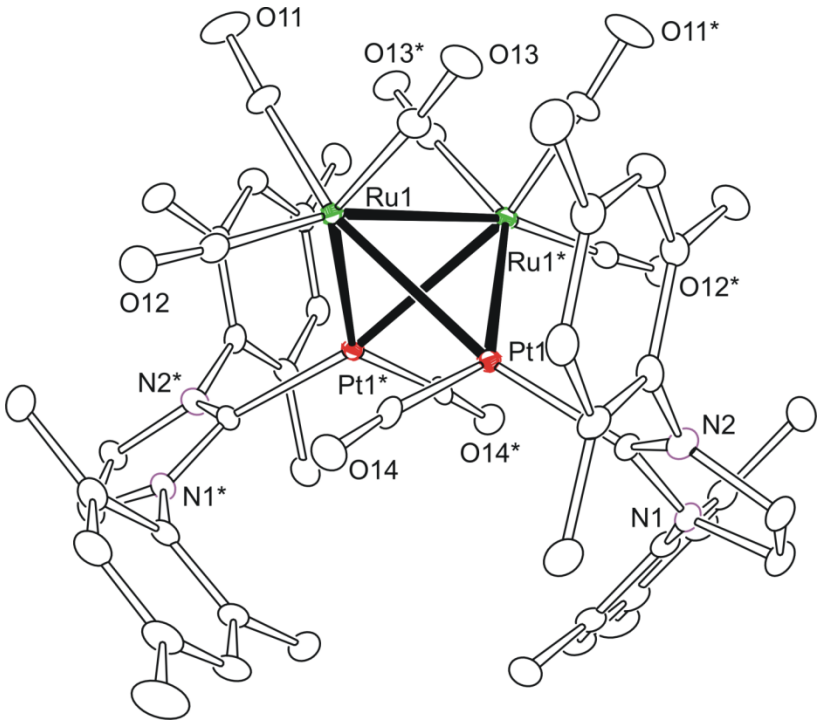

Figure D.6. The molecular structure of $Ru_2Pt_2(IMes)_2(CO)_8(\mu\text{-}H)_2$, **5.6**.

Table D.1. Crystallographic data for compounds $Ru_3Pt(IMes)_2(CO)_{11}$, 5.1 and $Ru_3Pt_2(IMes)_2(CO)_{12}$, 5.2.

	5.1	**5.2**
Empirical formula	$PtRu_3C_{53}H_{48}N_4O_{11}$	$Pt_2Ru_3C_{54}H_{48}N_4O_{12}$
Formula weight	1415.25	1638.35
Crystal system	Monoclinic	Monoclinic
Lattice parameters		
a (Å)	18.081(1)	16.4415(9)
b (Å)	41.675(2)	15.8001(9)
c (Å)	16.910 (1)	20.6466(12)
α (deg)	90	90
β (deg)	90.162 (1)	90.086 (1)
γ (deg)	90	90
V (Å^3)	12742.1(13)	5363.5(5)
Space group	*P* $2_1/c$ (# 14)	*P* $2_1/n$ (# 14)
Z value	8	4
ρ_{calc} (g / cm^3)	1.475	2.029
μ (Mo Kα) (mm^{-1})	2.938	6.088
Temperature (K)	296	100
$2\Theta_{max}$ (°)	50.00	55.00
No. Obs. (I > 2σ(I))	12533	11033
No. Parameters	1298	689
Goodness of fit	1.114	1.110
Max. shift in cycle	0.001	0.002
Residuals*:R1; wR2	0.1055; 0.2239	0.0485; 0.1155
Absorption Correction, Max/min	Multi-scan 0.6199/ 0.4727	Multi-scan 0.8879/ 0.2805
Largest peak in Final Diff. Map (e$^-$ / Å^3)	2.068	3.970

*$R = \Sigma_{hkl}(\,|\,|F_{obs}|-|F_{calc}|\,|)/\Sigma_{hkl}|F_{obs}|$; $R_w = [\Sigma_{hkl}w(|F_{obs}|-|F_{calc}|)^2/\Sigma_{hkl}wF_{obs}^2]^{1/2}$, $w = 1/\sigma^2(F_{obs})$; $GOF = [\Sigma_{hkl}w(|F_{obs}|-|F_{calc}|)^2/(n_{data} - n_{vari})]^{1/2}$.

Table D.2. Crystallographic data for compounds $Ru_2Pt(IMes)(CO)_9$, 5.3 and $RuPt_2(IMes)_2(CO)_6$, 5.4.

	5.3	5.4
Empirical formula	$PtRu_2C_{30}H_{20}N_2O_9$	$Pt_2RuC_{48}H_{48}N_4O_6$
Formula weight	949.71	1268.15
Crystal system	Triclinic	Monoclinic
Lattice parameters		
a (Å)	9.0916(3)	22.2711(9)
b (Å)	10.8002(4)	10.6747(4)
c (Å)	18.0566(7)	22.7224(9)
α (deg)	81.060 (1)	90
β (deg)	80.374 (1)	117.779 (1)
γ (deg)	72.777 (1)	90
V ($Å^3$)	1659.06(10)	4779.4(3)
Space group	$P\ \bar{1}$ (# 2)	$P\ 2_1/c$ (# 14)
Z value	2	4
ρ_{calc} (g / cm^3)	1.901	1.762
μ (Mo Kα) (mm^{-1})	5.156	6.201
Temperature (K)	296	296
$2\Theta_{max}$ (°)	56.00	50.00
No. Obs. ($I > 2\sigma(I)$)	7404	7411
No. Parameters	397	562
Goodness of fit	1.081	1.031
Max. shift in cycle	0.004	0.007
Residuals*:R1; wR2	0.0231; 0.0573	0.0497; 0.1350
Absorption Correction, Max/min	Multi-scan 0.7461/ 0.5443	Multi-scan 0.8860/ 0.3702
Largest peak in Final Diff. Map (e^- / $Å^3$)	0.735	7.935

*$R = \Sigma_{hkl}(\ |\ |F_{obs}|\ -\ |F_{calc}|\ |\ )/\Sigma_{hkl}|F_{obs}|$; $R_w = [\Sigma_{hkl}w(\ |F_{obs}|\ -\ |F_{calc}|\ )^2/\Sigma_{hkl}wF_{obs}^2]^{1/2}$, $w = 1/\sigma^2(F_{obs})$; $GOF = [\Sigma_{hkl}w(\ |F_{obs}|\ -\ |F_{calc}|\ )^2/(n_{data} - n_{vari})]^{1/2}$.

Table D.3. Crystallographic data for the compound $Ru_4(IMes)(CO)_{11}(\mu\text{-}H)_4$, 5.5 and $Ru_2Pt_2(IMes)_2(CO)_8(\mu\text{-}H)_2$, 5.6.

	5.5	**5.6**
Empirical formula	$Ru_4C_{32}H_{28}N_2O_{11}$	$Pt_2Ru_2C_{50}H_{48}N_4O_8 \bullet 2\ CH_2Cl_2$
Formula weight	1020.84	1595.10
Crystal system	Triclinic	Monoclinic
Lattice parameters		
a (Å)	11.1505(5)	18.1662(9)
b (Å)	11.3048(5)	17.0073(9)
c (Å)	15.8466(7)	12.9425(7)
α (deg)	108.061 (1)	90
β (deg)	99.189 (1)	130.8510(10)
γ (deg)	94.688 (1)	90
V ($Å^3$)	1856.31(14)	3024.7(3)
Space group	$P\ \bar{1}$ (# 2)	$C\ 2$ (# 5)
Z value	2	2
ρ_{calc} (g / cm^3)	1.826	1.751
μ (Mo Kα) (mm^{-1})	1.653	5.327
Temperature (K)	296	100
$2\Theta_{max}$ (°)	60.00	62.00
No. Obs. ($I > 2\sigma(I)$)	7738	8914
No. Parameters	460	331
Goodness of fit	1.000	1.056
Max. shift in cycle	0.002	0.002
Residuals*:R1; wR2	0.0324; 0.0623	0.0309; 0.0939
Absorption Correction, Max/min	Multi-scan 0.7461/ 0.6543	Multi-scan 0.7465/ 0.4030
Largest peak in Final Diff. Map (e^- / $Å^3$)	0.509	4.561

*$R = \Sigma_{hkl}(\ |\ |F_{obs}|\ -\ |F_{calc}|\ |\ )/\Sigma_{hkl}|F_{obs}|$; $R_w = [\Sigma_{hkl}w(\ |F_{obs}|\ -\ |F_{calc}|\ )^2/\Sigma_{hkl}wF_{obs}^2]^{1/2}$, $w = 1/\sigma^2(F_{obs})$; $GOF = [\Sigma_{hkl}w(\ |F_{obs}|\ -\ |F_{calc}|\ )^2/(n_{data} - n_{vari})]^{1/2}$.

Table D.4. Selected intramolecular distances and angles for compound $Ru_3Pt(IMes)_2(CO)_{11}$, 5.1.[a]

(a) Distances

atom	atom	distance (Å)	atom	atom	distance (Å)
Pt(1)	C(71)	2.02(3)	Ru(2)	C(24)	2.10(3)
Pt(1)	C(24)	2.03(3)	Ru(2)	Ru(3)	2.915(3)
Pt(1)	C(14)	2.08(3)	Ru(3)	C(92)	2.07(3)
Pt(1)	Ru(2)	2.690(2)	Ru(4)	Ru(5)	2.890(3)
Pt(1)	Ru(1)	2.699(2)	Ru(4)	Ru(6)	2.908(3)
Pt(2)	Ru(4)	2.679(2)	Ru(5)	Ru(6)	2.887(2)
Pt(2)	Ru(5)	2.690(2)	N(1)	C(71)	1.35(3)
Ru(1)	C(14)	2.11(3)	N(2)	C(71)	1.38(3)
Ru(1)	Ru(3)	2.890(3)	N(3)	C(92)	1.41(3)
Ru(1)	Ru(2)	2.892(3)	N(4)	C(92)	1.42(3)

(b) Angles

atom	atom	atom	angle (deg)
C(71)	Pt(1)	Ru(2)	146.6(8)
C(24)	Pt(1)	Ru(2)	50.5(7)
C(14)	Pt(1)	Ru(2)	115.0(8)
C(71)	Pt(1)	Ru(1)	148.4(9)
C(24)	Pt(1)	Ru(1)	115.4(7)
C(14)	Pt(1)	Ru(1)	50.3(8)
Ru(2)	Pt(1)	Ru(1)	64.91(6)
Ru(4)	Pt(2)	Ru(5)	65.12(6)
Pt(1)	Ru(1)	Ru(3)	117.92(8)
Pt(1)	Ru(1)	Ru(2)	57.39(6)
Ru(3)	Ru(1)	Ru(2)	60.54(6)
Pt(1)	Ru(2)	Ru(1)	57.70(6)
Pt(1)	Ru(2)	Ru(3)	117.38(8)
Ru(1)	Ru(2)	Ru(3)	59.69(6)
Pt(2)	Ru(4)	Ru(5)	57.61(5)
Pt(2)	Ru(4)	Ru(6)	117.33(8)
Ru(5)	Ru(4)	Ru(6)	59.71(6)
Pt(2)	Ru(5)	Ru(6)	117.72(8)
Pt(2)	Ru(5)	Ru(4)	57.26(6)
Ru(6)	Ru(5)	Ru(4)	60.46(6)
Ru(5)	Ru(6)	Ru(4)	59.82(6)

[a]Estimated standard deviations in the least significant figure are given in parentheses.

Table D.5. Selected intramolecular distances and angles for compound $Ru_3Pt_2(IMes)_2(CO)_{12}$, 5.2.[a]

(a) Distances

atom	atom	distance (Å)	atom	atom	distance (Å)
Pt(1)	C(10)	1.912(12)	Ru(1)	C(13)	2.093(11)
Pt(1)	C(41)	2.054(10)	Ru(1)	Ru(2)	2.7299(13)
Pt(1)	C(23)	2.096(13)	Ru(1)	Ru(3)	2.7419(13)
Pt(1)	Ru(2)	2.8331(10)	Ru(2)	C(23)	1.984(11)
Pt(1)	Ru(1)	2.9382(10)	Ru(2)	C(14)	2.191(11)
Pt(1)	Ru(3)	2.9392(10)	Ru(2)	Ru(3)	2.9533(12)
Pt(2)	C(20)	1.912(14)	Ru(3)	C(33)	1.988(12)
Pt(2)	C(71)	2.055(11)	Ru(3)	C(13)	2.155(11)
Pt(2)	C(33)	2.119(13)	N(1)	C(41)	1.367(14)
Pt(2)	Ru(3)	2.8102(10)	N(2)	C(41)	1.375(14)
Pt(2)	Ru(2)	2.9125(10)	N(3)	C(71)	1.366(14)
Pt(2)	Ru(1)	2.9947(10)	N(4)	C(71)	1.354(15)
Ru(1)	C(14)	2.046(11)			

(b) Angles

atom	atom	atom	angle (deg)	atom	atom	atom	angle (deg)
Ru(2)	Pt(1)	Ru(1)	56.42(3)	Ru(1)	Ru(2)	Pt(1)	63.73(3)
Ru(2)	Pt(1)	Ru(3)	61.51(3)	C(14)	Ru(2)	Pt(2)	94.0(3)
Ru(1)	Pt(1)	Ru(3)	55.62(3)	Ru(1)	Ru(2)	Pt(2)	64.02(3)
Ru(3)	Pt(2)	Ru(2)	62.11(3)	Pt(1)	Ru(2)	Pt(2)	113.40(3)
Ru(3)	Pt(2)	Ru(1)	56.26(3)	C(14)	Ru(2)	Ru(3)	104.6(3)
Ru(2)	Pt(2)	Ru(1)	55.03(3)	Ru(1)	Ru(2)	Ru(3)	57.53(3)
C(14)	Ru(1)	Ru(2)	52.3(3)	Pt(1)	Ru(2)	Ru(3)	61.01(3)
C(13)	Ru(1)	Ru(2)	115.5(3)	Pt(2)	Ru(2)	Ru(3)	57.25(2)
Ru(2)	Ru(1)	Ru(3)	65.33(3)	C(13)	Ru(3)	Ru(1)	48.8(3)
C(14)	Ru(1)	Pt(1)	78.7(3)	C(13)	Ru(3)	Pt(2)	81.2(3)
C(13)	Ru(1)	Pt(1)	94.1(3)	Ru(1)	Ru(3)	Pt(2)	65.27(3)
Ru(2)	Ru(1)	Pt(1)	59.84(3)	C(13)	Ru(3)	Pt(1)	92.8(3)
Ru(3)	Ru(1)	Pt(1)	62.21(3)	Ru(1)	Ru(3)	Pt(1)	62.17(3)
C(14)	Ru(1)	Pt(2)	94.8(3)	Pt(2)	Ru(3)	Pt(1)	113.27(3)
C(13)	Ru(1)	Pt(2)	77.8(3)	C(13)	Ru(3)	Ru(2)	105.4(3)
Ru(2)	Ru(1)	Pt(2)	60.96(3)	Ru(1)	Ru(3)	Ru(2)	57.14(3)
Ru(3)	Ru(1)	Pt(2)	58.47(3)	Pt(2)	Ru(3)	Ru(2)	60.65(3)
Pt(1)	Ru(1)	Pt(2)	108.08(3)	Pt(1)	Ru(3)	Ru(2)	57.47(2)

[a]Estimated standard deviations in the least significant figure are given in parentheses.

Table D.6. Selected intramolecular distances and angles for compound $Ru_2Pt(IMes)(CO)_9$, 5.3.[a]

(a) Distances

atom	atom	distance (Å)	atom	atom	distance (Å)
Pt(1)	C(24)	2.020(3)	Ru(1)	C(14)	2.205(3)
Pt(1)	C(14)	2.024(3)	Ru(1)	Ru(2)	2.8658(4)
Pt(1)	C(31)	2.026(3)	Ru(2)	C(15)	2.171(3)
Pt(1)	Ru(2)	2.7161(3)	Ru(2)	C(24)	2.176(3)
Pt(1)	Ru(1)	2.7241(3)	N(1)	C(31)	1.361(4)
Ru(1)	C(15)	2.120(4)	N(2)	C(31)	1.357(4)

(b) Angles

atom	atom	atom	angle (deg)
C(24)	Pt(1)	Ru(2)	52.21(9)
C(14)	Pt(1)	Ru(2)	116.39(9)
C(31)	Pt(1)	Ru(2)	147.96(8)
C(24)	Pt(1)	Ru(1)	115.79(9)
C(14)	Pt(1)	Ru(1)	52.89(9)
C(31)	Pt(1)	Ru(1)	148.28(8)
Ru(2)	Pt(1)	Ru(1)	63.576(8)
C(15)	Ru(1)	Pt(1)	106.95(10)
C(14)	Ru(1)	Pt(1)	47.05(8)
C(15)	Ru(1)	Ru(2)	48.87(10)
C(14)	Ru(1)	Ru(2)	105.07(8)
Pt(1)	Ru(1)	Ru(2)	58.077(7)
C(15)	Ru(2)	Pt(1)	105.68(10)
C(24)	Ru(2)	Pt(1)	47.20(8)
C(15)	Ru(2)	Ru(1)	47.34(10)
C(24)	Ru(2)	Ru(1)	105.54(8)
Pt(1)	Ru(2)	Ru(1)	58.347(8)

[a]Estimated standard deviations in the least significant figure are given in parentheses.

Table D.7. Selected intramolecular distances and angles for compound $RuPt_2(IMes)_2(CO)_6$, 5.4.[a]

(a) Distances

atom	atom	distance (Å)	atom	atom	distance (Å)
Pt(1)	C(13)	2.009(8)	Pt(2)	Ru(1)	2.7288(8)
Pt(1)	C(31)	2.030(8)	Ru(1)	C(13)	2.155(8)
Pt(1)	C(10)	2.072(9)	Ru(1)	C(20)	2.223(8)
Pt(1)	Pt(2)	2.6477(4)	N(3)	C(61)	1.344(11)
Pt(1)	Ru(1)	2.6893(8)	N(2)	C(31)	1.368(11)
Pt(2)	C(20)	2.015(9)	N(4)	C(61)	1.350(11)
Pt(2)	C(61)	2.037(8)	N(1)	C(31)	1.350(10)
Pt(2)	C(10)	2.089(9)			

(b) Angles

atom	atom	atom	angle (deg)
C(13)	Pt(1)	Pt(2)	112.9(3)
C(31)	Pt(1)	Pt(2)	148.3(2)
C(10)	Pt(1)	Pt(2)	50.8(2)
C(13)	Pt(1)	Ru(1)	52.2(2)
C(31)	Pt(1)	Ru(1)	149.5(2)
C(10)	Pt(1)	Ru(1)	112.0(2)
Pt(2)	Pt(1)	Ru(1)	61.494(18)
C(20)	Pt(2)	Pt(1)	113.3(2)
C(10)	Pt(2)	Pt(1)	50.2(2)
C(20)	Pt(2)	Ru(1)	53.4(2)
C(10)	Pt(2)	Ru(1)	110.0(2)
Pt(1)	Pt(2)	Ru(1)	60.004(17)
C(14)	Ru(1)	Pt(1)	93.7(2)
C(11)	Ru(1)	Pt(1)	146.4(4)
C(12)	Ru(1)	Pt(1)	82.4(4)
C(13)	Ru(1)	Pt(1)	47.4(2)
C(20)	Ru(1)	Pt(1)	105.1(2)
C(14)	Ru(1)	Pt(2)	87.3(3)
C(11)	Ru(1)	Pt(2)	153.5(4)
C(12)	Ru(1)	Pt(2)	84.6(4)
C(13)	Ru(1)	Pt(2)	105.3(2)
C(20)	Ru(1)	Pt(2)	46.7(2)
Pt(1)	Ru(1)	Pt(2)	58.502(18)

[a]Estimated standard deviations in the least significant figure are given in parentheses.

Table D.8. Selected intramolecular distances and angles for compound $Ru_4(CO)_{11}(IMes)(\mu\text{-}H)_4$, 5.5.[a]

(a) Distances

atom	atom	distance (Å)	atom	atom	distance (Å)
Ru(1)	C(51)	2.110(3)	Ru(2)	Ru(3)	2.9348(4)
Ru(1)	Ru(2)	2.9908(4)	Ru(3)	Ru(4)	2.7785(4)
Ru(1)	Ru(3)	3.0154(4)	N(1)	C(51)	1.364(4)
Ru(1)	Ru(4)	3.0156(4)	N(2)	C(51)	1.365(4)
Ru(2)	Ru(4)	2.7891(4)			

(b) Angles

atom	atom	atom	angle (deg)
C(51)	Ru(1)	Ru(2)	115.89(9)
C(51)	Ru(1)	Ru(3)	115.14(9)
Ru(2)	Ru(1)	Ru(3)	58.499(8)
C(51)	Ru(1)	Ru(4)	168.56(9)
Ru(2)	Ru(1)	Ru(4)	55.337(8)
Ru(3)	Ru(1)	Ru(4)	54.866(9)
Ru(4)	Ru(2)	Ru(3)	58.013(9)
Ru(4)	Ru(2)	Ru(1)	62.783(8)
Ru(3)	Ru(2)	Ru(1)	61.170(8)
Ru(4)	Ru(3)	Ru(2)	58.365(9)
Ru(4)	Ru(3)	Ru(1)	62.571(9)
Ru(2)	Ru(3)	Ru(1)	60.331(9)
Ru(3)	Ru(4)	Ru(2)	63.621(9)
Ru(3)	Ru(4)	Ru(1)	62.564(9)
Ru(2)	Ru(4)	Ru(1)	61.881(9)

[a]Estimated standard deviations in the least significant figure are given in parentheses.

Table D.9. Selected intramolecular distances and angles for compound $Ru_2Pt_2(CO)_8(IMes)_2(\mu\text{-}H)_2$, 5.6.[a]

(a) Distances

atom	atom	distance (Å)	atom	atom	distance (Å)
Pt(1)	C(14)	1.849(6)	Ru(1)	Ru(1)*	2.7695(8)
Pt(1)	C(15)	2.061(5)	Ru(1)	Pt(1)*	2.8356(5)
Pt(1)	Ru(1)	2.7136(5)	N(1)	C(15)	1.353(6)
Pt(1)	Ru(1)*	2.8357(5)	N(2)	C(15)	1.379(7)

(b) Angles

atom	atom	atom	angle (deg)
C(14)	Pt(1)	C(15)	99.0(2)
C(14)	Pt(1)	Ru(1)	82.72(17)
C(15)	Pt(1)	Ru(1)	166.71(14)
C(14)	Pt(1)	Ru(1)*	142.21(17)
C(15)	Pt(1)	Ru(1)*	118.58(14)
Ru(1)	Pt(1)	Ru(1)*	59.831(16)
C(11)	Ru(1)	Pt(1)	160.3(2)
C(13)	Ru(1)	Pt(1)	82.22(17)
C(12)	Ru(1)	Pt(1)	103.78(17)
C(11)	Ru(1)	Ru(1)*	98.2(2)
C(13)	Ru(1)	Ru(1)*	87.05(18)
C(12)	Ru(1)	Ru(1)*	165.20(17)
Pt(1)	Ru(1)	Ru(1)*	62.275(12)
C(11)	Ru(1)	Pt(1)*	100.91(19)
C(13)	Ru(1)	Pt(1)*	143.03(18)
C(12)	Ru(1)	Pt(1)*	114.82(17)
Pt(1)	Ru(1)	Pt(1)*	71.681(12)
Ru(1)*	Ru(1)	Pt(1)*	57.893(12)

[a]Estimated standard deviations in the least significant figure are given in parentheses.

VITA

Sumit Saha was born in Kolkata, India, on October 12th, 1984. His parents are Chandra Sekhar Saha and Mala Saha, and his younger brother is Souvik Saha, who is a Senior System Engineer at IBM. Sumit earned his B.S. in Chemistry from Jadavpur University, Kolkata, India, and M.S. in Chemistry from the Indian Institute of Technology, Roorkee, India. Right after that, he joined the University of Miami in Fall 2008 as a doctoral student in Chemistry. As a Research Assistant in the Chemistry Department, Sumit has worked on Organometallic Chemistry and X-Ray Crystallography, and published four first-authored research articles in prestigious peer-reviewed scientific journals. He worked as a Provost Teaching Fellow and Graduate Teaching Assistant in the Department of Chemistry from 2008 to 2013. He also worked as a Language Partner in Hindi (National Language of India) at the Directed Independent Language Study Program at the University of Miami. He received the "Excellence in Education" Award, "Lifetime Teaching Assistant" Award, "Perpetually Outstanding Teaching" Award from the Chemistry Department. He is also a recipient of "Who's Who Among Students in American Universities and Colleges" award from the University of Miami in recognition of his outstanding merit and accomplishment as a student in 2013. During his graduate studies at the University of Miami, Sumit served as Graduate Student Association Vice President and Media Relations Officer. He also served as Graduate Council Member and Graduate Student Representative on the Board of Trustees Academic Affairs and Master Planning committees at the University of Miami. Outside of academia, Sumit's hobbies include singing, dancing, travelling, playing soccer, volleyball and swimming. He is proud to be a Miami Hurricane.